Aalborg Universitet

From Global to local Functional Connectivity

Application to Listening Effort

Baboukani, Payam Shahsavari

Publication date:
2022

Document Version
Publisher's PDF, also known as Version of record

[Link to publication from Aalborg University]

FROM GLOBAL TO LOCAL FUNCTIONAL CONNECTIVITY: APPLICATION TO LISTENING EFFORT

BY
PAYAM SHAHSAVARI BABOUKANI

DISSERTATION SUBMITTED 2022

AALBORG UNIVERSITY
DENMARK

From Global to local Functional Connectivity: Application to Listening Effort

Ph.D. Dissertation
Payam Shahsavari Baboukani

Dissertation submitted 2022

Abstract

Listening to speech under adverse conditions such as background noise and competing talkers can demand higher effort and be challenging for hearing-impaired individuals. The higher effort can lead to adverse effects such as fatigue. The cognitive factors related to the higher demand are not considered in the traditional measurements of the performance of a listening task. Therefore, the concept of listening effort was defined and highly studied to improve the evaluation of hearing disability.

Several methods and tools have been used to estimate correlates of listening effort, among which electroencephalography (EEG) has gained attraction due to being non-invasive and having high temporal resolution. EEG is a method to record the brain's electrical activity by electrodes placed on the scalp. The relationship between and within different regions of the brain can be measured by assessing the statistical dependencies between and within EEG signals through the functional connectivity (FC) analysis, which can provide insights into the cognitive functions of the listening effort.

The objective of this thesis was to utilize FC analysis in the EEG to estimate correlates of listening effort. We divided our FC analysis into global- and local-scale analyses based on the distance between EEG electrodes. A directional measure, conditional transfer entropy (TE), was selected regarding global-scale connectivity assessment in EEG signals. We proposed a new estimator for conditional TE estimation and a new directed dependency measure based on conditional TE by which we could get higher accuracy in simulated data and real-world intracranial EEG data recorded during seizures. However, the estimation of correlates of listening effort by using global-scale connectivity analysis in real-world EEG data led to negative results.

Regarding local connectivity assessment in response to speech in adverse conditions, an existing multivariate phase synchrony measure called circular omega complexity (COC) was selected. The local connectivity was shown in this thesis to have the capability to estimate correlates of listening effort during a continuous long speech in noise task. Finally, we studied the effect of noise reduction (NR) schemes in hearing aid (HA) on local connectivity in EEG signals.

Resumé

Danish Abstract At lytte til tale mens der er baggrundsstøj eller hvor der er andre personer, som taler samtidigt - kan være en stor udfordring for høre-hæmmede personer, som ofte skal anstrenge sig for at forstå hvad der bliver sagt. Det fører til en øget kognitiv indsats, som kan føre til træthed og andre uønskede effekter. Traditionelle målinger i forbindelse med udførelsen af en lytteopgave tager ikke de kognitive faktorer relateret til en øget anstrengelse i betragtning. For at imødekomme dette er begrebet lytteindsats blevet defineret og benyttet til i bl.a. evalueringer af et hørehandikap.

Adskillige metoder og værktøjer er blevet brugt til at estimere korrelater af lytteindsatsen, blandt hvilke elektroencefalografi (EEG) ofte foretrækkes da det ikke er invasivt og da det har en høj tidsmæssig opløsning. EEG er en metode til at registrere hjernens elektriske aktivitet ved hjælp af elektroder placeret på hovedbunden. EEG-signaler i forskellige områder af hjernen kan måles og deres statistiske afhængigheder kan kvantificeres ved en funktionel koblingsanalyse (functional connectivity (FC)), som giver indsigt i lytteindsatsens kognitive relationer.

Formålet med denne ph.d.-afhandling var at bruge FC-analyser af EEG-signaler til at estimere korrelater af lytteindsatsen. Vi opdelte vores FC-analyser i global- og lokalskala analyser baseret på afstanden mellem EEG elektroderne. En analysemetode baseret på retningsbestemt betinget over-førselsentropi (TE) blev benyttet til global-skala analysen af EEG-signaler. Vi foreslog her en ny estimator til betinget TE-estimering og et nyt retnings-bestemt afhængighedsmål baseret på den betingede TE, hvorved vi kunne opnå en højere nøjagtighed på simuleret data samt på intrakranielle EEG-signaler målt på en person som havde et epilepsi anfald. Korrelaterne for lytteindsatsen fundet i forbindelse med global-skala forbindelsesanalysen af EEG-signaler, hvor en person udsættes for akustiske stimuli, førte til negative resultater.

Til lokal-skala forbindelsesanalysen af EEG-signaler blev et multivariat fasesynkroniseringsmål benyttet. Det blev påvist at lokal-skala forbindelsesanalysen muliggjorde en kontinuerlig estimering af korrelater af lytteindsatsen i et studie med kontinuerlig tale i støj. Lokal-skalaforbindelsesanalysen blev

også brugt til at undersøge effekten af støjreduktionsmetoder i høreapparater.

Contents

Contents

Contents

Contents

List of Publications

Thesis Title: From Global to local Functional Connectivity: Application to Listening Effort

    Ph.D. Student: Payam Shahsavari Baboukani

    Supervisor: Professor Jan Østergaard, Aalborg University

                        Assistant Professor Dr. Carina Graversen, Aalborg University

The main body of this dissertation is based on the following papers:

[A]:P. S. Baboukani, C. Graversen, , E. Alickovic, and J. Østergaard, *Estimating conditional transfer entropy in timeseries using mutual information and nonlinear prediction*. Entropy 22, 11–24, 2020.

[B]: P. S. Baboukani, S. Theodoridis, and J. Østergaard, *A stimuli-relevant directed dependency index for time series*, IEEE International Conference on Acoustics, Speech and Signal Processing (ICASSP). IEEE, pp. 5812–5816, 2022.

[C]: P. S. Baboukani, C. Graversen, , E. Alickovic, and J. Østergaard, *EEG phase synchrony reflects snr levels during ncontinuous speech-in-noise tasks*, 43rd Annual International Conference of the IEEE Engineering in Medicine & Biology Society (EMBC), 531–534, 2021.

[D]: P. S. Baboukani, C. Graversen, , E. Alickovic, and J. Østergaard, *Speech to noise ratio improvement induces nonlinear parietal phase synchrony in hearing aid users*, Frontiers in Neuroscience, p. 1173, 2022.

In addition to the aforementioned papers, one more paper was also published:

[1] P. S. Baboukani, C. Graversen , and J. Østergaard, *Estimation of directed dependencies in time series using conditional mutual information and non-linear prediction*, 28th European Signal Processing Conference (EUSIPCO), 2388–2392, 2020.

List of Publications

Preface

This thesis documents the scientific work conducted as part of the PhD project "From Global to local Functional Connectivity: Application to Listening Effort". The thesis is submitted to the Technical Doctoral School of IT and Design at Aalborg University in partial fulfillment of the requirements for the degree of Doctor of Philosophy. The project was carried out within the Centre for Acoustic Signal Processing Research (CASPR), at the Section for Artificial Intelligence and Sound, Department of Electronic Systems, Aalborg University, Aalborg, Denmark. Parts of the work were conducted during a research stay at the Eriksholm research center, part of Oticon, Denmark.

The thesis includes introduction and a collection of scientific papers. The purpose of the introduction is to provide the reader with some basic concepts to understand the research area, objectives and the contributions of the project. The papers elaborate more in details on the methods and discussing the results.

I would like to thank all the people who contributed to this PhD project. First and foremost, a great thank goes to my supervisor Jan Østergaard for his support, helpful advice, and guidance, which have not only big impacts on this work, but also on my way to conduct research. I am also so grateful to Emina Alickovic for her help, guidance, and support. Although her name is not mentioned as a supervisor in this thesis, her impacts on this work was as big as a very good supervisor. I also would like to thank my co-supervisor Carina Graversen. Last but not least, I would like to thank my family and friends whose support made this journey possible.

<div align="right">
Name
Aalborg University, November 23, 2022
</div>

Part I

Introduction

Introduction

Listening to speech under adverse conditions such as the presence of background noise and competing talkers can demand higher effort and be challenging for both hearing-impaired (HI) and normal-hearing individuals. A higher effort can lead to negative effects such as fatigue. An example of adverse listening conditions and their possible negative effects are shown in Figure 1, where the listener faces music in the background and a competing talker at a dining table. The cognitive factors related to the higher demand are not considered in the traditional measurements of the performance of a listening task. The concept of listening effort was therefore defined and highly studied to improve the evaluation of hearing disability [1] and enhance the rehabilitation strategy [2].

Several methods and tools have been used to estimate correlates of listening effort, among which electroencephalography (EEG) has gained attraction due to being non-invasive and having high temporal resolution [3]. Most studies in which correlates of listening effort were estimated by EEG have focused on spectral power analysis. The objective of this Ph.D. was to utilize functional connectivity (FC) analysis in EEG signals to estimate correlates of listening effort. The relationship between and within different regions of the brain can be measured by assessing the statistical dependencies between

Fig. 1: An example of adverse listening conditions such as competing talkers and background noise (music in this example) and its possible negative effects such as fatigue.
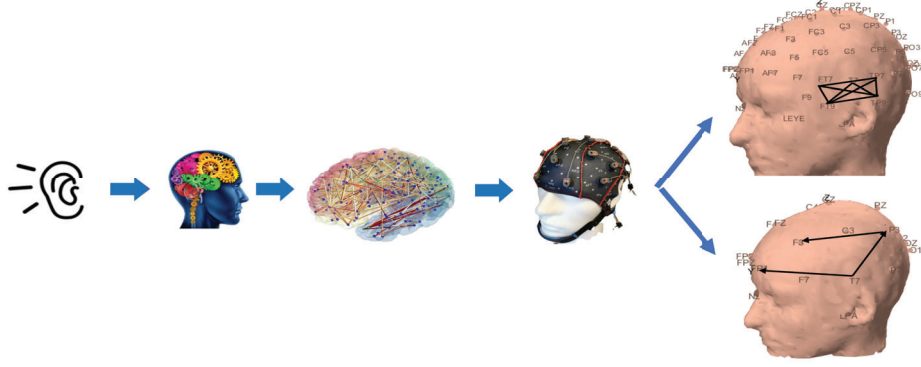
Fig. 2: Schematic presentation of the considered analysis in this thesis. The listening effort's cognitive functions can be assessed using FC analysis of EEG signals. The FC analysis can be divided into global- and local-scale based on the distance between EEG electrodes. The last right column of pictures shows examples of local- and global-scale connectivity. The FC within a region of interest (ROI) near the auditory cortex is considered as an example of local connectivity (top picture). The FC between the temporal, parietal, and frontal ROIs are considered an examples of global-scale connectivity (bottom picture).

neural data through the FC analysis [4]. Considering the brain as a complex system, characterization of the dependency between and within time-varying subsystems (different regions of the brain) can provide insights about the cognitive functions of the listening effort. In summary, as shown in Figure 2 , the cognitive functions related to listening to speech in noisy environments can lead to interaction between and within different areas of the brain, which can be assessed through a FC analysis of EEG signals.

We divided our FC analysis based on the distance between the electrodes recording neural data into global- and local-scale analysis, where the local-scale connectivity is FC within an ROI and the global-scale connectivity is FC between two ROIs (cf. figure 2). Regarding global-scale connectivity assessment in EEG signals, conditional transfer entropy (TE) was initially selected [5]. The conditional TE is able to assess the direction in addition to strength of the dependency between EEG electrodes [5]. This is an information-theoretic measure that is based on conditional mutual information. An estimator is therefore required before applying that to the EEG signals to assess global-scale connectivity. After implementing the existing estimators of conditional TE on the EEG signals, we found that reliable estimation of global-scale connectivity has limitations such as:

1. Low accuracy in detection of global-scale connectivity.

2. No guarantee that the estimated value is due to the change in external stimuli.

We addressed the above limitations in this thesis. First, we improved estimators' accuracy using a weighted combination of nonlinear prediction and

4

mutual information estimation, see Paper A. It was shown on synthetic data that the accuracy was significantly improved compared to existing methods. We could also get higher performance for the proposed algorithm when the volume conduction effect was higher in the synthetic data. Moreover, improvements were also demonstrated on real-world intracranial EEG signals recorded during seizures.

To take external stimuli into account, we developed a stimuli-relevant directed dependency metric based on the difference between two conditional TEs, See Paper B. We showed in a simulation study that the proposed metric more accurately predicts the true dependencies than for traditional conditional TE. However, estimation of correlates of listening effort using global-scale connectivity analysis of EEG signals led to negative results (as exemplified and explained the possible reasons for the negative results in Section 2.4).

As far as assessing the local connectivity in response to speech in adverse conditions is concerned, we found that:

1. Currently, there is no reliable estimate of correlates of listening effort based on the local connectivity assessed by phase synchrony.

2. Traditional power analysis failed to detect effects of noise reduction (NR) processing at different SNR values during a continuous speech in noise (SiN) task on correlates of listening effort [6].

An existing multivariate phase synchrony metric, called circular omega complexity (COC) [7], was chosen to assess the local connectivity. We showed that local connectivity estimated by the COC has the possibility to estimate correlates of listening effort. First, we demonstrated that the change of correlates of listening effort induced by the change in SNR value in a continuous SiN task could be detected by the local connectivity analysis, See Paper C. Then, we demonstrated the nonlinear trend (i.e. inverted U-shape) of local connectivity due to NR processing at different SNR values during a continuous long SiN task, See Paper D.

The rest of the introduction is organized as follows: we review basic concepts about EEG and listening effort in Section 1. Then, Sections 2 and 3 explain basic concepts related to the global- and local-scale connectivity, respectively. Finally, we provide a summary of the contributions and future work directions.

1   EEG and Listening Effort
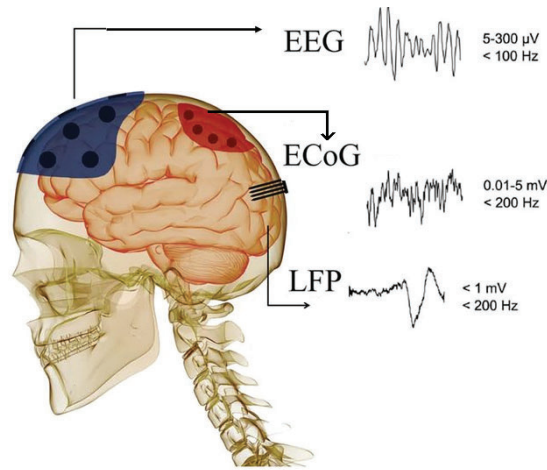
Fig. 3: Electrode location, amplitude, and frequency range of ECOG and LFP. The figure is modified version of Figure 1 in [8]

1.1   EEG

EEG is a method to record the brain's electrical activity by electrodes placed on the scalp [3]. The EEG history dates back to 1875, when Richard Keaton first recorded it. The first existing EEG recording on humans was made in 1924 by Hans Berger [3]. The amplitude and frequency ranges are 5-300 mV and 0-100 Hz, respectively [3].

There are other ways to record the electrical activity of the brain. The main difference between these methods is the location of the electrodes, as shown in Figure 3. Two examples include:

- Electrocorticography (ECOG): In this method, electrodes are placed on the brain's surface. The ECOG signal amplitude and frequency ranges are 0.01-5 microvolts (μV) and 0-200 Hz, respectively [8].

- Local field potential (LFP): In this method, electrodes are placed inside the brain. The amplitude and frequency ranges of the LPF signals are 0-1 millivolts (MV) and 0-200 Hz, respectively [8].

Although ECOG and LPF provide more accurate local information about brain activity, EEG has two significant advantages over the other two methods, which are [3]:

1. Non-invasiveness: In medical methods, a crucial factor is that the used method causes the least harm to the person [3]. It is known that ECOG and LPF require surgery to record, but EEG does not require surgery [3].

2. High temporal resolution.

Anatomy and Physiology of Neurons

Every neuron in the brain contains axons, dendrites, and cell body [3]. Perhaps a straightforward description of the functions of different parts of a neuron is as follows [3]:

1. The cell body is responsible for generating an action potential [3].

2. The axon is responsible for transmitting the action potential [3].

3. The dendrites are responsible for receiving the action potential [3].

The action potential is created by the displacement and change of ions in neurons [3]. The action potential is a temporary change in potential that spreads to all parts of the axon, usually starting in the cell body and moving in one direction [3].

The junction of two neurons is called a synapse [3]. At the site of synapses, the axon terminals do not attach to dendrites or cell bodies of other neurons, but there is a small space called the synaptic space [3]. Neural communication refers to the transmission of messages at the site of synapses [3]. The transmission of neural messages is mediated by specific chemicals. These chemicals are made in the cell body of neurons and stored in sacs at the axon terminals [3]. When a neural message reaches the axon terminals, these sacs reach the axon membrane and rupture, releasing chemicals inside the synaptic space [3]. The chemicals stimulate other neurons.

EEG Recording

To record multichannel EEG, caps are used on which all the electrodes are placed [3]. The material of the electrodes is usually aluminum or aluminum chloride [3]. Conductor gel is usually used to reduce the impedance between the head's skin and the electrodes resulting in a better recording [3].

A standard EEG method is needed to compare different EEG recordings. The International Federation of EEG and Clinical Neurophysiology, therefore, has developed a standard method called the 10-20 system for electrodes positions [3]. The reason behind the name of 10-20 system is the distance of 10% and 20% of the electrodes from each other, As shown in Figure 4. The distance between the nasion and inion is divided into two parts of 10% and four parts of 20%. The same procedure applies to the distance between two ears for which specific anatomical locations of the ears, such as mastoids, are used [3].

The electrode names consist of two parts: letters and numbers. The letters indicate the lobe (or the area) on which the electrodes are located [3]. The human brain consists of 4 lobes: frontal lobe, parietal lobe, occipital lobe, and temporal lobe, as shown in Figure 5. For example, F represents the parietal
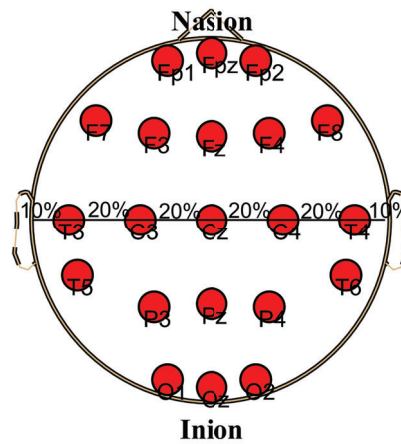
Fig. 4: Schematic presentation of the electrode position in 10-20 EEG system.
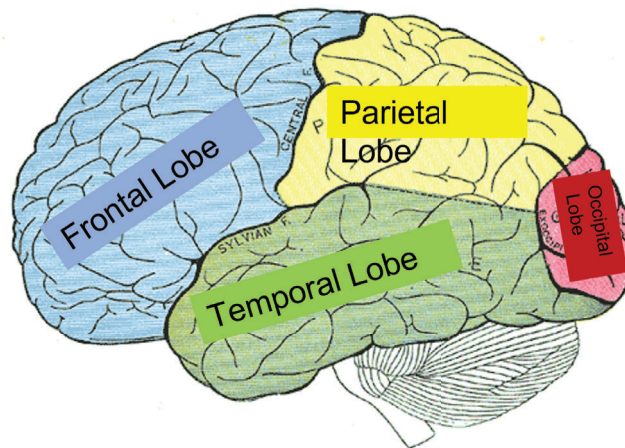
Fig. 5: Different lobes of the brain, which include frontal, temporal, parietal and occipital lobes. The figure is modified version of the figure 728 in [9].

lobe. The letter C says the electrode is located on the central area of the brain (note that there is no central lobe in the brain). Numbers are divided into three categories: even and odd numbers and the letter z. The even and odd numbers indicate that the electrode is in the right and left hemispheres, respectively. The letter z shows that the electrode is on the central part of the brain.

Three referencing methods are used to record EEG signals:

1. Mono-polar reference recording: The potential of all electrodes is measured relative to one reference electrode [3]. We normally assume that the reference electrode does not have any electrical activity [3]. The reference electrode is typically considered as the left , right, or the average of both earlobes.

2. Bipolar reference recording: The potential difference between the two

8

desired electrodes is measured [3].

3. Mean average reference recording: The potential of electrodes is measured relative to the mean of all electrodes at each moment [3].

EEG Frequency Bands

Brain frequency bands refer to the frequency components in the EEG. It has been shown that the frequency bands are related to particular states of the individuals [3]. It should be noted that the characteristics of brain rhythms can vary from person to person and also for a person at different ages [3]. Many brain disorders and cognitive functions are also characterized by the frequency analysis. There are four well-known brain frequency bands, which from low to high frequency are, as shown in Figure 6, [3]:

- Delta (δ) wave: The delta wave is in the frequency range of 0 to 4 Hz. The delta wave is the most observed wave in the EEG during deep sleep [3].

- Theta (θ) wave: This wave is in the frequency range of 4 to 8 Hz. It usually occurs between sleep and wakefulness [3].

- Alpha (α) wave: The frequency range of this wave is between 8 and 13 Hz and is usually present in the back of the brain. Alpha waves are involved in brain activities such as language learning and analysis [3].

- Beta (β) wave: The frequency range of this wave is between 13 and 39 Hz. This wave is related to the state of awakening, such as thinking and being alert. The beta wave tends to appear in the brain's central and frontal areas [3].

EEG artifacts and pre-processing

EEG signals can be affected by two types of artifacts. The first category of the artifacts is those internally originated from the subject [3]. Some examples include eye movements, breathing, heart-related, and muscle-related artifacts [3]. The second type of artifact is system-based such as 50/60 Hz electricity power supply interference and impedance fluctuation [3]. Figure 7 demonstrates two examples of the artifacts in the EEG signals.

A pre-processing step is typically applied to the EEG signals to reduce the artifacts' effect. This step tends to include a 0.5 Hz high-pass filter to reduce the effect of the disturbing very low frequency components such as those of breathing [3]. Furthermore, low-pass filters with a cut-off frequency of approximately $50 - 100$ Hz are applied to mitigate the high-frequency noise, such as muscle activity [3]. A 50/60 Hz notch filter is often applied to reduce
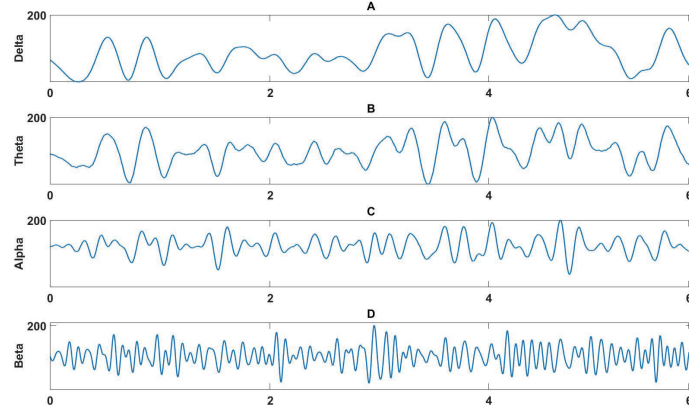
Fig. 6: Frequency bands in EEG signals. A) Delta, B) Theta, C) Alpha, and D) Beta frequency bands. It should be noted that this example is not from real EEG data.
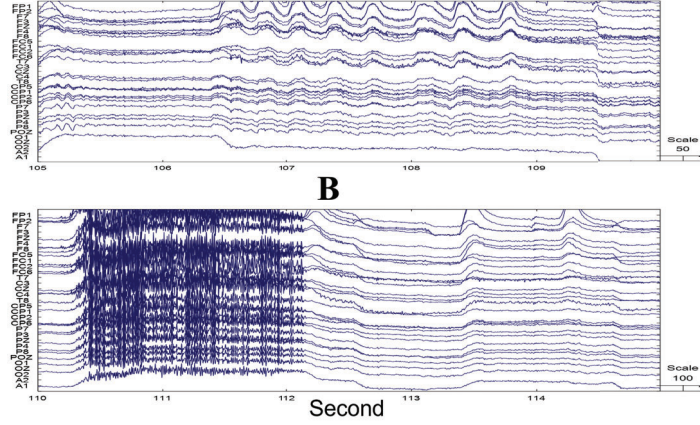
Fig. 7: Two examples of EEG artifacts. A) Eye blinking which is considered to have very low frequency specification and B) Muscle activity which is considered to have very high frequency.

the power supply noise [3]. Finally, an independent component analysis algorithm is often applied to decrease artifacts caused by eye movements, eye blinks, muscle activity, heartbeats, and single-channel noise [10, 11]. The independent component analysis usually decomposes the EEG signals to their constituent components [10, 11]. The noise component is then visually identified. The noise components usually have specific features identified by time, frequency, and space projections. An example of the time, frequency, and space projections of an eye movement component are shown in Figure 8.

1.2 Functional Connectivity

After the pre-processing step, the main analysis is applied to extract the relevant information from the EEG signals. Several signal processing and
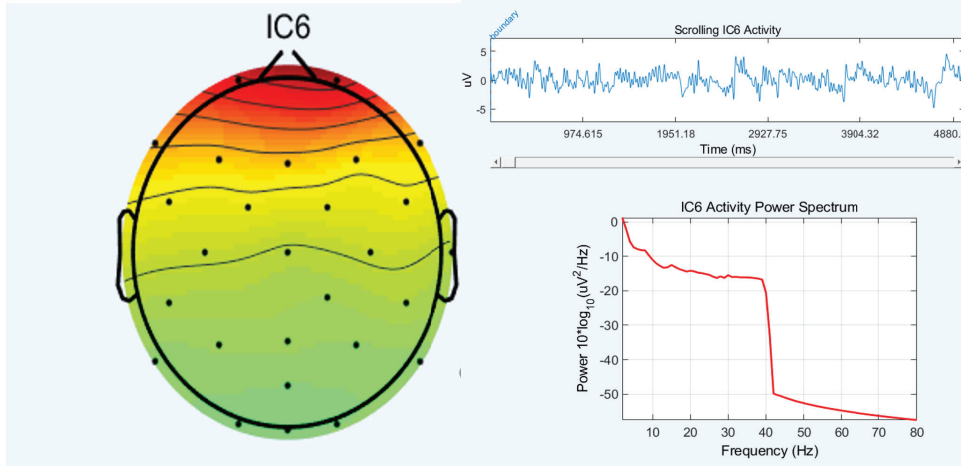
Fig. 8: Eye movement component of the independent component analysis decomposition. As shown in the figure, the projection of the component to the sensor level is only active in the frontal area. The time component show activity like an eye blink. The activity power spectrum also shows a smooth decrease, which tends to be related to the eye blink activity.

information theory approaches have been used toward this end. Some examples include time analysis such as event-related potential (ERP) [12], frequency analysis such as power analysis in the conventional EEG frequency bands [13], and connectivity analysis [14]. After the main analysis, a statistical test [15], or a classifier is applied to evaluate the extracted information.

Connectivity analysis tends to determine the relationship between and within different areas of the brain, which can be divided into functional and effective analysis in the EEG signals[1]. Functional connectivity can be referred to the statistical dependencies between neural data [17]. The neural data can be recorded by electrodes located on the scalp in EEG signals. The information extracted by this analysis can provide insights into how the brain functions. Cognitive functions related to auditory processing in the brain have been studied through functional connectivity analysis of EEG signals [4, 14, 17, 18].

The term effective connectivity can stem from the cause and effect property in causal measures [19, 20]. The measures used in the EEG processing literature to extract effective connectivity can sometimes over- or underestimate the causal effect [19, 20]. Two popular approaches, Granger causality and TE, are based on Wiener's definition, which is based on prediction [21]. Wiener's definition states that a causal effect exists from X to Y when the prediction of the future value of a time series Y from its own past can be improved by incorporating the past value of another time series X [21]. Despite

---

[1]It should be noted that there is another type of connectivity in the brain called structural connectivity. This connectivity refers to the existence of white matter tracts physically interconnecting brain regions, which are generally investigated by diffusion magnetic resonance imaging (MRI) [16]. We will not investigate structural connectivity in this dissertation.

the use of the term "causal" in Wiener's definition, it has been demonstrated that measures quantifying it under- or over-estimate the causal effect in certain cases [19, 20]. The term "directed dependencies" is therefore used in this dissertation to describe the property of time series or processes meeting Wiener's definition.

Functional connectivity can be divided into global- and local-scale connectivity based on the distance between the regions of the brain from which neural data is recorded. Global-scale connectivity describes the statistical dependency between the two regions. Functional connectivity within a localized region is described by local-scale connectivity.

1.3   Listening Effort

Listening to speech in an environment with competing talkers and background noise can be challenging for hearing-impaired people, which can lead to negative effects like fatigue [22–24], disengagement from conversations [25], and social withdrawal [26]. However, the cognitive factors related to effortful listening are not necessarily taken into account in current listening tests such as speech reception threshold [27, 28].

The concept of listening effort was defined in [29] as "the deliberate allocation of mental resources to overcome obstacles in goal pursuit when carrying out a task, with listening effort applying more specifically when tasks involve listening." The listener faces acoustic challenges as a combination of cognitive factors, such as linguistic ability and memory capacity, and acoustic characteristics, such as level of background noise and competing talker [30], as shown in Figure 9.

The listener's motivation might also modulate the listening effort [29, 30]. Figures 10A and B illustrate a relationship between acoustic challenge and listening effort and accuracy, respectively. At low levels of acoustic challenge, the cognitive demand is not high as the speech comprehension is mostly automatic [30]. As acoustic challenges increase, the cognitive processing needed to comprehend speech increases [30]. The figures illustrate that accuracy remains high when the acoustic challenge is moderate but requires additional effort. Listeners might lose the motivation to spend cognitive resources at very high levels of acoustic challenge when they understand that they will not be able to comprehend successfully (dotted line in Figure 10A), which can lead to nonlinear relationship between correlates of the listening effort and acoustic challenge levels [30].

Through advanced signal processing techniques, modern hearing aids (HA) can help individuals with hearing loss [31–33]. Particularly, noise reduction (NR) processing reduces the effect of background noise and improves the SNR. It has been shown that NR processing has the capability to reduce the listening effort [28, 34]. The activation of NR processing can improve
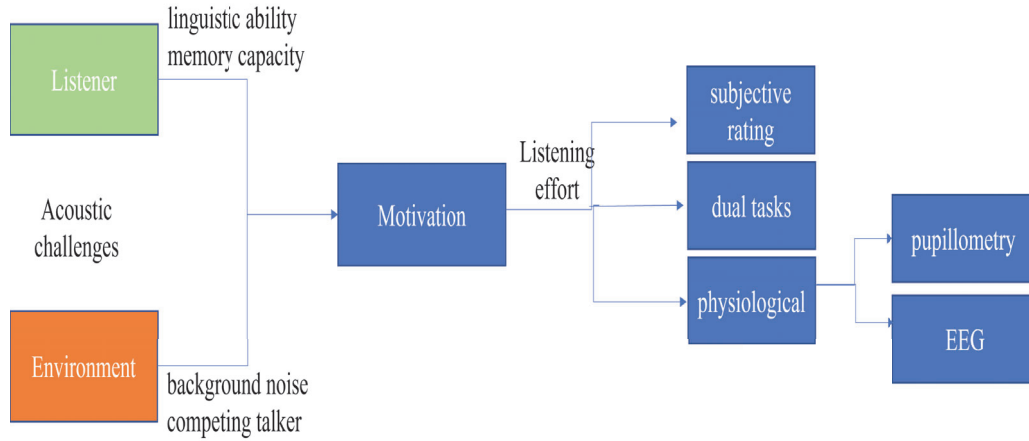
Fig. 9: A schematic presentation of acoustic challenges including cognitive factors and acoustic characteristics. Different estimators of the listening effort are also schematically demonstrated.

speech ineligibility at low SNRs. The activation of the NR processing in HAs can provide an additional effect in addition to improved speech ineligibility when it comes to listening effort [34]. Furthermore, when HA users are asked to perform a selective attention task, NR schemes can improve their performances [35, 36].

The purpose of researching listening effort is to provide a reliable measurement tool, which can be simultaneously used with speech recognition tests and improve the evaluation of hearing disability and enhance the rehabilitation strategy [1, 2].

A wide variety of methods and tools have been used to estimate correlates of listening effort. These include:

- Subjective rating such as scales [37] and questioner [38].

- Dual tasks which are based on the limited cognitive capacity hypothesis. The effort spent on the primary task (such as understanding the speech in noise) can be measured by the performance of the secondary task (such as recalling the words in the speech) [39].

- Physiological measures such as pupillometry [40, 41] and neuroimaging [41].

Figure 9 shows a schematic presentation of the acoustic challenges and different approaches to estimating correlates of listening effort.

EEG Estimates of Correlates of Listening Effort

EEG is a neuroimaging method that has gained particular attraction to estimate correlates of listening effort due to its advantages(c.f. Section 1.1). A wide variety of signal processing and information theory methods have
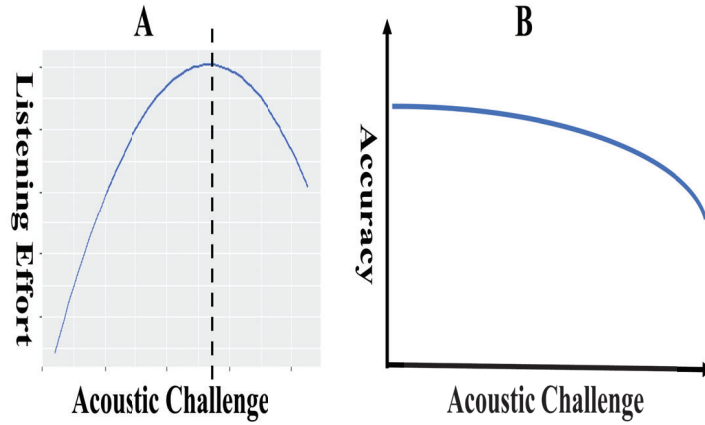
Fig. 10: Relationship between acoustic challenge and A) listening effort and B) accuracy. Listening effort is low at low levels of acoustic challenge as speech comprehension is mostly automatic. At moderate levels of acoustic challenges, the accuracy remains high, but the listening effort increases as speech comprehension demands higher effort. Listeners lose motivation at very high levels of listening effort (the dotted line) and both listening effort and accuracy decrease. This would lead to nonlinear relationship between acoustic challenges and listening effort. It should be noted that figure A is generated from the real correlates of listening effort obtained by the local connectivity analysis of EEG signals. Figure B is the replicated version of figure 2C in [30].

been used to analyze the EEG and estimate the correlate of listening effort. Power analysis on conventional EEG frequency bands is the most studied signal processing approach in the literature. Pwelch [42], wavelet [43] and short-time Fourier transform [44] were used in the literature to extract event-related spectral perturbation. Other analyzing methods can include phase synchrony, speech tracking, and functional connectivity. In addition, we can also categorize the EEG estimates of correlates of listening effort based on the conventional EEG frequency bands and the location of the electrodes on which the analysis is performed. The alpha frequency band in the parietal region and theta frequency band in the frontal region are the most investigated bands and regions. Finally, EEG estimates of listening can be divided depending on whether the analysis is performed on the sensor or source level. Table 1 summarizes the state-of-the-art of EEG estimates of correlates of listening effort based on the analyzing methodology, frequency band, location of the electrode on which the analysis was performed, and if the analysis was performed on source level or sensor level.

2 Global-scale Connectivity

An information theoretic-based metric was selected regarding global-scale connectivity assessment in EEG signals. This section reviews some basic concepts of information theory, such as entropy and mutual information. Then,

14

Table 1: State of the art of EEG estimates of correlates of listening effort. N.A is the abbreviation of not applicable in the table, which means that in the papers, they did not filter the data to the conventional EEG frequency bands. All regions in the last column of the table means that authors of the articles performed a comprehensive analysis on the all electrodes located at all regions.

Refere––nces	Analyzing Methodology	Frequency Band	Source/ Sensor	Location of the electrodes
[1, 6, 45] [41, 46, 47] [48–50] [2, 51, 52]	Power	Alpha	Sensor	Parietal
[13, 48]	Power	All Bands	Source	All Regions
[47, 53, 54]	Power	Alpha	Source	All Regions
[41, 48, 52, 55]	Power	Theta	Sensor	Frontal
[56]	Power	Theta	Source	Frontal
[12]	ERP	N.A	Sensor	Parietal
[57]	Functional Connectivity	N.A	Sensor	All Regions
[4, 18]	Functional Connectivity	N.A	Source	All Regions
[45, 58, 59] [32, 33]	Phase Synchrony	Theta	Sensor	Right Mastoid
[60]	Phase Synchrony	Theta	Sensor	All Regions
[53] [54]	Speech tracking	Delta Theta	Source	Frontal Temporal

we provide an example of negative results obtained by applying conditional TE on EEG signals to estimate correlates of listening effort. Finally, we discuss the possible reasons for the negative results.

2.1 State-of-the-art

Several signal processing and information theoretic-based approaches have been proposed to quantify functional connectivity. The first subdivision of these methods can be based on whether the metrics quantify the direction of the interaction [61]. One limitation of non-directional approaches is that they are not able to distinguish the direction of the interaction. On the other hand, directional metrics are able to assess the direction in addition to strength of the dependency between the neural data. Coherence coefficient, Pearson correlation coefficient [4], phase locking value [62], and mutual information [63] are the measures that have been used to quantify non-directional dependency. Granger causality [64] and TE [5] are the two popular approaches in the literature to assess directional functional connectivity. These measures are based on Wiener's definition, which is based on the concept of predic-
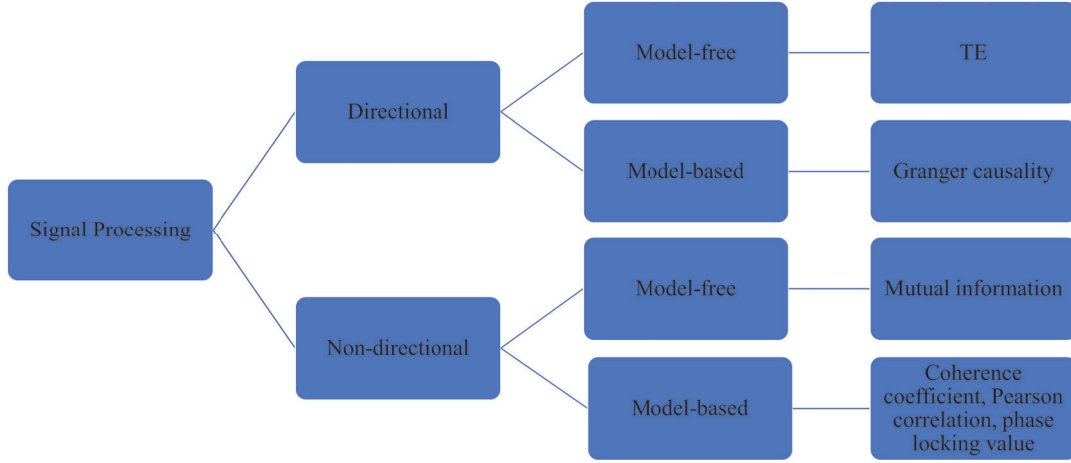
Fig. 11: Schematic presentation of the metrics used in the literature to assess functional connectivity.

tion [21]. Wiener's definition states that a causal effect exists from *X* to *Y* when the prediction of the future value of a time series *Y* from its own past can be improved by incorporating the past value of another time series *X* [21].

The functional connectivity metrics can also be divided based on if they depend on a model or linearity assumption [61]. The model-based measures include Pearson correlation coefficient, Coherence coefficient, phase locking value, and Granger causality. These measures are only capable of assessing linear interaction between neural data, while the model-free measures such as mutual information and TE tend to be able to capture the nonlinear dependencies. Figure 11 illustrates the state-of-the-art measures utilized to quantify functional connectivity, which includes the described subdivisions and mentioned metrics. We note that although there are several metrics in the literature that we did not mention in this section (see for example [65] where 42 methods were described for functional connectivity quantification), the state-of-the-art described in this section provides a general point of view and mentions the most widely used measures.

2.2 Information Theory

The field of information theory originally began by Claud Shannon in 1948 [63]. Although addressing the problems in communication was the original motivation for the development of the information theory, Shannon's measures and their extensions have been extensively used in many fields, such as signal processing and neuroscience. One example is TE, an extended form of mutual information widely used in neuroscience and economics to quantify directed dependency. In this section, we review basic concepts in information theory, which can help better understand TE that is used to assess global-scale connectivity in this dissertation.

16
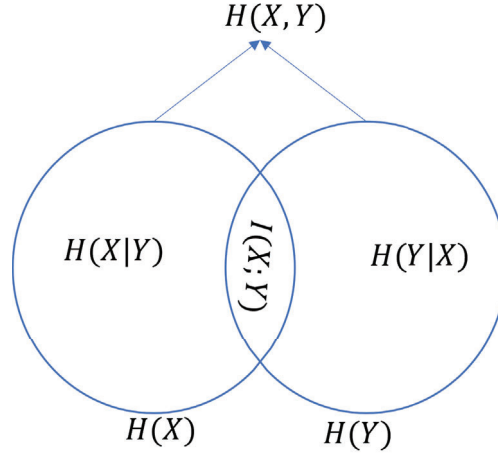
Fig. 12: Venn diagram showing the area associated with $H(X)$, $H(Y)$, $H(Y|X)$, $H(X|Y)$, $H(X,Y)$ and $I(X;Y)$

Entropy

Consider a random variable X with probability mass function (PMS) $p(x)$, the entropy of X is noted by $H(X)$ and defined as follows [63]:

$$H(X) = - \sum_{x \in \mathcal{X}} p(x) log_2 p(x), \tag{1}$$

where $\mathcal{X}$ is the alphabet of X. An entropy value measures the average degree of uncertainty associated with a random variable. The logarithms base is 2. The entropy is then measured in bits. Therefore, entropy is the average number of bits needed to describe the random variable [63]. It shoulb be note that we consider discrete random variables here but similar concept exists for continuous random variables.

The amount of remaining uncertainty in the random variable X conditioned on the knowledge of another random variable Y is defined by conditional entropy $H(X|Y)$ as [63]:

$$H(X|Y) = - \sum_{x \in \mathcal{X}, y \in \mathcal{Y}} p(x,y) log_2 \frac{p(x,y)}{p(y)}, \tag{2}$$

where $p(x,y)$ is the joint PMS of x and y. The alphabet of Y is noted by $\mathcal{Y}$.

The uncertainty associated with both random variables X and Y is described by their joint entropy $H(X,Y)$ as [63]:

$$H(X,Y) = - \sum_{x \in \mathcal{X}} \sum_{x \in \mathcal{Y}} p(x,y) \log_2 p(x,y). \tag{3}$$

Mutual Information

The information that a random variable X has about another random variable Y is described by mutual information $I(X;Y)$ as [63]:

$$I(X;Y) = \sum_{x \in \mathcal{X} y \in \mathcal{Y}} p(x,y) \log_2 \frac{p(x,y)}{p(x)p(y)}. \tag{4}$$

Relative entropy (or Kullback–Leibler distance) describes the distance between two probability mass functions [63]. The relative entropy $D(P||Q)$ is defined as [63]:

$$D(P||Q) = \sum_{x \in \mathcal{X}} p(x) log_2 \frac{p(x)}{q(x)}. \tag{5}$$

The mutual information $I(X;Y)$ can be written as the relative entropy between joint distribution $p(x,y)$ and product distribution $p(x)p(y)$ [63]. We should note that two random variables X and Y are mutually independent if $p(x,y) = p(x)p(y)$. Therefore, mutual information can describe the distance between the joint entropy of two random variables and the condition that they are independent. Mutual information is also a non-directional measure of linear and nonlinear dependencies between two time series.

Figure 12 shows a Venn diagram in which the relationship between various information measures related to two random variables X and Y are expressed.

Next measure is conditional mutual information $I(X;Y|Z)$, which is the information that X and Y have in common when Z is given [63]. The conditional mutual information is described as:

$$\begin{aligned} I(X;Y) &= \sum_{x \in \mathcal{X} y \in \mathcal{Y} z \in \mathcal{Z}} p(x,y,z) \log_2 \frac{p(x,y|z)}{p(x|z)p(y|z)} \\ &= \sum_{z \in \mathcal{Z}} p(z) \sum_{x \in \mathcal{X} y \in \mathcal{Y}} p(x,y|z) \log_2 \frac{p(x,y|z)}{p(x|z)p(y|z)}, \end{aligned} \tag{6}$$

where $\mathcal{Z}$ is the alphabet of random variable Z.

The mutual information and its conditional version can be described by the entropy as [63]:

$$\begin{aligned} I(X;Y) &= H(X) - H(X|Y) = H(X) + H(Y) - H(X,Y) \\ I(X;Y|Z) &= H(X|Z) - H(X|Z,Y). \end{aligned} \tag{7}$$

2.3 Directed Information Theory

Unlike mutual information, TE is a directional measure that is able to assess the direction in addition to the strength of dependencies between two time

series [5]. TE is based on Wiener's definition, which states that a causal effect exists from X to Y when the prediction of the future value of a time series Y from its own past can be improved by incorporating the past value of another time series X [21]. Schreiber proposed TE which can also be considered as the reformulation of Wiener's definition based on information theory [66]. A different approach based on Wiener's definition relies on works by Granger on causality [64, 67], referred to as Granger causality. Time series are modeled as autoregressive models and their interactions as linear. Granger causality is, therefore, only capable of assessing linear dependencies, while TE is a model-free measure that can assess both linear and nonlinear interactions [68]. It was shown in [57, 69] that linear implementation of TE and Granger causality are equivalent in the Gaussian case.

Another information theoretic-based framework to assess directed dependencies relies on the works by Marko [70] and Massey [71]. A bidirectional channel's information flow can be calculated by using conditional probabilities based on Markovian dependencies, as proposed by Marko [70]. The directed information flow from the input to the output of a channel with feedback was formally defined by Massey based on Marko's initial work [71]. In fact, TE is part of the directed information flow proposed by Massey, except that Schreiber did not take into account the possible instantaneous causal dependencies of a time series on another [69]. Directed information flow has been used to infer neural networks in neural spike training recording [72, 73].

Transfer Entropy

TE, and its extensions such as phase TE [74], lag specific TE [75, 76] and compensated TE [77], have been used to infer the directed dependencies in physiological systems [78, 79]. Let the stationary stochastic processes $X = (X_1, X_2, \ldots, X_N)$ describe the time series $X[n], n \in 1, 2, \ldots, N$ over time, similar notation applies to $Y = (Y_1, Y_2, \ldots, Y_N)$. Let X_n and Y_n be stochastic variables obtained by sampling the processes X and Y at the present time n, respectively. Additionally, let the past of X up until X_{n-1} be described by a random vector $X_n^- = [X_{n-1}, X_{n-2}, \ldots]$, similar notation applies to Y_n^- and Z_n^-. TE from X to Y is then defined as [5]:

$$I(X \rightarrow Y) \triangleq I(Y_n; X_n^- \mid Y_n^-). \tag{8}$$

It was proposed in [66] that Taken's delay embedding (which is referred to as uniform embedding in [80]) and Kraskov–Stögbauer–Grassberger (KSG) estimator can be used to estimate of the past of the processes and the conditional mutual information in Eq. 8, respectively. In a complex network, there could be a third process, say $Z = (Z_1, Z_2, \ldots, Z_N)$, through which shared information or indirect dependencies are mediated. In this case, conditional

TE from an individual source X to the target Y conditioned on Z is defined as [80]:

$$I(X \rightarrow Y|Z) \triangleq I(Y_n; X_n^- \mid Y_n^-, Z_n^-). \tag{9}$$

2.4 Estimation of Correlates of Listening Effort using Transfer Entropy

In this thesis, conditional TE was chosen to assess global-scale connectivity in EEG signals to estimate correlates of listening effort. Reliable estimation of the conditional TE in networks, including high number of nodes such as EEG signals, is limited by the so-called "curse of dimensionality" problem since we only have access to a limited number of realizations. Non-uniform embedding algorithms are proposed to reduce this effect and improve the reliability of the conditional TE estimators [80, 81]. In this section, we will report the negative results of applying existing and proposed non-uniform embedding algorithms to estimate correlates of listening effort. The EEG data used in this section were utilized in [82, 83], where more details can be found. Briefly, Twenty-two native HI Danish speakers listened to 40 Danish news clips with two levels of SNR (3 dB and 8dB). We are interested in the change of correlates of listening effort induced by the change in SNR value, which the global-scale connectivity can estimate. The EEG data were recorded using 64 channels BioSemi ActiveTwo amplifier system (Biosemi, Amsterdam, Netherlands). As we were interested in assessing global-scale connectivity in this analysis, we selected 19 electrodes that were used in the international 10-20 system, which are shown in Figure 4.

The existing non-uniform embedding algorithm proposed in [80] was initially utilized to calculate conditional TE in EEG in response to acoustic stimuli with two different SNR values. Next, Two sample t-test was applied to the obtained values to check the significant different global-scale connectivity. As demonstrated in Figure 13A, a high number of connectivities are statistically different, some of which are higher for the easier condition (3 dB) and some others are higher for the more difficult condition (8 dB). We could not find any neuroscience-based hypothesis which can explain the obtained results.

One possible explanation for the obtained results could be that the existing non-uniform embedding algorithm cannot reliably detect global-scale connectivity. We, therefore, proposed a new non-uniform embedding algorithm by which we could get higher accuracy than that of state-of-the-art ones in simulated data, specifically when the data are highly directly interacted [84]. We could also get better performance for the proposed algorithm when the volume conduction effect was higher in the simulated data [84]. The highly coupled data and volume conduction effect could be the possible reasons for the negative results of the existing algorithm [85].
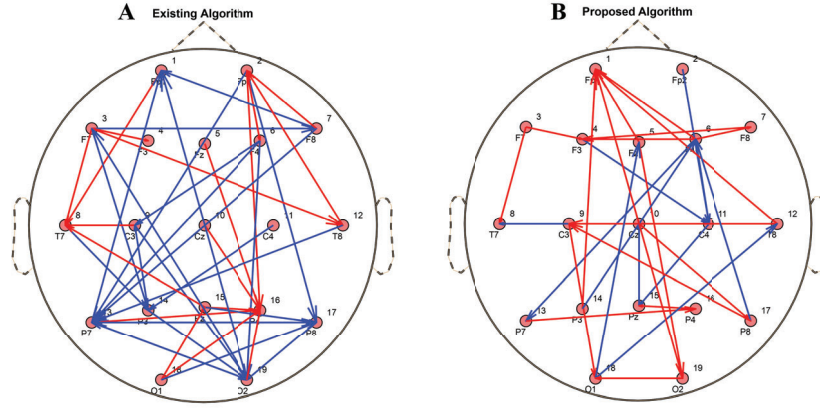
Fig. 13: significantly different global-scale connectivity in response speech with two different SNR values. The red arrows show that the connectivity has higher values at 8 dB and the blue color demonstrates otherwise. A) Existing non-uniform embedding algorithm. B) Proposed non-uniform embedding algorithm.

The proposed algorithm was utilized to calculate conditional TE in EEG in response to acoustic stimuli with two different SNR values. Figure 13B shows statistically significant different global-scale connectivity. As shown in 13B, a lower number of connectivities are found to be different due to the change in SNR value. However, we could not find any neuroscience-based hypothesis that can explain the obtained results.

It should be noted that we also employed graph theory measures to analyze the results shown in Figure 13, but the results were again not in line with any neuroscience-based hypothesis.

Another contradictory global-scale connectivity result obtained by conditional TE can be found in [85, 86]. Both papers analyzed the global-scale connectivity in resting state EEG data using conditional TE and the same non-uniform embedding algorithm. A statistically different front-to-back propagation was found during eye-closed situation [85] while a back-to-front information flow was found in [86].

Altogether, we got negative results regarding estimating correlates of the listening effort using global-scale connectivity. The possible reasons could be low accuracy in the detection of the large-scale connectivity due to the volume conduction effect and no guarantee that estimated connectivity is due to the change of acoustic stimuli. The effect of the volume conduction can be reduced by applying source localization techniques. Regarding the latter, we proposed a metric that quantifies an external stimulus's effect on the coupling strength between other time series, which is called stimuli-relevant directed dependency index [87]. Applying source localization and stimuli-relevant directed dependency index to assess the global-scale connectivity for estimating correlates of listening effort are considered as future directions

of this thesis.

3 Local Scale Connectivity

A phase synchrony-based measure was selected for local-scale connectivity assessment in EEG signals. In this section, we review some concepts related to phase synchrony.

3.1 State-of-the-art

Local connectivity is defined as functional connectivity within localized regions of the brain. Local connectivity assessment in EEG signals has been used to classify motor imagery movements [88], estimate cognitive workload [89], investigate schizophrenia [90] and Alzheimer [91].

Generally, there are two approaches to estimating local connectivity. The first approach is to calculate the functional connectivity within the electrodes located in a localized region of the brain using a metric by which the interaction can be assessed. An example can be the assessment of the functional connectivity within cluster of locations defined by the electrode itself and the surrounding electrodes that belong to its first neighbor [90]. The second approach is to calculate the interaction between all pair-wise electrodes and recruit the graph theory measures such as local efficiency, which can assess the local connectivity [18]. In this thesis, we will use the first approach.

All the metrics mentioned in Section 2.1 can also be used to estimate the local connectivity. A phase synchrony measure was chosen to estimate local connectivity. Phase synchrony analysis has also been utilized to estimate correlates of the listening effort. In particular, wavelet phase synchronization stability was reported to be higher for more effortful listening conditions [58]. The same index of listening effort has shown sensitivity to the effect of age and hearing loss [59]. The distribution of the mapped phase mean vector on the unit circle was also used as an index of phase synchrony, and higher effort corresponded to higher phase synchrony. Noise reduction schemes in hearing aids decreased the listening effort, and phase synchrony [32]. The entropy of the instantaneous phase of EEG signals has also been used to estimate correlates of listening effort [33, 60].

3.2 Phase Synchrony

The timing of neural activity can be reflected by the phase of neural data and phase synchrony can be used to describe the interaction between or within brain regions in neural networks [92]. Extracting the instantaneous phase is the first step in calculating phase synchrony. Several approaches, such as Hilbert-based and wavelet-based, have been proposed in the literature [93,

94]. Each approach has its advantages and disadvantages. We will use a Hilbert-based approach to extract the instantaneous phase in this thesis due to advantages mentioned in [93], such as simplicity. The required assumption to recruit the Hilbert-based approach is that the signal is mono-component, i.e., in the time-frequency domain, its distribution represents a single time-varying ridge [7]. It is possible to reduce the multi-component nature of non-stationary signals such as EEG signals by filtering to narrow frequency bands. This procedure will improve the estimation of the instantaneous phase signals by filtering to narrow frequency bands.

Consider a discrete signal $X[n]$, the analytical signal $Z[n]$ is defined as [44]:

$$Z[n] = X[n] + \hat{X}[n] = a[n]e^{i\phi_X[n]}, \tag{10}$$

where $\hat{X}[n]$ is the Hilbert transform of $X[n]$ and $i = \sqrt{-1}$. The instantaneous amplitude and phase are denoted by $a[n]$ and $\phi_X[n]$, respectively. The instantaneous phase signal $\phi_X[n]$ is then defined as [44]:

$$\phi_X[n] = \tan^{-1}\left(\frac{\hat{X}[n]}{X[n]}\right). \tag{11}$$

Bivariate Phase Synchrony

The signals $X[n]$ and $Y[n]$ with the corresponding instantaneous phases of $\phi_X[n]$ and $\phi_Y[n]$ are said to be phase locked of order $m : n$ (where m and n are integers) if their IP signals satisfy the equation below [62]:

$$m\phi_X[n] - \phi_Y[n] < \alpha \tag{12}$$

where α is a constant integer. A statistical metric is typically used to quantify the degree of phase locking in these methods, whereby phase synchrony can be measured. Some examples include recruiting Shannon entropy to quantify the uncertainty of IP differences [95] and mutual information to measure the interaction between the instantaneous phases [96]. Considering the particular case where $m = n = 1$, the degree of phase locking can be quantified using the phase locking value (PLV) metric, which is defined as [62]:

$$PLV = \frac{1}{N}\sum_{n=1}^{N} e^{i(\phi_X[n] - \phi_Y[n])}, \tag{13}$$

where N is the length signals X and Y.

Another widely utilized phase synchrony metric is the coherence coefficient which is equivalent to the time domain cross-correlation in the frequency domain [61]. The coherence coefficient is defined as [61]:

$$Coherence = \frac{\left|\frac{1}{N}\sum_{n=1}^{N} a_X(\omega,n)a_Y(\omega,n)e^{i(\phi_X(\omega,n) - \phi_Y(\omega,n))}\right|}{\sqrt{\left(\frac{1}{N}\sum_{n=1}^{N} a_X^2(\omega,n)\right)}\sqrt{\left(\frac{1}{N}\sum_{n=1}^{N} a_Y^2(\omega,n)\right)}}, \tag{14}$$

where $a_X(\omega, n)$ and $\phi_X(\omega, n)$ are the instantaneous amplitude and phase at frequency ω, respectively. The PLV can also be written as the special case of the coherence coefficient if replace $a_X(\omega, n) = 1$ and $a_Y(\omega, n) = 1$ [61]. The PLV is, therefore, a linear metric.

Multivariate Phase Synchrony

The phase synchrony ratio within several electrodes located in a brain's area needs to be calculated to extract local connectivity. Phase synchrony within a multivariate signal is traditionally quantified by first assessing all pair-wise phase synchrony between channels and then averaging them. The averaging over bivariate values may not be sufficient to provide global phase synchrony [7, 97–100]. For example, suppose we have three nodes network with the corresponding mutually independent phase signals ϕ_A, ϕ_B and ϕ_C. Furthermore, let $\phi_B = \phi_C \oplus \phi_A$ where $\oplus$ denotes XOR operator. Then, all the bivariate mutual information values are zero (such as $I(\phi_A; \phi_B) = 0$), which leads to zero average value. However, considering the information of the third node can lead to a non-zero value, as is the case for $I(\phi_A; \phi_B | \phi_c) = H(\phi_A)$.

The multivariate phase synchrony metrics are alternatives to bivariate ones, which generalize the pair-wise phase synchrony concept to multivariate signals. An example can be a co-integration-based phase synchrony measure [98]. This metric is based on the ratio of the number of linear combinations of instantaneous phases that results in a stationary process and the maximum possible number, which is the number of channels [98]. Another example is Hyper-Torus phase synchrony (HTS) which is based on a hyperdimensional coordinate system [100].

More recently, a multivariate phase synchrony metric was proposed based on the concept of circular statistics and state space. This metric, circular omega complexity (COC), quantifies the dimensionality of the state space formed by the instantaneous phases, which showed sensitivity to the degree of multivariate phase synchrony [7]. The COC metric has been shown to be more effective than conventional multivariate phase synchrony metrics in some specific applications [7]. Therefore, the COC metric was chosen to extract local connectivity in this thesis.

4 Summary of the Contributions

This thesis aims to derive an EEG-based reliable estimation of the correlates of listening effort. Toward this end, an FC analysis in the EEG signals was chosen. We divided our FC analysis based on the distance between neural data into global- and local-scale analysis. The conditional TE metric was selected to assess global-scale connectivity. After implementing the existing

estimators of conditional TE on the EEG signals, we found that reliable estimation of large-scale connectivity has limitations and needs improvement. Regarding local-connectivity analysis, the COC metric was selected.

Following this introduction, we formed five research questions:

Q1: Can the combination of nonlinear prediction and transfer entropy improve the estimation of directed functional connectivity?

Q2: Can the change in functional connectivity induced by external stimuli be estimated using transfer entropy?

Q3: Can global-scale connectivity assessed by transfer entropy estimate the correlates of listening effort?

Q4: Can local-scale connectivity assessed by phase information estimate the correlates of listening effort?

Q5: Is local-scale connectivity assessed by phase information depending upon the noise reduction processing in hearing aids?

Except research question 3, where we found negative results (cf. Section 2.4), our investigations on the rest of the research questions led to positive results (See Papers A-D). The main contributions are as follows:

1. Global-scale connectivity estimator that significantly mitigates the effect of volume conduction.

2. Global-scale connectivity estimator that outperforms when the data is highly directly interacted.

3. Global-scale connectivity metric that can detect effects due to a particular stimuli.

4. New neural estimate of correlates of listening effort based on local connectivity assessed by phase information.

5. Providing further evidence that noise reduction processing help hearing aids users in their everyday natural listening environments.

Four papers that constitute the main body of this thesis are introduced below. In addition to those, one conference paper [101] was also published, which is not included in this thesis.

4.1 Paper A- Estimating Conditional Transfer Entropy in Time Series Using Mutual Information and Nonlinear Prediction

In this paper, we propose a new non-uniform embedding algorithm. Each variable is ranked based on its contribution to providing new information

and improving prediction accuracy. In an iterative process, the most informative subsets are then selected using a greedy approach. In cases where the highest ranked variable does not significantly increase the prediction accuracy over that obtained with the existing subsets, the algorithm terminates. The proposed algorithm demonstrated higher accuracy than state-of-the-art ones in a simulation study, especially when the data are highly directly interacted. Furthermore, the volume conduction effect in neuro-physiological time series like EEG can be considered as an instantaneous coupling. We showed that the proposed algorithm has lower false detection of directed dependencies compared to existing ones due to zero-lag coupling. Finally, we showed an application of the proposed algorithm in real-world intracranial EEG data recorded during seizures.

4.2 Paper B- A Stimuli-Relevant Directed Dependency Index for Time Series

In this paper, we proposed a metric that quantifies the effect a given time series (e.g., external stimuli) has on the coupling strength between other time series. This is accomplished by defining a directed dependency index based on the difference between two causally conditioned TEs. A lower bound for the proposed dependency index is then provided, and its efficient computation is demonstrated on synthetic data. Finally, we showed that the proposed index more accurately predicts the true dependencies in a simulation study than for traditional conditional TE.

4.3 Paper C- EEG Phase Synchrony Reflects SNR Levels During Continuous Speech-in-Noise Tasks

In this paper, we investigated how local-scale FC, i.e., functional connectivity within a localized region of the brain, is affected by two levels of SNR of the speech stimuli. A continuous speech in noise task was performed by 22 participants at two different SNRs (+3 dB and +8 dB). The COC metric estimated the local connectivity within eight regions of interest on EEG data. The results showed that the correlates of listening effort, as estimated by local connectivity in the parietal and frontal area, increased by increasing SNR value.

4.4 Paper D- Speech to Noise Ratio Improvement Induces Nonlinear Parietal Phase Synchrony in Hearing Aid Users

An assessment of NR processing (inactive, where NR was turned off, vs. active, where NR was turned on) effect on listening effort across two different background noise levels [+3 dB signal-to-noise ratio (SNR) and +8 dB SNR]

is the goal of this study. Toward this goal, a new estimate of the correlate of listening effort, local connectivity analysis, was used to evaluate listening effort. During continuous speech in noise (SiN) tasks, 22 HI participants fitted with hearing aids recorded their electroencephalograms (EEGs). A multivariate phase synchrony measure was used to quantify local connectivity within eight regions of interest (ROIs) and four conventional EEG bands. The results showed that the activation of NR in HAs affects the EEG local connectivity in parietal ROI at low SNR value, differently than high SNR value. The results also demonstrated that there was a nonlinear relationship between conditions of the listening task and phase synchrony in the parietal ROI. We contend that the effects of HAs in HI individuals under ecological listening conditions can be observed by studying the local connectivity as estimated by phase synchrony.

5 Conclusion and Future Directions

We studied the feasibility of FC analysis in EEG signals for estimating the correlates of listening effort. We were interested in changes in correlates of listening effort induced by the change in SNR value and NR schemes in HAs. We divided our FC analysis based on the distance between EEG electrodes recording neural data into global- and local-scale analysis.

Conditional TE which is able to assess the direction in addition to the strength of dependencies was selected to assess global-scale connectivity in EEG signals. Although estimation of correlates of listening effort using this analysis led to negative results, we could improve the methodology and estimators related to existing conditional TE metric and get higher performance in simulation data, particularly, when the simulation data were highly directly interacted and in the presence of volume conduction effect (instantaneous coupling).

Altogether, we got negative results regarding estimation of the correlates of the listening effort using global-scale connectivity. The possible reasons could be low accuracy in detection of the global-scale connectivity due to volume conduction effect and no guarantee that estimated connectivity is due to the change of acoustic stimuli. The effect of the volume conduction can be reduced by applying source localization techniques. Regarding the latter, the stimuli-relevant directed dependency index can improve the estimation of true connectivity. Applying source localization and stimuli-relevant directed dependency index to assess the global-scale connectivity for estimating correlates of listening effort are considered as future directions of this thesis.

The local-scale connectivity estimated using COC metric which is multivariate phase synchrony. This analysis showed that increase in SNR value during a continuous long speech in noise task leads to increase in EEG-based

phase synchrony. The same analysis demonstrated that activation of the NR processing in HAs non-linearly affects the local connectivity as estimated by phase synchrony. These results provided evidence that EEG-based phase synchrony quantified by COC within localized regions of brain contains informative features which can be used as an estimate of correlate of listening effort.

We also considered a more comprehensive study including more SNR values of the acoustic stimuli as the future works of this study, which can lead us to observe a complete inverted U-shape of the relationship of the estimate of the correlates of listening effort and listening conditions.

References

[1] B. T. Paul, J. Chen, T. Le, V. Lin, and A. Dimitrijevic, "Cortical alpha oscillations in cochlear implant users reflect subjective listening effort during speech-in-noise perception," *Plos one*, vol. 16, no. 7, p. e0254162, 2021.

[2] K. Miles, C. McMahon, I. Boisvert, R. Ibrahim, P. De Lissa, P. Graham, and B. Lyxell, "Objective assessment of listening effort: Coregistration of pupillometry and eeg," *Trends in hearing*, vol. 21, p. 2331216517706396, 2017.

[3] S. Sanei and J. A. Chambers, *EEG signal processing*. John Wiley & Sons, 2013.

[4] G. M. Bidelman, M. K. Davis, and M. H. Pridgen, "Brainstem-cortical functional connectivity for speech is differentially challenged by noise and reverberation," *Hearing Research*, vol. 367, pp. 149–160, 2018.

[5] T. Schreiber, "Measuring information transfer," *Physical review letters*, vol. 85, no. 2, p. 461, 2000.

[6] L. Fiedler, T. S. Ala, C. Graversen, E. Alickovic, T. Lunner, and D. Wendt, "Hearing aid noise reduction lowers the sustained listening effort during continuous speech in noise—a combined pupillometry and eeg study," *Ear and hearing*, vol. 42, no. 6, pp. 1590–1601, 2021.

[7] P. S. Baboukani, G. Azemi, B. Boashash, P. Colditz, and A. Omidvarnia, "A novel multivariate phase synchrony measure: Application to multichannel newborn eeg analysis," *Digital Signal Processing*, vol. 84, pp. 59–68, 2019.

[8] N. Lago and A. Cester, "Flexible and organic neural interfaces: a review," *Applied Sciences*, vol. 7, no. 12, p. 1292, 2017.

[9] H. Gray, *Anatomy of the human body*. Lea & Febiger, 1878, vol. 8.

[10] A. J. Bell and T. J. Sejnowski, "An information-maximization approach to blind separation and blind deconvolution," *Neural computation*, vol. 7, no. 6, pp. 1129–1159, 1995.

[11] A. Delorme and S. Makeig, "Eeglab: an open source toolbox for analysis of single-trial eeg dynamics including independent component analysis," *Journal of neuroscience methods*, vol. 134, no. 1, pp. 9–21, 2004.

References

[12] J. Obleser and S. A. Kotz, "Multiple brain signatures of integration in the comprehension of degraded speech," *Neuroimage*, vol. 55, no. 2, pp. 713–723, 2011.

[13] M. G. Wisniewski, A. C. Zakrzewski, D. R. Bell, and M. Wheeler, "Eeg power spectral dynamics associated with listening in adverse conditions," *Psychophysiology*, vol. 58, no. 9, p. e13877, 2021.

[14] G. Zhang, Y. Si, and J. Dang, "Revealing the dynamic brain connectivity from perception of speech sound to semantic processing by eeg," *Neuroscience*, vol. 415, pp. 70–76, 2019.

[15] H. Madsen and P. Thyregod, *Introduction to general and generalized linear models*. CRC Press, 2010.

[16] P. Babaeeghazvini, L. M. Rueda-Delgado, J. Gooijers, S. P. Swinnen, and A. Daffertshofer, "Brain structural and functional connectivity: A review of combined works of diffusion magnetic resonance imaging and electro-encephalography," *Frontiers in human neuroscience*, p. 585, 2021.

[17] Y. Zhu, J. Liu, T. Ristaniemi, and F. Cong, "Distinct patterns of functional connectivity during the comprehension of natural, narrative speech," *International journal of neural systems*, vol. 30, no. 03, p. 2050007, 2020.

[18] G. M. Bidelman, M. S. Mahmud, M. Yeasin, D. Shen, S. R. Arnott, and C. Alain, "Age-related hearing loss increases full-brain connectivity while reversing directed signaling within the dorsal–ventral pathway for speech," *Brain Structure and Function*, vol. 224, no. 8, pp. 2661–2676, 2019.

[19] R. G. James, N. Barnett, and J. P. Crutchfield, "Information flows? a critique of transfer entropies," *Physical review letters*, vol. 116, no. 23, p. 238701, 2016.

[20] J. T. Lizier and M. Prokopenko, "Differentiating information transfer and causal effect," *The European Physical Journal B*, vol. 73, no. 4, pp. 605–615, 2010.

[21] N. Wiener, "The theory of prediction," *Modern mathematics for engineers*, 1956.

[22] S. E. Kramer, T. S. Kapteyn, and T. Houtgast, "Occupational performance: Comparing normally-hearing and hearing-impaired employees using the amsterdam checklist for hearing and work: Desempeño laboral: Comparación de empleados con audición normal o alterada usando el listado amsterdam para audición y trabajo," *International journal of audiology*, vol. 45, no. 9, pp. 503–512, 2006.

[23] Y. Wang, G. Naylor, S. E. Kramer, A. A. Zekveld, D. Wendt, B. Ohlenforst, and T. Lunner, "Relations between self-reported daily-life fatigue, hearing status, and pupil dilation during a speech perception in noise task," *Ear and Hearing*, vol. 39, no. 3, p. 573, 2018.

[24] S. L. Mattys, M. H. Davis, A. R. Bradlow, and S. K. Scott, "Speech recognition in adverse conditions: A review," *Language and Cognitive Processes*, vol. 27, no. 7-8, pp. 953–978, 2012.

[25] A. Jaworski and D. Stephens, "Self-reports on silence as a face-saving strategy by people with hearing impairment," *International Journal of Applied Linguistics*, vol. 8, no. 1, pp. 61–80, 1998.

References

[26] B. E. Weinstein and I. M. Ventry, "Hearing impairment and social isolation in the elderly," *Journal of Speech, Language, and Hearing Research*, vol. 25, no. 4, pp. 593–599, 1982.

[27] R. Houben, M. van Doorn-Bierman, and W. A. Dreschler, "Using response time to speech as a measure for listening effort," *International journal of audiology*, vol. 52, no. 11, pp. 753–761, 2013.

[28] A. Sarampalis, S. Kalluri, B. Edwards, and E. Hafter, "Objective measures of listening effort: Effects of background noise and noise reduction," 2009.

[29] M. K. Pichora-Fuller, S. E. Kramer, M. A. Eckert, B. Edwards, B. W. Hornsby, L. E. Humes, U. Lemke, T. Lunner, M. Matthen, C. L. Mackersie *et al.*, "Hearing impairment and cognitive energy: The framework for understanding effortful listening (fuel)," *Ear and hearing*, vol. 37, pp. 5S–27S, 2016.

[30] J. E. Peelle, "Listening effort: How the cognitive consequences of acoustic challenge are reflected in brain and behavior," *Ear and hearing*, vol. 39, no. 2, p. 204, 2018.

[31] A. Winneke, M. De Vos, K. C. Wagener, P. Derleth, M. Latzel, J. Appell, and F. Wallhoff, "Listening effort and eeg as measures of performance of modern hearing aid algorithms," *Audiology Online*, vol. 24198, pp. 1–13, 2018.

[32] C. Bernarding, D. J. Strauss, R. Hannemann, H. Seidler, and F. I. Corona-Strauss, "Objective assessment of listening effort in the oscillatory eeg: Comparison of different hearing aid configurations," in *2014 36th Annual International Conference of the IEEE Engineering in Medicine and Biology Society*. IEEE, 2014, pp. 2653–2656.

[33] C. Bernarding, D. J. Strauss, R. Hannemann, H. Seidler, and F. I. Corona Strauss, "Neurodynamic evaluation of hearing aid features using eeg correlates of listening effort," *Cognitive neurodynamics*, vol. 11, no. 3, pp. 203–215, 2017.

[34] B. Ohlenforst, D. Wendt, S. E. Kramer, G. Naylor, A. A. Zekveld, and T. Lunner, "Impact of snr, masker type and noise reduction processing on sentence recognition performance and listening effort as indicated by the pupil dilation response," *Hearing research*, vol. 365, pp. 90–99, 2018.

[35] E. Alickovic, T. Lunner, D. Wendt, L. Fiedler, R. Hietkamp, E. H. N. Ng, and C. Graversen, "Neural representation enhanced for speech and reduced for background noise with a hearing aid noise reduction scheme during a selective attention task," *Frontiers in neuroscience*, vol. 14, p. 846, 2020.

[36] E. Alickovic, E. H. N. Ng, L. Fiedler, S. Santurette, H. Innes-Brown, and C. Graversen, "Effects of hearing aid noise reduction on early and late cortical representations of competing talkers in noise," *Frontiers in Neuroscience*, vol. 15:636060, 2021.

[37] M. Krueger, M. Schulte, T. Brand, and I. Holube, "Development of an adaptive scaling method for subjective listening effort," *The Journal of the Acoustical Society of America*, vol. 141, no. 6, pp. 4680–4693, 2017.

[38] S. G. Hart and L. E. Staveland, "Development of nasa-tlx (task load index): Results of empirical and theoretical research," in *Advances in psychology*. Elsevier, 1988, vol. 52, pp. 139–183.

References

[39] J.-P. Gagne, J. Besser, and U. Lemke, "Behavioral assessment of listening effort using a dual-task paradigm: A review," *Trends in hearing*, vol. 21, p. 2331216516687287, 2017.

[40] A. A. Zekveld, T. Koelewijn, and S. E. Kramer, "The pupil dilation response to auditory stimuli: Current state of knowledge," *Trends in hearing*, vol. 22, p. 2331216518777174, 2018.

[41] T. Seifi Ala, C. Graversen, D. Wendt, E. Alickovic, W. M. Whitmer, and T. Lunner, "An exploratory study of eeg alpha oscillation and pupil dilation in hearing-aid users during effortful listening to continuous speech," *Plos one*, vol. 15, no. 7, p. e0235782, 2020.

[42] P. Welch, "The use of fast fourier transform for the estimation of power spectra: a method based on time averaging over short, modified periodograms," *IEEE Transactions on audio and electroacoustics*, vol. 15, no. 2, pp. 70–73, 1967.

[43] A. Grossmann and J. Morlet, "Decomposition of hardy functions into square integrable wavelets of constant shape," *SIAM journal on mathematical analysis*, vol. 15, no. 4, pp. 723–736, 1984.

[44] B. Boashash, *Time-frequency signal analysis and processing: a comprehensive reference*. Academic press, 2015.

[45] L. Decruy, D. Lesenfants, J. Vanthornhout, and T. Francart, "Top-down modulation of neural envelope tracking: the interplay with behavioral, self-report and neural measures of listening effort," *European Journal of Neuroscience*, vol. 52, no. 5, pp. 3375–3393, 2020.

[46] E. B. Petersen, M. Wöstmann, J. Obleser, S. Stenfelt, and T. Lunner, "Hearing loss impacts neural alpha oscillations under adverse listening conditions," *Frontiers in psychology*, vol. 6, p. 177, 2015.

[47] J. Obleser, M. Wöstmann, N. Hellbernd, A. Wilsch, and B. Maess, "Adverse listening conditions and memory load drive a common alpha oscillatory network," *Journal of Neuroscience*, vol. 32, no. 36, pp. 12 376–12 383, 2012.

[48] M. G. Wisniewski, E. R. Thompson, and N. Iyer, "Theta-and alpha-power enhancements in the electroencephalogram as an auditory delayed match-to-sample task becomes impossibly difficult," *Psychophysiology*, vol. 54, no. 12, pp. 1916–1928, 2017.

[49] C. M. McMahon, I. Boisvert, P. de Lissa, L. Granger, R. Ibrahim, C. Y. Lo, K. Miles, and P. L. Graham, "Monitoring alpha oscillations and pupil dilation across a performance-intensity function," *Frontiers in Psychology*, vol. 7, 2016.

[50] M. Wostmann, S.-J. Lim, and J. Obleser, "The Human Neural Alpha Response to Speech is a Proxy of Attentional Control," *Cerebral Cortex*, vol. 27, no. 6, pp. 3307–3317, 2017.

[51] M. Wostmann, B. Herrmann, A. Wilsch, and J. Obleser, "Neural alpha dynamics in younger and older listeners reflect acoustic challenges and predictive benefits," *Journal of Neuroscience*, vol. 35, no. 4, pp. 1458–1467, 2015.

[52] P. Marsella, A. Scorpecci, G. Cartocci, S. Giannantonio, A. G. Maglione, I. Venuti, A. Brizi, and F. Babiloni, "Eeg activity as an objective measure of

cognitive load during effortful listening: A study on pediatric subjects with bilateral, asymmetric sensorineural hearing loss," *International Journal of Pediatric Otorhinolaryngology*, vol. 99, pp. 1–7, 2017.

[53] A. Dimitrijevic, M. L. Smith, D. S. Kadis, and D. R. Moore, "Cortical alpha oscillations predict speech intelligibility," *Frontiers in Human Neuroscience*, vol. 11, 2017.

[54] ——, "Neural indices of listening effort in noisy environments," *Scientific Reports*, vol. 9, no. 1, pp. 1–10, 2019.

[55] M. G. Wisniewski, N. Iyer, E. R. Thompson, and B. D. Simpson, "Sustained frontal midline theta enhancements during effortful listening track working memory demands," *Hearing Research*, vol. 358, pp. 37–41, 2018.

[56] M. G. Wisniewski, E. R. Thompson, N. Iyer, J. R. Estepp, M. N. Goder-Reiser, and S. C. Sullivan, "Frontal midline θ power as an index of listening effort," *Neuroreport*, vol. 26, no. 2, pp. 94–99, 2015.

[57] K. Mehta and J. Kliewer, "Directional and causal information flow in eeg for assessing perceived audio quality," *IEEE Transactions on Molecular, Biological and Multi-Scale Communications*, vol. 3, no. 3, pp. 150–165, 2017.

[58] C. Bernarding, F. I. Corona-Strauss, M. Latzel, and D. J. Strauss, "Auditory streaming and listening effort: an event related potential study," in *2010 Annual International Conference of the IEEE Engineering in Medicine and Biology*. IEEE, 2010, pp. 6817–6820.

[59] C. Bernarding, D. J. Strauss, R. Hannemann, H. Seidler, and F. I. Corona-Strauss, "Neural correlates of listening effort related factors: Influence of age and hearing impairment," *Brain research bulletin*, vol. 91, pp. 21–30, 2013.

[60] C. Bernarding, D. J. Strauss, R. Hannemann, and F. I. Corona-Strauss, "Quantification of listening effort correlates in the oscillatory eeg activity: a feasibility study," in *2012 Annual International Conference of the IEEE Engineering in Medicine and Biology Society*. IEEE, 2012, pp. 4615–4618.

[61] A. M. Bastos and J.-M. Schoffelen, "A tutorial review of functional connectivity analysis methods and their interpretational pitfalls," *Frontiers in systems neuroscience*, vol. 9, p. 175, 2016.

[62] J.-P. Lachaux, E. Rodriguez, J. Martinerie, and F. J. Varela, "Measuring phase synchrony in brain signals," *Human brain mapping*, vol. 8, no. 4, pp. 194–208, 1999.

[63] T. M. Cover, *Elements of information theory*. John Wiley & Sons, 1999.

[64] C. W. Granger, "Investigating causal relations by econometric models and cross-spectral methods," *Econometrica: journal of the Econometric Society*, pp. 424–438, 1969.

[65] H. E. Wang, C. G. Bénar, P. P. Quilichini, K. J. Friston, V. K. Jirsa, and C. Bernard, "A systematic framework for functional connectivity measures," *Frontiers in neuroscience*, vol. 8, p. 405, 2014.

References

[66] M. Lindner, R. Vicente, V. Priesemann, and M. Wibral, "Trentool: A matlab open source toolbox to analyse information flow in time series data with transfer entropy," *BMC neuroscience*, vol. 12, no. 1, pp. 1–22, 2011.

[67] L. Barnett and A. K. Seth, "The mvgc multivariate granger causality toolbox: a new approach to granger-causal inference," *Journal of neuroscience methods*, vol. 223, pp. 50–68, 2014.

[68] P.-O. Amblard and O. J. Michel, "On directed information theory and granger causality graphs," *Journal of computational neuroscience*, vol. 30, no. 1, pp. 7–16, 2011.

[69] ——, "Measuring information flow in networks of stochastic processes," *arXiv preprint*, 2009.

[70] H. Marko, "The bidirectional communication theory-a generalization of information theory," *IEEE Transactions on communications*, vol. 21, no. 12, pp. 1345–1351, 1973.

[71] J. Massey *et al.*, "Causality, feedback and directed information," in *Proc. Int. Symp. Inf. Theory Applic.(ISITA-90)*, 1990, pp. 303–305.

[72] C. J. Quinn, T. P. Coleman, N. Kiyavash, and N. G. Hatsopoulos, "Estimating the directed information to infer causal relationships in ensemble neural spike train recordings," *Journal of computational neuroscience*, vol. 30, no. 1, pp. 17–44, 2011.

[73] Z. Cai, C. L. Neveu, D. A. Baxter, J. H. Byrne, and B. Aazhang, "Inferring neuronal network functional connectivity with directed information," *Journal of neurophysiology*, vol. 118, no. 2, pp. 1055–1069, 2017.

[74] M. Lobier, F. Siebenhühner, S. Palva, and J. M. Palva, "Phase transfer entropy: a novel phase-based measure for directed connectivity in networks coupled by oscillatory interactions," *Neuroimage*, vol. 85, pp. 853–872, 2014.

[75] L. Faes, D. Marinazzo, A. Montalto, and G. Nollo, "Lag-specific transfer entropy as a tool to assess cardiovascular and cardiorespiratory information transfer," *IEEE Transactions on Biomedical Engineering*, vol. 61, no. 10, pp. 2556–2568, 2014.

[76] M. Wibral, N. Pampu, V. Priesemann, F. Siebenhühner, H. Seiwert, M. Lindner, J. T. Lizier, and R. Vicente, "Measuring information-transfer delays," *PloS one*, vol. 8, no. 2, p. e55809, 2013.

[77] L. Faes, G. Nollo, and A. Porta, "Compensated transfer entropy as a tool for reliably estimating information transfer in physiological time series," *Entropy*, vol. 15, no. 1, pp. 198–219, 2013.

[78] L. Faes, D. Kugiumtzis, G. Nollo, F. Jurysta, and D. Marinazzo, "Estimating the decomposition of predictive information in multivariate systems," *Physical Review E*, vol. 91, no. 3, p. 032904, 2015.

[79] L. Faes and A. Porta, "Conditional entropy-based evaluation of information dynamics in physiological systems," in *Directed information measures in neuroscience*. Springer, 2014, pp. 61–86.

References

[80] A. Montalto, L. Faes, and D. Marinazzo, "Mute: a matlab toolbox to compare established and novel estimators of the multivariate transfer entropy," *PloS one*, vol. 9, no. 10, p. e109462, 2014.

[81] J. Zhang, "Low-dimensional approximation searching strategy for transfer entropy from non-uniform embedding," *PloS one*, vol. 13, no. 3, p. e0194382, 2018.

[82] P. S. Baboukani, C. Graversen, E. Alickovic, and J. Østergaard, "Eeg phase synchrony reflects snr levels during continuous speech-in-noise tasks," in *2021 43rd Annual International Conference of the IEEE Engineering in Medicine & Biology Society (EMBC)*. IEEE, 2021, pp. 531–534.

[83] P. Shahsavari Baboukani, C. Graversen, E. Alickovic, and J. Østergaard, "Speech to noise ratio improvement induces nonlinear parietal phase synchrony in hearing aid users," *Frontiers in Neuroscience*, p. 1173.

[84] ——, "Estimating conditional transfer entropy in time series using mutual information and nonlinear prediction," *Entropy*, vol. 22, no. 10, p. 1124, 2020.

[85] L. Faes, D. Marinazzo, G. Nollo, and A. Porta, "An information-theoretic framework to map the spatiotemporal dynamics of the scalp electroencephalogram," *IEEE Transactions on Biomedical Engineering*, vol. 63, no. 12, pp. 2488–2496, 2016.

[86] E. Olejarczyk, L. Marzetti, V. Pizzella, and F. Zappasodi, "Comparison of connectivity analyses for resting state eeg data," *Journal of neural engineering*, vol. 14, no. 3, p. 036017, 2017.

[87] P. S. Baboukani, S. Theodoridis, and J. Østergaard, "A stimuli-relevant directed dependency index for time series," in *ICASSP 2022-2022 IEEE International Conference on Acoustics, Speech and Signal Processing (ICASSP)*. IEEE, 2022, pp. 5812–5816.

[88] P. S. Baboukani, S. Mohammadi, and G. Azemi, "Classifying single-trial eeg during motor imagery using a multivariate mutual information based phase synchrony measure," in *2017 24th National and 2nd International Iranian Conference on Biomedical Engineering (ICBME)*. IEEE, 2017, pp. 1–4.

[89] P. Zarjam, J. Epps, F. Chen, and N. H. Lovell, "Estimating cognitive workload using wavelet entropy-based features during an arithmetic task," *Computers in biology and medicine*, vol. 43, no. 12, pp. 2186–2195, 2013.

[90] M. Jalili, S. Lavoie, P. Deppen, R. Meuli, K. Q. Do, M. Cuénod, M. Hasler, O. De Feo, and M. G. Knyazeva, "Dysconnection topography in schizophrenia revealed with state-space analysis of eeg," *PloS one*, vol. 2, no. 10, p. e1059, 2007.

[91] M. Jalili, E. Barzegaran, and M. G. Knyazeva, "Synchronization of eeg: bivariate and multivariate measures," *IEEE Transactions on Neural Systems and Rehabilitation Engineering*, vol. 22, no. 2, pp. 212–221, 2013.

[92] M. Wöstmann, L. Fiedler, and J. Obleser, "Tracking the signal, cracking the code: Speech and speech comprehension in non-invasive human electrophysiology," *Language, Cognition and Neuroscience*, vol. 32, no. 7, pp. 855–869, 2017.

[93] M. Le Van Quyen, J. Foucher, J.-P. Lachaux, E. Rodriguez, A. Lutz, J. Martinerie, and F. J. Varela, "Comparison of hilbert transform and wavelet methods for the analysis of neuronal synchrony," *Journal of neuroscience methods*, vol. 111, no. 2, pp. 83–98, 2001.

References

[94] J. Sun and M. Small, "Unified framework for detecting phase synchronization in coupled time series," *Physical Review E*, vol. 80, no. 4, p. 046219, 2009.

[95] M. ROSENBLUM, P. TASS, J. Kurths, J. VOLKMANN, A. SCHNITZLER, and H.-J. FREUND, "Detection of phase locking from noisy data: application to magnetoencephalography," in *Chaos In Brain?* World Scientific, 2000, pp. 34–51.

[96] M. Palus, "Detecting phase synchronization in noisy systems," *Physics Letters A*, vol. 235, no. 4, pp. 341–351, 1997.

[97] R. T. Canolty, C. F. Cadieu, K. Koepsell, R. T. Knight, and J. M. Carmena, "Multivariate phase-amplitude cross-frequency coupling in neurophysiological signals," *IEEE Transactions on Biomedical Engineering*, vol. 59, no. 1, pp. 8–11, 2011.

[98] A. Omidvarnia, G. Azemi, P. B. Colditz, and B. Boashash, "A time–frequency based approach for generalized phase synchrony assessment in nonstationary multivariate signals," *Digital Signal Processing*, vol. 23, no. 3, pp. 780–790, 2013.

[99] K. Oshima, C. Carmeli, and M. Hasler, "State change detection using multivariate synchronization measure from physiological signals," *Journal of Signal Processing*, vol. 10, no. ARTICLE, pp. 223–226, 2006.

[100] M. Al-Khassaweneh, M. Villafane-Delgado, A. Y. Mutlu, and S. Aviyente, "A measure of multivariate phase synchrony using hyperdimensional geometry," *IEEE Transactions on Signal Processing*, vol. 64, no. 11, pp. 2774–2787, 2016.

[101] P. S. Baboukani, C. Graversen, and J. Østergaard, "Estimation of directed dependencies in time series using conditional mutual information and non-linear prediction," in *2020 28th European Signal Processing Conference (EUSIPCO)*. IEEE, 2021, pp. 2388–2392.

References

Part II

Papers

Paper A

Estimating Conditional Transfer Entropy in Time Series Using Mutual Information and Nonlinear Prediction

Payam Shahsavari Baboukani, Carina Graversen, Emina Alickovic and Jan Østergaard

Abstract

We propose a new estimator to measure directed dependencies in time series. The dimensionality of data is first reduced using a new non-uniform embedding technique, where the variables are ranked according to a weighted sum of the amount of new information and improvement of the prediction accuracy provided by the variables. Then, using a greedy approach, the most informative subsets are selected in an iterative way. The algorithm terminates, when the highest ranked variable is not able to significantly improve the accuracy of the prediction as compared to that obtained using the existing selected subsets. In a simulation study, we compare our estimator to existing state-of-the-art methods at different data lengths and directed dependencies strengths. It is demonstrated that the proposed estimator has a significantly higher accuracy than that of existing methods, especially for the difficult case, where the data are highly correlated and coupled. Moreover, we show its false detection of directed dependencies due to instantaneous couplings effect is lower than that of existing measures. We also show applicability of the proposed estimator on real intracranial electroencephalography data.

Keywords

directed dependency; conditional transfer entropy; non-uniform embedding; nonlinear prediction; mutual information

1   Introduction

Real-world interconnected technological systems such as car traffic and distributed power grids as well as biological systems such as the human brain can be represented in terms of complex dynamical systems that contain subsystems. Characterizing the subsystems and their interdependencies can help understanding the overall system behavior on a local and global scale. For example, different regions of the brain such as the cortices can be considered as subsystems. An assessment of the interaction between the cortices may provide insights into how the brain functions [1]. In order to identify the interactions, several time series analyses methods ranging from information theoretical to signal processing approaches have been proposed in the literature [2–4]. In particular, the directional methods have gained increasing attention because, unlike symmetric measures such as mutual information [2] and phase synchronization [3, 5], directional measures are generally able to assess the direction in addition to the strength of the interactions between subsystems [4, 6–9].

A popular approach used in the literature to assess directed dependencies uses Wiener's definition, which is based on the concept of prediction [10]. According to the Wiener's definition, if the prediction of the future value of a time series X_t from its own past values can be improved by incorporating

41

past values of another time series Y_t, then there are causal dependencies from Y_t to X_t [10]. Although the term "causal" was used in Wiener's definition, it has been shown that measures quantifying the Wiener's definition over- or under-estimate the causal effect in certain cases [11, 12]. In this paper, we use the term "directed dependencies" to refer to the property of time series or processes satisfying Wiener's definition.

Schreiber [4] formalized directed dependencies by using the concept of conditional mutual information (CMI) and proposed a new measure called transfer entropy (TE). TE does not depend on any model in its formulation, which makes this method able to assess both linear and nonlinear interactions [13]. Additionally, estimating TE by using the combination of data-efficient and model-free estimators like Kraskov–Stögbauer–Grassberger (KSG) [14], and uniform embedding state space reconstruction schemes [15, 16] has increased the popularity of TE. TE has been used for quantifying directed dependencies between joint processes in neuro-physiological [15, 16] and economical [17] applications.

As an example, assume that we are interested in measuring TE between processes which, for example, represent sensor measurement data from different regions of the brain, e.g., multi-channel electroencephalography (EEG) data. The recorded EEG data are spatially auto-correlated due to the phenomenon known as the volume conduction effect in neuro-physiological time series [18]. The spatial auto-correlation in such data can lead to overestimate in the estimated TE and eventually lead to false positives detection of TE. A possible approach to reduce such effect is to use a conditional version of TE [19, 20], which is referred to as conditional transfer entropy (CTE).

It is preferred to condition out all other variables in the network to ensure that the obtained CTE values reflect the true directed dependencies from an individual source to the target. On the other hand, the more variables we include in the conditioning, the higher the dimension of the problem becomes and the less accurate CTE estimators are, since we only have access to a limited number of realizations. Considering the fact that we are interested in estimating directed dependencies and we need to condition out past variables related to the remaining variables, the dimension of the conditioning process increases even more and reliable estimation of CTE in multi-channel data (such as EEG data) by using the classical uniform embedding technique is limited by the so-called "curse of dimensionality" problem [13, 21–23].

Non-uniform embedding (NUE) approaches reconstruct the past of the system with respect to a target variable by selecting the most relevant past and thereby decreases the dimensionality [13, 19, 22, 24–26]. The information theoretical-based NUE algorithm proposed in [13] is a greedy strategy, which uses CMI for selecting the most informative candidates. The authors in [13] showed a significant improvement of NUE over uniform embedding. The author in [21] stated that,

as the iteration of the NUE algorithm increases and more variables are selected, estimation of the higher dimensional CMI may become less accurate. The author in [21] then suggested to use a low-dimensional approximation (LA) of the CMI, and proposed a new NUE algorithm.

Adding more variables in the conditioning process decreases accuracy of the CTE estimator. The key problem is therefore how to decide whether we should include more variables, or terminate the algorithm. The existing NUE algorithms terminate if they fulfill a termination criterion defined by a bootstrap statistical-based test [13, 21, 23, 26]. The bootstrap test is used to approximate a confidence bound (or a critical value) by which the NUE algorithm is terminated. A higher bootstrap size, up to a threshold, generally leads to better approximation of the confidence bound [27], which can further influence the accuracy of the NUE algorithms. A bootstrap size of at most 100 is generally used in the literature [13, 19, 21, 22] due to computational complexity reasons. It has been shown that using an alternative to the bootstrap-based termination criterion can improve the accuracy and computational efficiency of the greedy algorithms [27, 28]. For example, the Akaike information criterion (AIC) and kernel density estimation (KDE)-based regression were proposed in [27] as an alternative to bootstrap methods for input variable selection techniques

In the present study, inspired by [27] and originated from our initial work in [29], we propose an alternative approach to the bootstrap-based termination criterion used in the existing NUE algorithms. Specifically, to aid in making the decision of whether to include a variable or terminate the algorithm, we propose to measure the relevance of the new candidate variable by assessing the effect of it on the accuracy of the nonlinear prediction of the target variable. The nonlinear prediction is based on nearest neighbor (NN)-based regression [30]. We show that it is also advantageous to use the nonlinear prediction strategy for selecting the pool of candidates in the first place. We then introduce a new NUE algorithm which uses a weighted combination of CMI and the accuracy of the nonlinear prediction for selection of candidates and present the new termination criterion for stopping the algorithm. Finally, we demonstrate that our proposed NUE procedure is more accurate than the existing NUE algorithms on both synthetic and real-world data.

The effect of instantaneous coupling (IC) on the NUE algorithms will also be investigated. IC can occur due to simultaneous (zero lag) information sharing like source mixing as a result of volume conduction in EEG signals [19, 31] and may lead to spurious detection of TE or CTE.

The remainder of this paper is structured as follows. In Section 1, the necessary background on CTE and the existing NUE algorithms will be briefly reviewed. Then, the proposed termination criterion and NUE procedure will be introduced in Sections 2 and 3, respectively. This is followed by the de-

scription of our simulation study in Section 4, which is based on Henon maps and nonlinear autoregressive (AR) models. The results of applying the proposed NUE algorithm on real EEG data will be reported in Section 5. Section 6 will discuss the results. The same section will also conclude the paper.

sectionBackground

1.1 Conditional Transfer Entropy

Let us consider a complex system which consists of L interacting subsystems. We assume that we are interested in assessing the directed dependencies between subsystems $\mathcal{X}$ and $\mathcal{Y}$. Let stationary stochastic processes $X = (X_1, X_2, \ldots, X_N)$ and $Y = (Y_1, Y_2, \ldots, Y_N)$ describe the state visited by the subsystem $\mathcal{X}$ and $\mathcal{Y}$ over time, respectively. We denote $X_n \in \mathbb{R}$ and $Y_n \in \mathbb{R}$ as stochastic variables obtained by sampling the processes X and Y at the present time n, respectively. Furthermore, we denote the past of X up until X_{n-1} by a random vector $X_n^- = [X_{n-1}, X_{n-2}, \ldots]$. TE from X to Y is then defined as [4].

$$\text{TE}(X \to Y) \triangleq I(Y_n; X_n^- \mid Y_n^-), \tag{A.1}$$

where $I(\,.\,;\,.\mid.)$ is CMI. However, in a complex network, it is not guaranteed that (A.1) only describes the directed dependencies from X to Y. For example, there could be a third process, say Z, through which shared information is mediated to X and Y. In this case, the shared information will lead to an increase in TE. To reduce the effect of common information being shared through other process, it has been suggested to use CTE [13, 19]. Let us consider the $L = 6$ nodes network in Figure A.1, where we are interested in assessing the directed dependencies from node $\mathcal{X}$ to $\mathcal{Y}$ and which is not due to indirect paths through the remaining nodes $\mathcal{Z} = \{\mathcal{Z}^1, \mathcal{Z}^2, \mathcal{Z}^3, \mathcal{Z}^4\}$. We denote $Z^i = (Z_1^i, Z_2^i, \ldots, Z_N^i)$ as a stochastic process describes the state visited by $\mathcal{Z}^i$ and $\mathbf{Z} = [Z^1, Z^2, \ldots, Z^4]$ as a 4-variate stochastic process which describes state visited by $\mathcal{Z}$ over time. CTE from an individual source X to the target Y excluding information from $\mathbf{Z}$ is then defined as

$$\text{CTE}(X \to Y|\mathbf{Z}) \triangleq I(Y_n; X_n^- \mid Y_n^-, \mathbf{Z}_n^-), \tag{A.2}$$

where $\mathbf{Z}_n^- = [\mathbf{Z}_{n-1}, \mathbf{Z}_{n-2}, \ldots]$ denotes the past of up $\mathbf{Z}$ until but not including $\mathbf{Z}_n$.

1.2 Existing Non-Uniform Embedding Algorithm

Prior to estimating CTE in (A.2), it is mandatory to approximate the possibly infinite-dimensional random vectors which represent the past of the processes. Let us denote the approximated past vector variable X_n^- by V_n^X.
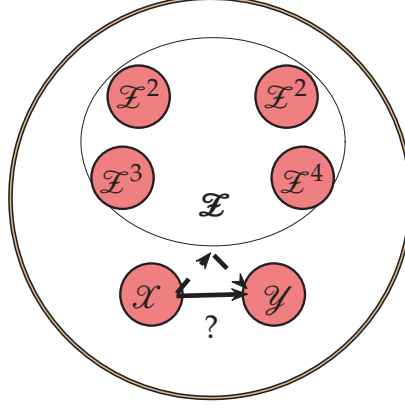
Fig. A.1: An example of $L = 6$ nodes network where indirect paths through the remaining channels $\mathcal{Z}$ may cause a falsely (dashed line) detected directed dependency (solid line) from X to Y.

The same notation applies to V_n^Y and V_n^Z. The basic idea behind reconstructing the past of the processes X, Y, and $\mathbf{Z}$ by assuming Y as the target process is to form a low dimensional embedding vector $\mathcal{S}$ comprising the most informative past variables about the present state of the target Y. Traditionally, the past of the system is reconstructed by using the uniform embedding scheme in which each component of $\mathcal{S}$ is approximated separately. For example, V_n^Y is approximated as $V_n^Y = [Y_{n-m}, Y_{n-2m}, \ldots, Y_{n-dm}]$, where m and d are the embedding delay and embedding dimension, respectively [13, 15]. Then, the V_n^X and V_n^Z are estimated using the same approach and the final embedding vector $\mathcal{S} = [V_n^X, V_n^Y, V_n^Z]$ is formed and utilized to estimated CTE in (A.2).

The uniform embedding scheme may lead to selection of redundant past variables and ignore relevant variables, as a result decrease the accuracy of the CTE estimation. This can limit applications in high dimensional data [13, 21, 23]. Alternatively, the NUE schemes try to select the most relevant and least redundant past variables and form a new embedding vector [13, 21, 23].

Bootstrap-Based Non-Uniform Embedding Algorithm

The NUE algorithm, as suggested in [13], can be described as follows:

1. Choose embedding delay d and embedding dimension m and construct the candidate set $\mathscr{C} = [X_{n-m}, \ldots, X_{n-md}, Y_{n-m}, ..Y_{n-md}, \mathbf{Z}_{n-m}, \ldots, \mathbf{Z}_{n-md}]$.

2. Initialize the algorithms by an empty set of the selected candidates $\mathcal{S}_n^0 = \varnothing$.

3. Run a forward search to find the most informative candidate among the candidate set $\mathscr{C}$. This can be achieved by quantifying the amount of

information that each candidate W_n has about Y_n which is not provided by the selected candidates from the last iteration $\mathscr{S}_n^{k-1}$. To formalize this, at each iteration $k \geq 1$, select the candidate W_n^k, such that CMI between W_n and Y_n conditioned on $\mathscr{S}_n^{k-1}$ is maximized

$$W_n^k = \underset{W_n \in \mathscr{C} \setminus \mathscr{S}_n^{k-1}}{\text{argmax}} \; \mathrm{I}\left(Y_n; W_n \mid \mathscr{S}_n^{k-1}\right), \tag{A.3}$$

where $\mathscr{S}_n^{k-1} = \bigcup\limits_{i=0}^{k-1} W_n^i$ denotes the set of the selected candidates up till iteration $k-1$ and $\mathscr{C} \setminus \mathscr{S}_n^{k-1}$ denotes the remaining candidates in $\mathscr{C}$. We estimate the CMI given in (A.3) by using the KSG approach [13, 14, 32] in this study (cf. Appendix A.1).

4. Stop the iteration if the termination criterion is fulfilled and return $\mathscr{S}_n^{k-1}$ as the desired embedding vector.

The flow chart of the NUE algorithm is shown in Figure A.2. After obtaining the embedding vector $\mathscr{S}_n^{k-1}$, CTE is estimated by using (A.2) in which case $[X_n^-, Y_n^-, \mathbf{Z}_n^-]$ is replaced by $\mathscr{S}_n^{k-1}$ and $[Y_n^-, \mathbf{Z}_n^-]$ is replaced by $\mathscr{S}_n^{k-1}$ excluding the past of X_n. CTE is written as the sum/difference of four differential entropies and is estimated by using KSG approach (In this paper, we use the KSG approach to estimate CTE and CMI. The KSG estimator is designed to estimates differential entropies. Therefore, we assumed that variables used in this paper are continuous.) [13, 14, 32] (cf. Appendix A.1).

The existing NUE algorithm proposed in [13] utilizes a bootstrap-based termination criterion. The goal of the bootstrap test in the NUE algorithm is to estimate an upper bound on the CMI between independently selected candidate $\widehat{W_n^k}$ and the target variable $\widehat{Y_n}$ given $\mathscr{S}_n^{k-1}$, $I(\widehat{W_n^k}; \widehat{Y_n} | \mathscr{S}_n^{k-1})$. The estimation is accomplished by drawing 100 independent randomly shuffled realizations of Y_n and W_n^k, estimating the CMI between the randomized W_n^k and the randomized Y_n given the original $\mathscr{S}_n^{k-1}$, and then finding the 95th percentile I^{95} of the generated distribution. The obtained value I^{95} can be used as a critical value (at 5% confidence level) of $I(W_n^k; Y_n | \mathscr{S}_n^{k-1})$ so that if $I(W_n^k; Y_n | \mathscr{S}_n^{k-1}) > I^{95}$ then the candidate is included in the embedding vector and the algorithm continues to search for more candidates in iteration $k+1$. Otherwise, the termination criterion is fulfilled and the algorithm is ended and $\mathscr{S}_n^{k-1}$ is returned as the embedding vector.

Low-Dimensional Approximation-Based Non-Uniform Embedding Algorithm

The LA-based strategy follows the same flow chart as the existing NUE algorithm, shown in Figure A.2, except that the CMI in (A.3) is substituted

by its LA [21]. It is suggested in [21, 23] that using LA of the CMI in (A.3) can increase the accuracy of estimation of the CMI and may outperform the accuracy of the NUE algorithm. The author in [21] proposed two LA alternatives to the CMI and concluded based on a simulation study that the LA of the CMI used in this study for the sake of comparison with our proposed NUE algorithm, outperforms another LA of the CMI. The criterion for finding the most informative candidates (i.e., Equation (A.3)) in the LA-based NUE algorithm is then given by

$$W_n^k = \underset{W_n \in \mathscr{C} \setminus \mathscr{S}_n^{k-1}}{\operatorname{argmax}} \{I(W_n; Y_n) - \frac{2}{|\mathscr{S}_n^{k-1}|} \sum_{W_j \in \mathscr{S}_n^{k-1}} I(W_n; W_j) + \frac{2}{|\mathscr{S}_n^{k-1}|} \sum_{W_j \in \mathscr{S}_n^{k-1}} I(W_n; W_j | Y_n)\},$$

(A.4)

where $|.|$ denotes the cardinality of a set. The mutual information and CMI are estimated using the KSG approach [13, 14, 32] (cf. Appendix A.1). The LA-based NUE algorithm also uses the bootstrap-based termination criterion. It should be noted that the LA of the CMI (i.e., Equation (A.4)) is used to estimate I^{95}.

Akaike Information Criterion-Based Non-Uniform Embedding Algorithm

AIC is used to assess the trade-off between accuracy and complexity of a model. It was adapted to quantify the trade-off between accuracy and complexity of a KDE-based prediction as an alternative to the bootstrap termination criterion in an input variable selection approach in [27, 28]. AIC can also be adapted to act as a termination criterion for stopping the NUE algorithm. Therefore, an AIC-based NUE algorithm could follow the same flow chart as the existing NUE algorithm, shown in Figure A.2, except that the the termination criterion will be replaced with the AIC-based termination criterion as is described below.

After selecting the most informative candidate W_n^k by using (A.3), the target variable Y_n is predicted given $\mathscr{U}_n^k = [W_n^k, \mathscr{S}_n^{k-1}] \in \mathbb{R}^k$, by using KDE-based prediction (cf. Appendix A.2). Let $y_n = (y_n(1), y_n(1), \dots, y_n(N))$ be N realizations of Y_n. The AIC at iteration k is then given as:

$$AIC_k = N \log \left(\frac{1}{N} \sum_{i=1}^{N} (y_n(i) - \widehat{y}_n(i|\mathscr{U}_n^k))^2 \right) + 2p,$$

(A.5)

where the ith realization of Y_n is denoted by $y_n(i)$ and $\widehat{y}_n(i|\mathscr{U}_n)$ is an estimator for the prediction of $y_n(i)$ given $\mathscr{U}_n$. The total number of realization of Y_n is N and p is the measure of complexity and for KDE-based regression, it is given as [27, 33]:

$$p = \sum_{n=1}^{N} \frac{K_h(u_n^k(i), u_n^k(i))}{\sum_{j=1}^{N} K_h(u_n^k(i), u_n^k(j))},$$

(A.6)
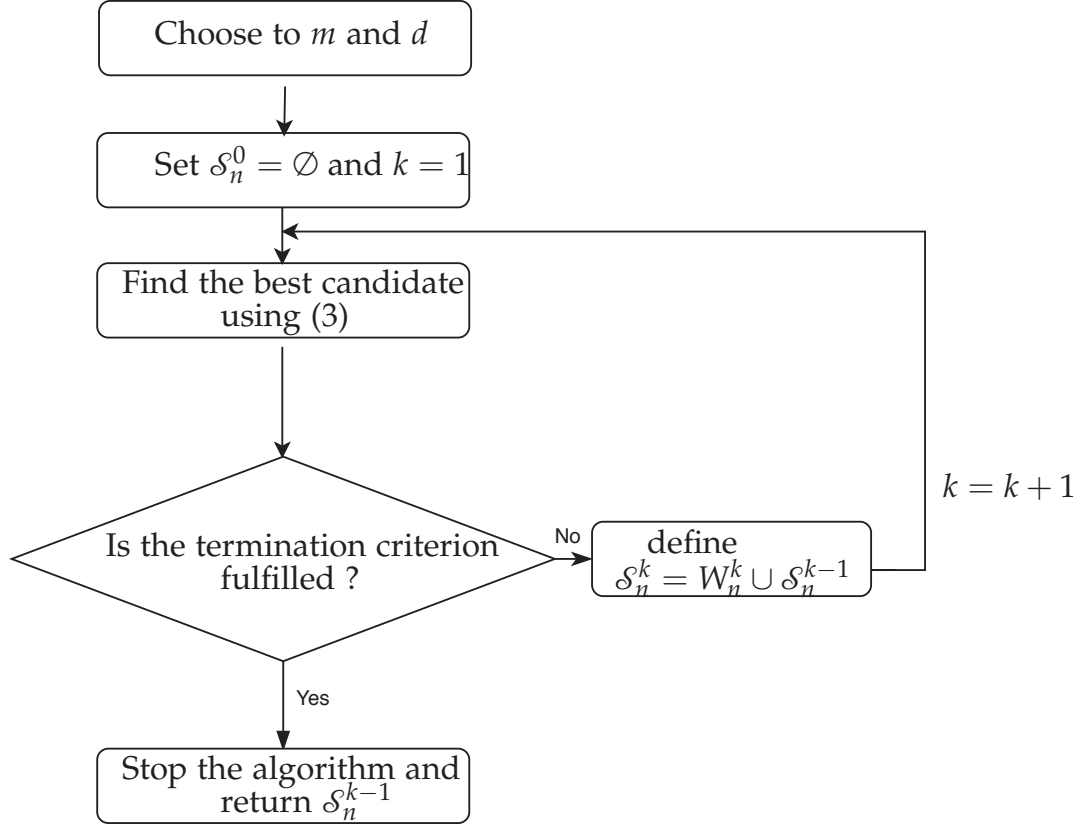
Fig. A.2: The flow chart of the NUE algorithm.

where $u_n^k(i)$ is i^{th} realization of $\mathcal{U}_n^k$ (see equation (7) for more details) and K_h is a Gaussian kernel with Mahalonobis distance and Gaussian reference kernel bandwidth (cf. Appendix A.2). During the NUE algorithm, if $AIC_k > AIC_{k-1}$ then, W_n^k is included in the embedding vector $\mathcal{S}_n^k$. Otherwise, the algorithm stops and $\mathcal{S}_n^{k-1}$ will be considered as the desired reconstructed past state of the system.

2 Proposed Termination Criterion

In this section, inspired by [27], we present a new termination criterion. Our proposed criterion is based on nonlinear prediction of the target variable, similar to the AIC approach. We modify NN-based regression [30] in order to be able to assess the effect of the selected candidate W_n^k on the accuracy of the prediction of Y_n.

We are interested in nonlinear prediction of the random variable Y_n given the random vector $\mathcal{U}_n^k = [W_n^k, \mathcal{S}_n^{k-1}] \in \mathbb{R}^k$. We denote the set of N realizations of W_n^k by $w_n^k = (w_n^k(1), w_n^k(2) \ldots, w_n^k(N))$ and set of N realizations of $\mathcal{U}_n^k$ be

the $N \times k$ matrix

$$u_n^k = \begin{bmatrix} w_n^k(1) & w_n^{k-1}(1) & \cdots & w_n^1(1) \\ w_n^k(2) & w_n^{k-1}(2) & \cdots & w_n^1(2) \\ \vdots & \vdots & \ddots & \vdots \\ w_n^k(N) & w_n^{k-1}(N) & \cdots & w_n^1(N) \end{bmatrix}. \tag{A.7}$$

The ith row of the matrix u_n^k is a realization of the random vector $\mathcal{U}_n^k$. Let $t(i)$ be the set of indices of the T nearest neighbors of the ith realization of $\mathcal{U}_n^k$. For example, $t(i) = \{3,7,9\}$ shows that 3rd, 7th, and 9th rows of u_n^k are the $T = 3$ nearest neighbors of its ith row. The Euclidean distance is used as the distance metric for finding the nearest neighbors in the NN-based prediction. The prediction of the ith realization of Y_n (i.e., $y_n(i)$) given $\mathcal{U}_n^k$ is then calculated as an average of the realizations of Y_n whose indices are specified by the neighbor search in u_n^k. The average of the y-values having the same conditioned past is not an optimal estimator. However, it is simple, works well in the cases that we have considered, and has also been used in previous work on non-conditional NN-based prediction. The $\widehat{y}_n(i|\mathcal{U}_n^k)$ is given as:

$$\widehat{y}_n(i|\mathcal{U}_n^k) \triangleq \frac{1}{T} \sum_{v \in t(i)} y_n(v). \tag{A.8}$$

For example, if $t(i) = \{3,7,9\}$ then $\widehat{y}(i|\mathcal{U}_n^k)$ is equal to the mean of $\{y_n(3), y_n(7), y_n(9)\}$. The residual $r(i|\mathcal{U}_n^k)$ can be computed as:

$$r(i|\mathcal{U}_n^k) = y_n(i) - \widehat{y}_n(i|\mathcal{U}_n^k). \tag{A.9}$$

In the NUE algorithm, the most informative candidate at iteration k, W_n^k, will be included in the embedding vector, if it significantly improves the accuracy of the prediction of the target variable Y_n given $\mathcal{U}_n^k$ compared to the prediction accuracy from the iteration $k-1$. The accuracy of the prediction can be calculated as the mean of the squared prediction residual (MSR):

$$\text{MSR}(Y_n \mid \mathcal{U}_n^k) = \frac{1}{N} \sum_{i=1}^{N} r(i|\mathcal{U}_n^k)^2, \tag{A.10}$$

where the smaller MSR, the better prediction.

We first assume that the NUE algorithm contains at least $k = 2$ iterations and the termination test is performed from the second iteration. Accordingly, at each iteration $k \geq 2$, if $\text{MSR}(Y_n|\mathcal{U}_n^{k-1}) - \text{MSR}(Y_n|\mathcal{U}_n^k) > \gamma$, then W_n^k is included in $\mathcal{S}_n^k$ and the algorithm proceeds to search for more candidates at iteration $k+1$. Otherwise, the algorithm ends and $\mathcal{S}_n^{k-1}$ is considered as the desired embedding vector. The non-negative parameter γ defines how

much the accuracy of the prediction needs to be improved before a variable is selected. Basically, by increasing the non-negative parameter γ which we have introduced, our proposed algorithm terminates sooner, and hence less variables are selected. In other words, the parameter γ controls the balance between true positives and true negatives, which can be useful, for example, in taking care of the confounder effects like IC. We will show in Section 5.2.2 that, by choosing a proper γ value, the number of true negatives significantly increases while the number of true positives does not decrease significantly in data in which the IC may cause spurious detection of directed dependencies.

3 Proposed Non-Uniform Embedding Algorithm

Our proposed NUE algorithm (referred to as MSR-based) uses a weighted combination of the CMI and MSR for selecting the most informative candidate and our proposed termination criterion for ending the algorithm. The details of the proposed NUE algorithm are as follows:

1. Choose γ, λ, embedding delay d and embedding dimension m and construct the candidate set $\mathscr{C} = [X_{n-m}, \ldots, X_{n-md}, Y_{n-m}, ..Y_{n-md}, \mathbf{Z}_{n-m}, \ldots, \mathbf{Z}_{n-md}]$.

2. Initialize by setting $\mathscr{S}_n^0 = \varnothing$,

3. At first iteration $k = 1$, find the first most relevant candidate W_n^1 by using a weighted combination of MSR and mutual information as:
$$W_n^1 = \underset{W_n \in \mathscr{C}}{\operatorname{argmax}} \left[(1 - \lambda) \, \mathrm{I}\,(Y_n; W_n) - \lambda \, \mathrm{MSR}(Y_n \mid W_n) \right], \qquad \text{(A.11)}$$

   where $0 \leq \lambda \leq 1$ is the weight. Then, set $\mathscr{S}_n^1 = [W_n^1]$.

4. At each iteration $k \geq 2$, run a search procedure to select the candidate which leads to the highest amount of new information about target variable Y_n and the best prediction of Y_n given the random vector $\mathscr{U}_n^k = [W_n, \mathscr{S}_n^{k-1}]$. It can be formalized by:

$$W_n^k = \underset{W_n \in \mathscr{C} \setminus \mathscr{S}_n^{k-1}}{\operatorname{argmax}} \left[(1 - \lambda) \, \mathrm{I}\left(Y_n; W_n \mid \mathscr{S}_n^{k-1}\right) - \lambda \, \mathrm{MSR}\left(Y_n \mid \mathscr{U}_n^k\right) \right],$$
$$\text{(A.12)}$$

   where $\mathscr{S}_n^{k-1} = \bigcup_{i=0}^{k-1} W_n^i$ denotes the set of selected candidates up till iteration $k-1$ and $\mathscr{C} \setminus \mathscr{S}_n^{k-1}$ refers to all elements of $\mathscr{C}$ except the elements of $\mathscr{S}_n^{k-1}$. Similar to the existing NUE algorithms, mutual information and CMI are estimated using the KSG approach [13, 14, 32] (cf. Appendix A.1).

Fig. A.3: The flow chart of our proposed NUE algorithm.

5. Include the candidate W_n^k in the embedding vector $\mathcal{S}_n^k$ if $\mathrm{MSR}(Y_n|\mathcal{U}_n^{k-1}) - \mathrm{MSR}(Y_n|\mathcal{U}_n^k) > \gamma$ and continue the algorithm to find more candidate. Otherwise, terminate the algorithm and return $\mathcal{S}_n^{k-1}$ as the desired embedding vector.

The flow chart of the proposed algorithm is shown in Figure A.3. CTE is then estimated by replacing $[X_n^-, Y_n^-, \mathbf{Z}_n^-]$ and $[Y_n^-, \mathbf{Z}_n^-]$ with $\mathcal{S}_n^{k-1}$ and $\mathcal{S}_n^{k-1}$ excluding the past of X_n, respectively. The CTE is finally estimated using the KSG approach [13, 14, 32] (cf. Appendix A.1).

4 Simulation Study

In this section, we use simulated data in order to compare the performance of our proposed NUE algorithm with the existing algorithms described in Section 1.2. We investigate the effect of the data length, strength of directed dependency and instantaneous coupling effect on the NUE algorithms. The execution time of the NUE algorithms are also investigated. The main reason

for using simulated data are to be able to obtain well-defined ground truth. Therefore, it is possible to compare the NUE algorithms by computing their accuracies. The termination criterion of the NUE algorithms is also utilized for testing the significance of the estimated CTE in the simulation study: if the embedding vector $\mathcal{S}_n$ of the target variable Y_n does not include any lagged component of the node $\mathcal{X}$, then CTE from $\mathcal{X}$ to $\mathcal{Y}$ is zero and, otherwise its CTE is positive. The results are used to calculate true positive (TP), i.e., number of truly detected directed coupled nodes, true negative (TN), false positive (FP), and false negative (FN). The accuracy (ACC), true positive rate (TPR), and true negative rate (TPR) of the NUE algorithms are then defined as:

$$
\begin{aligned}
\text{ACC} &= 100 \times \tfrac{TP+TN}{TP+TN+FP+FN} \\
\text{TNR} &= 100 \times \tfrac{TN}{TN+FP} \\
\text{TPR} &= 100 \times \tfrac{TP}{TP+FN}.
\end{aligned}
\tag{A.13}
$$

The TPR shows the ability of NUE algorithms to include the candidates in the embedding vector related to correctly coupled nodes, and TNR represents the ability to exclude the candidates related to uncoupled nodes. The ACC, TPR and TNR are computed as an average over 100 generated realizations because the simulated data depends on the random initial condition. The embedding delay m and dimension d are chosen as 1 and 5 samples, respectively. For estimation of the CMI and MSR, $T = 10$ nearest neighbors are considered.

4.1   Henon Map Model

The Henon map model has been frequently utilized in the literature to generate multivariate data with a controlled amount of directed interaction [13, 21, 22]. A 5 nodes Henon map can be defined as [13, 21, 22]:

$$
\begin{aligned}
Y_{l,n} &= 1.4 - Y_{l,n-1}^2 + 0.3 Y_{l,n-2}, \quad \text{for } l = 1, 5 \\
Y_{l,n} &= 1.4 - [0.5Q(Y_{l-1,n-1} + Y_{l+1,n-1}) + (1 - Q)Y_{l,n-1}]^2 + 0.3 Y_{l,n-2}, \\
&\quad \text{for } l = 2, 3, 4,
\end{aligned}
\tag{A.14}
$$

where Q is the coupling strength and it varies between 0.2 to 0.8 in this study; it is guaranteed that the complete synchronization between any pair nodes is avoided [34]. The first and last nodes (Y_1 and Y_5) depend only on their own past (first row of (A.14)) and therefore they do not depend on other nodes. On the other hand, nodes $l = 2, 3, 4$ depend on the past of nodes Y_{l-1} and Y_{l+1}. Consequently, there are nonlinear directed dependencies with strength Q from nodes Y_{l-1} and Y_{l+1} to node Y_l for $l = 2, 3, 4$ (second row of
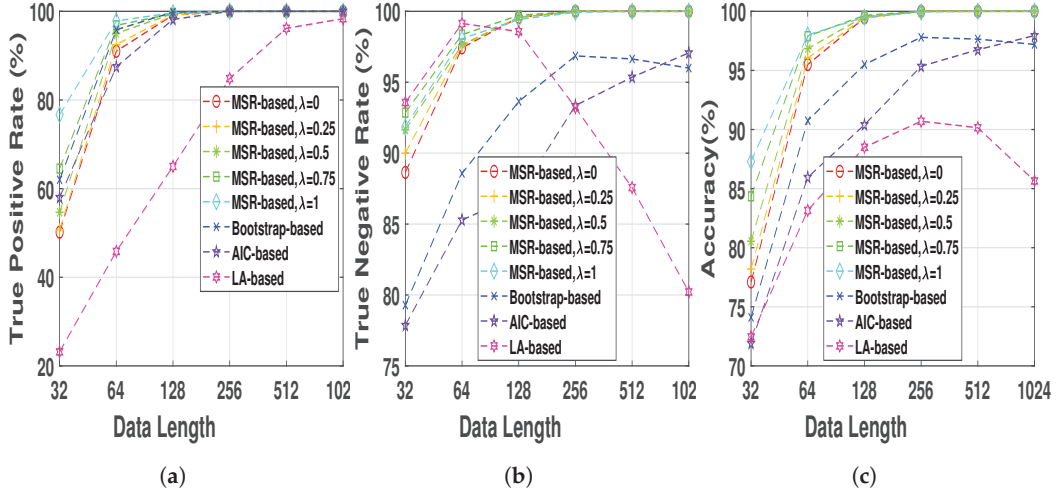
Fig. A.4: (a) true positive rates, (b) true negative rates and (c) accuracies of MSR-based, bootstrap-based, AIC-based, and LA-based NUE algorithms for the Henon map model at moderate fixed coupling strength $Q = 0.6$ and data length ranging from 32 to 1024. The results are shown as an average over 100 realizations.

(A.14)). The aforementioned connectivity is considered as the ground truth when comparing the performance of the NUE algorithms.

Data Length Effect

Henon map data sequences were generated at a fixed normal strength $Q = 0.6$ and different lengths, $N = 2^h, h = 5, 6, \ldots, 10$, in order to evaluate the effect of the data length on the performance of the NUE algorithms. The proposed NUE algorithm were used with five different weights, $\lambda = 0, 0.25, 0.5, 0.75, 1$, to demonstrate the effect of the weight. According to the fact that in this simulation there is no unobserved confounder effect like IC, we set the parameter $\gamma = 0$. Figure A.4 shows TPRs, TNRs and accuracies of the MSR-based NUE algorithm with five different λ's. In addition, shown in the figure, are the performances of the existing NUE algorithms. As Figure A.4c demonstrates, the accuracy of our proposed NUE algorithm (for any λ) increases as the data length increases up to 256 samples where the accuracy is nearly 100%. The proposed algorithm with higher λ attains better performance at data length under 128 samples. Figure A.4a,b show that the improvement of the accuracy by changing λ is mostly due to the better TPRs. As we can see in Figure A.4b, TNRs of bootstrap-based and LA-based algorithms decreases for data lengths greater than 256 and 64, respectively. The accuracy, TPR and TNR of the AIC-based algorithm increases by increasing the data length. Overall, the proposed algorithm with $\lambda = 1$ attains the greatest accuracy and the LA-based algorithm has the worst accuracy for all data lengths.

Fig. A.5: (**a**) true positive rates, (**b**) true negative rates and (**c**) accuracies of MSR-based, bootstrap-based, AIC-based, and LA-based NUE algorithms for the Henon map model at fixed data length $N = 512$ and coupling strength ranging from 0.2 to 0.8. The results are shown as an average over 100 realizations.

Coupling Strength Effect

The Henon map model at 512 data length was generated with different coupling strengths ranging from 0.2 to 0.8 in step of 0.2 in order to evaluate the NUE algorithms as a function of the strength of the directed dependencies. As Figure A.5b shows TNRs of the MSR-based algorithm (for any λ) is almost 100 % while the TNRs of the existing NUE algorithms tend to decrease as the strength of the directed dependency increase, which also causes a decrease in the accuracy. TPRs of the NUE algorithms are nearly equal except that at very low coupling strength the bootstrap-based algorithm has higher TPR. Changing λ at $Q = 0.2$ leads to slightly better TPR and accuracy. Overall, our proposed MSR-based algorithm has better accuracy compared to that of the existing NUE algorithms, except for $Q = 0.2$ where bootstrap-based algorithms yields better performance.

Execution Time

In this section the execution time of the proposed MSR-based algorithm with $\lambda = 1$ and $\lambda = 0$ (at fixed $\gamma = 0$) is compared with that of the existing NUE algorithms. The Henon Map data at length 512 samples and coupling strength $Q = 0.6$ was generated and execution time of the NUE algorithms are reported as an average over 100 realizations. The execution time was calculated in a single block-wise code where each NUE algorithms has a block. The function *tic* of MATLAB was set before each block and the function *toc* was used to calculate the execution time of the blocks related to the NUE algorithms. The code was run by a Intel(R) core(TM) i7-7600 CPU@2.10 GHz.

We use the ITS toolbox (available at http://www.lucafaes.net/its.html) for implementation of bootstrap-based NUE algorithm. The ITS toolbox was also modified for implementation of the LA-based algorithm by using a MATLAB code provided in [21]. We also modified ITS toolbox in order to implement the AIC-based and MSR-based NUE algorithms. The results are reported in Table A.1. In addition to execution time, the total number of iterations k that the algorithms were performed before they terminated, are reported.

Table A.1: The execution time and and total iterations before termination of the proposed MSR-based with $\lambda = 0, 1$ (at fixed $\gamma = 0$) as well as existing NUE algorithms for the Henon map data at data length 512. The results are reported as an average over 100 realizations.

NUE Algorithm	Bootstrap-Based	LA-Based	AIC-Based	MSR-Based, $\lambda = 1$	MSR-Based, $\lambda = 0$
Execution Time (second)	40.59	117.23	11.29	2.26	5.34
Total Number of Iterations	19.18	16.94	24.08	16.19	16.64

As Table A.1 indicates, the execution time of MSR-based with the known parameters $\lambda = 1$ and $\lambda = 0$, and AIC-based NUE algorithms are significantly less than that of the bootstrap-based and LA-based ones. However, the total number of iterations of the AIC-based algorithm before termination is on average higher in comparison with that of the MSR-based algorithm. The higher total number of iterations of the AIC-based algorithm increases its execution time. It is important to note that the execution time of the MSR-based with $\lambda = 1$ is less than that of with $\lambda = 0$. Overall, our proposed MSR-based NUE algorithm with $\lambda = 1$ and $\gamma = 0$ attains the best and the LA-based has the worst execution time.

4.2 Autoregressive Model

AR models have been widely used to generate multivariate data with controlled directed dependencies among them [13, 21, 22]. The considered nonlinear AR model is given as:

$$
\begin{aligned}
Y_{1,n} &= 0.95\sqrt{2}Y_{1,n-1} - 0.9125Y_{1,n-2} + \varepsilon_1 \\
Y_{2,n} &= 0.5Y_{1,n-2}^2 + \varepsilon_2 \\
Y_{3,n} &= -0.4Y_{1,n-3} + 0.4Y_{2,n-1} + \varepsilon_3 \\
Y_{4,n} &= -0.5Y_{1,n-1}^2 + 0.25\sqrt{2}Y_{4,n-1} + \varepsilon_4 \\
Y_{5,n} &= -0.25\sqrt{2}Y_{4,n-1} + 0.25\sqrt{2}Y_{5,n-2} + \varepsilon_5,
\end{aligned}
\tag{A.15}
$$

where $\varepsilon_1, \ldots, \varepsilon_5$ are mutually independent zero mean and unit variance white Gaussian noise processes. In accordance with (A.15), node 1 only depends on its own past and therefore there is no directed dependency from other nodes to node 1 (first row of (A.15)). On the other hand, nodes 2, 3 and 4 depend on the past of node 1 and therefore there are nonlinear directed dependencies
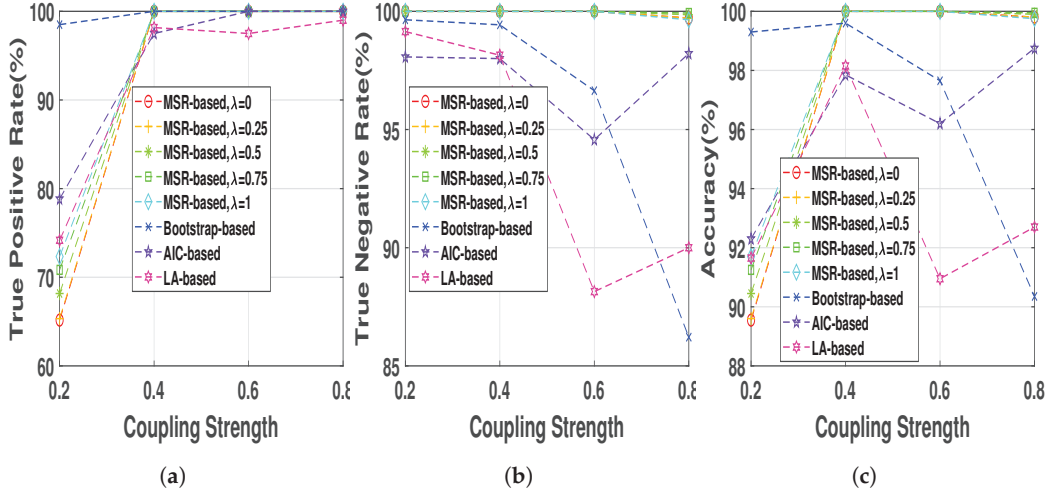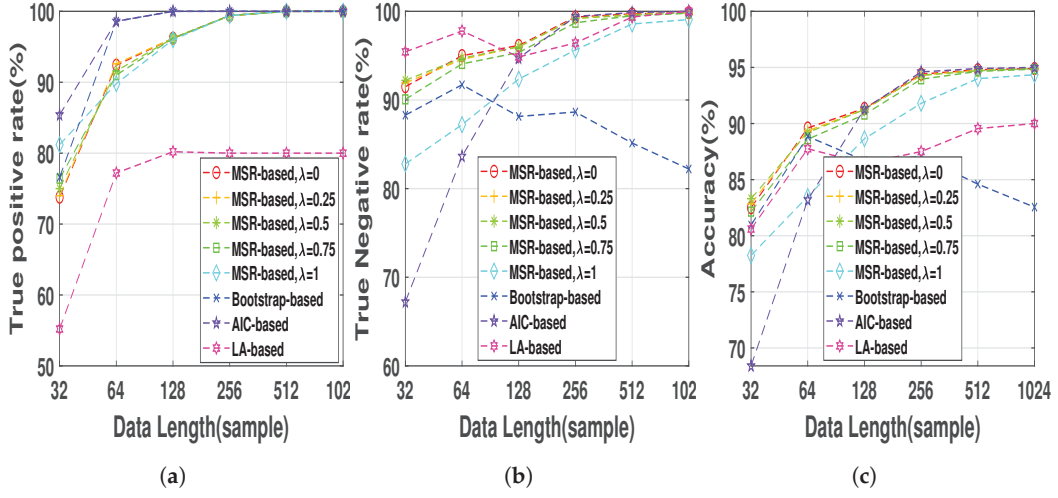
Fig. A.6: (**a**) true positive rates, (**b**) true negative rates and (**c**) accuracies of MSR-based, bootstrap-based, AIC-based, and LA-based NUE algorithms for the AR at data length ranging from 32 to 1024. The results are shown as an average over 100 realizations.

from node 1 and to nodes 2 and 4 (second and fourth rows of (A.15)) and linear directed dependencies from node 1 to node 3 (third row of (A.15)). There are also linear directed dependencies from nodes 2 and 4 to nodes 3 and 5, respectively (third and fifth rows of (A.15)). These dependencies describe the ground truth couplings when comparing TPR, TNR, and ACC of the NUE algorithms.

Data Length Effect

Nonlinear AR data series were first generated for 100 realizations at different lengths, $N = 2^h, h = 5, 6, \ldots, 10$, in order to evaluate the effect of data length on the performance of the NUE algorithms using AR data. We set the parameter $\gamma = 0$ since in this simulation there is no IC effect. Figure A.6 shows TPRs, TNRs and accuracies of the NUE algorithms for the AR model as a function of data lengths. As Figure A.6a illustrates, the LA-based NUE algorithm has significantly lower TPR compared to that of the other algorithms. It is also noteworthy that the TNR of the bootstrap-based algorithm tends to decrease as the data length increases. The MSR-based algorithm, for all λ except $\lambda = 1$, presents higher accuracy than that of the bootstrap-based and LA-based algorithms at all data lengths and higher accuracy than that of the AIC-based algorithms at data length smaller than 128.

Instantaneous Coupling Effect

IC can happen due to sharing information at same lag. In other words, it can occur due to fast sharing information [31]. For example, in neuro-

physiological time series like EEG, the recorded electrical activity at each electrode located at the scalp, is considered to be a mixture of the source generators because the sources pass through the volume conductor [18]. The volume conduction can be considered as the zero lag coupling which may lead to detection of false directed dependency by the NUE algorithms.

Let us consider the AR model defined in (A.15) at length N as the sources, which are instantly mixed to simulate the effect of IC. The considered mixing matrix is given as

$$
A = \begin{bmatrix}
(1-\alpha) & \alpha & \alpha & \alpha & \alpha \\
\alpha & (1-\alpha) & \alpha & \alpha & \alpha \\
\alpha & \alpha & (1-\alpha) & \alpha & \alpha \\
\alpha & \alpha & \alpha & (1-\alpha) & \alpha \\
\alpha & \alpha & \alpha & \alpha & (1-\alpha)
\end{bmatrix}.
\tag{A.16}
$$

where α varies between 0.1 and 0.3 in step of 0.1 in this paper. The greater α, the greater IC between the sources. Let $Y = [Y_1, Y_2, \ldots, Y_5]^T$ be $N \times 5$ matrix which includes all sequences (they are considered to simulate sources in the brain) generated by the AR model (A.15). The mixed matrix (it is considered to simulate the EEG signals recorded at the scalp level which is the mixture of all sources) is then defined as the matrix product between Y and A that is

$$
Y^{mixed} = YA.
\tag{A.17}
$$

Each column of A defines how the sources $Y_1, \ldots Y_5$ are mixed. As expected, for the nth mixed data sequence Y_n^{mixed}, the most important term is Y_n. This is more clear by looking at the main diagonal of the A.

The nonlinear AR data series were first generated for 100 realization at data lengths 512 using (A.15) and then mixed using (A.17) in order to evaluate the effect of IC on the performance of the NUE algorithms. As it was mentioned in Section 2, selecting a decent γ can control the balance between true positives and true negatives which can be useful, for example, to increase the accuracy of our proposed MSR-based NUE algorithm when there is an unobserved confounder effect like IC effect. Therefore, the proposed algorithm was implemented using six γs. We set a fixed $\lambda = 0.5$ since in this section the goal is to investigate effect of γ on the performance of the MSR-based algorithm. Figure A.7 demonstrates the TPRs, TNRs and accuracies of the MSR-based with six γ when they are applied on the data with three instantaneous couplings, i.e., $\alpha = 0.1, 0.2, 0.3$. As we can see in Figure A.7, the TNR of the MSR-based algorithm increases by increasing γ while the TPR gradually decreases up to a certain γ (e.g., $\gamma = 0.04$ for $\alpha = 0.1$) and then it significantly declines. Accordingly, the accuracy increases up to a certain γ due to the increasing of the TNR compensating for the slight decrease of the TPR. Table A.2 illustrates accuracies of the existing NUE algorithms
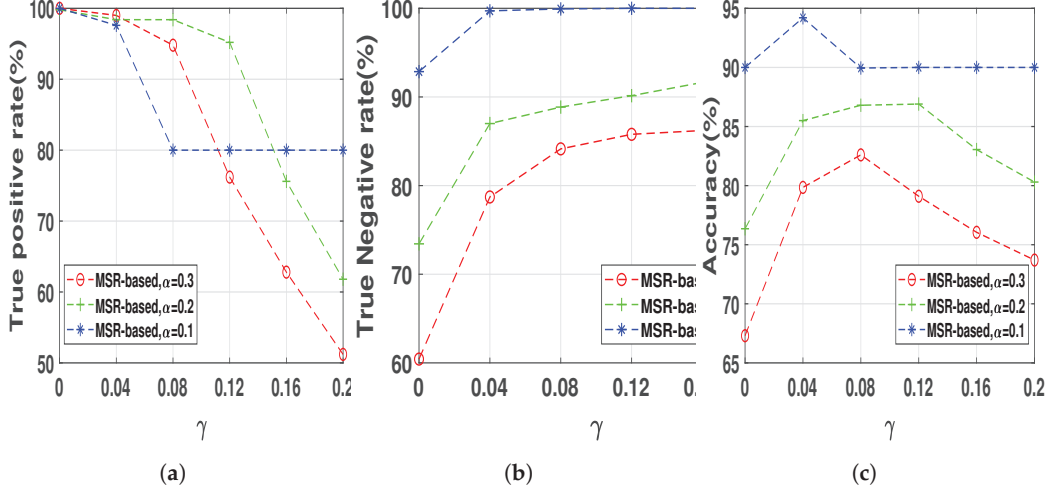
Fig. A.7: (**a**) true positive rates, (**b**) true negative rates and (**c**) accuracies of the MSR-based algorithm with different γ ranging from 0 to 0.2 in step of 0.04 when applied to the mixed AR data sequences at length 512 with different instantaneous coupling strength $\alpha = 0.1, 0.2, 0.3$. The results are shown as an average over 100 realizations.

as well as the best accuracy of the MSR-based algorithm which is obtained by a reported γ in the table. As Table A.2 demonstrates, accuracies of the NUE algorithms decrease by increasing instantaneous effect strength. Our proposed MSR-based NUE algorithm attains the greatest accuracy compared to the existing algorithms for all αs.

Table A.2: Accuracies of the bootstrap-based, LA-based and AIC-based algorithms as well as the proposed MSR-based algorithm. The γ leads to the best accuracies of the MSR-based algorithm are also reported in parenthesis after the accuraies. The results are reported as an average over 100 realizations.

NUE Algorithm	Bootstrap-Based	LA-Based	AIC-Based	MSR-Based (Best γ)
$\alpha = 0.1$	71.10	86.30	88.65	**94.20**($\gamma = 0.04$)
$\alpha = 0.2$	71.80	77.75	73.20	**86.90**($\gamma = 0.12$)
$\alpha = 0.3$	63.55	75.10	60.55	**82.60**($\gamma = 0.08$)

Execution Time

In this section the AR model data at length 512 was generated and execution time of the NUE algorithms is reported as an average over 100 realizations in Table A.3. Similar to the results reported in Section 4.1, the MSR-based algorithm with $\lambda = 1$ (at fixed $\gamma = 0$) is the fastest algorithm and LA-based one is the slowest one. Although the total number of iterations of the AIC-based and MSR-based algorithms with $\lambda = 0$ before termination are almost the same (around 10 iterations), the execution time of the AIC-based is slightly higher. It can be due to the fact that we did not have access to optimal code

for calculating the KDE-based regression while for the NN-based prediction we have used a mex file for the neighbor search which is provided by the ITS toolbox [19].

Table A.3: The execution time of our proposed MSR-based with $\lambda = 0, 1$ (at fixed $\gamma = 0$) as well as existing NUE algorithms for the AR data at length 512. The results are reported as an average over 100 realizations.

NUE Algorithm	Bootstrap-Based	LA-Based	AIC-Based	MSR-Based, $\lambda = 1$	MSR-Based, $\lambda = 0$
Execution Time	28.96	38.02	5.09	1.62	3.64
Total Number of Iterations	14.13	7.65	10.15	10.61	10.12

5   Application

In this section, we demonstrate the applicability of our proposed MSR-based algorithm on a real-world data. We consider a publicly available high dimensional intracranial EEG data from an epileptic patient. While our proposed estimator is defined for stationary stochastic processes, at least for this particular case of real world EEG data, our estimator is also able to provide good results when applied on non-stationary signals. The overall goal here is to apply NUE algorithms to estimate CTE and find patterns related to the onset and spread of the seizure. A total of 76 implanted electrodes was recorded, resulting in 76 time series. Electrodes 1–64 are cortical electrode grid and electrodes 65–76 are in-depth electrodes (six electrodes on each side). The data comprises 8 epileptic seizures (Ictal) and 8 periods just before the seizure onset (Pre-ictal) segments. Each segment is 10 seconds intracranial EEG data recorded at 400 Hz sampling frequency (more details about this data can be found in [35]). In this work, an anti-aliasing low-pass filter with a cut-off frequency of 50 Hz was applied prior to downsampling the signals to 100 Hz (Slow temporal auto-correlation of signals can induce a bias in the estimated conditional TE , nonlinear prediction and CMI in the NUE algorithms [36]. An approach used to correct this bias is called Theiler correction based on which too close observations in time should be discarded from the NN searches included in the estimation of TE, CMI and MSR [36]. In this paper, we down-sample the EEG data to avoid slow auto-correlation bias. In other words, the Theiler window is 4 samples.). The embedding delay and dimension were chosen as 1 and 8, respectively.

Epileptologists recognized the regions corresponding to one of the depth strips (electrodes 70 to 76) and the lower left corner of the grid (electrodes 1–4, 9–11 and 17) were resected during anterior temporal lobectomy as the seizure onset zone, which means synchronous activity of neurons in the specific regions of the brain becomes so strong, so that it can propagate its own activity to other distant regions [7, 13, 21, 23]. From an information theory point of

view, these nodes send information to other nodes, resulting in seizure onset. The amount of information each node sends to other nodes can be computed by the summation over each row of the directed dependencies matrix.

We applied our proposed in addition to bootstrap-based and LA-based NUE algorithms to estimate CTE in real high dimensional and redundant intracranial EEG data. The overall goal here is to compare advantages of our proposed NUE algorithms over the other algorithms reported in the literature. The MSR-based NUE algorithm was implemented with $\lambda = 1$ and $\gamma = 0.005$. The directed dependencies matrices obtained by our proposed algorithm as well as the existing algorithms are shown in Figure A.8. The directed dependencies matrices obtained by the bootstrap-based NUE algorithm (Figure A.8b,e) contain many connections in both pre-ictal and ictal conditions. Specifically, the diagonal pattern observed in the matrices obtained by the bootstrap-based NUE algorithm can be due to the volume conduction and conduction effect of the grid. On the other hand, our proposed (Figure A.8a,d) and LA-based NUE algorithms (Figure A.8c,f) are less sensitive to the volume conduction effect in comparison to that of the bootstrap-based algorithm.

Figure A.9 represents the total amount of information each electrode sends to other electrodes. As Figure A.9b demonstrates, due to the volume conduction effect there are some peaks even in the pre-ictal condition. On the other hand, the amount of information each electrode sends in the pre-ictal condition obtained by the MSR-based (Figure A.9a) and LA-based (Figure A.9c) NUE algorithms is approximately zero except for electrode 73. This electrode can be associated with the seizure onset although it is not yet clinically observable.

As mentioned earlier, electrodes 2–4, 9–11 and 17 are the seizure onset zones. Figure A.9d,f show that the magnitude of the peaks at electrodes 2–4 and 9–11 for the MSR-based algorithm is higher than the one of the LA-based procedure. It is also important to mention that the existing LA-based and bootstrap-based NUE algorithms are not able to detect the peak at electrode 17 as opposed to that of our proposed MSR-based NUE algorithm.

6   Discussion and Conclusions

Reliable estimation of the directed dependencies in conditional high dimensional data are limited by the so-called ´´curse of dimensionality" problem. A greedy approach called non-uniform embedding (NUE) algorithm was proposed in [13] to select the most relevant variables and reduce the dimension of the reconstructed state-space of the data. Then, the model-free directed dependencies measure, conditional transfer entropy (CTE) is estimated using the reconstructed state-space. The NUE strategy based on sequentially

(**a**) Pre-Ictal (MSR-based)   (**b**) Pre-Ictal (Bootstrap-based)   (**c**) Pre-Ictal (LA-based)

(**d**) Ictal (MSR-based)   (**e**) Ictal (Bootstrap-based)   (**f**) Ictal (LA-based)

Fig. A.8: directed dependency Matrices obtained by applying NUE algorithms on intracranial EEG data at epileptic seizures (Ictal) and just before the seizure onset (Pre-ictal) conditions. The directed dependency is shown from rows (driver) to the colomns (Targets). The darker color of an element, the higher the directed dependency is. The results are shown as an average over 8 segments.

selecting the best candidates in a greedy way will generally not lead to the same performance as would be obtained by using a brute-force combinatorial approach, where the performance is maximized over all possible sets of candidates. It has, however, been shown that NUE approaches often lead to an improved accuracy of the CTE compared to that of uniform embedding approaches [13, 19]. The NUE algorithm has been widely utilized to estimate the directed dependencies in neuro-physiological [15, 16] and economical [17] applications. It still has some obstacles like using a bootstrap-based termination criterion which highly depends on the bootstrap size [27]. It has been shown in [9, 28] that using an alternative to the bootstrap statistical test can be more accurate and computationally efficient.

In this paper, we proposed a new modification for the NUE algorithm

(a) Pre-Ictal (MSR-based)   **(b)** Pre-Ictal (Bootstrap-based)   **(c)** Pre-Ictal (LA-based)

(d) Ictal (MSR-based)   **(e)** Ictal (Bootstrap-based)   **(f)** Ictal (LA-based)
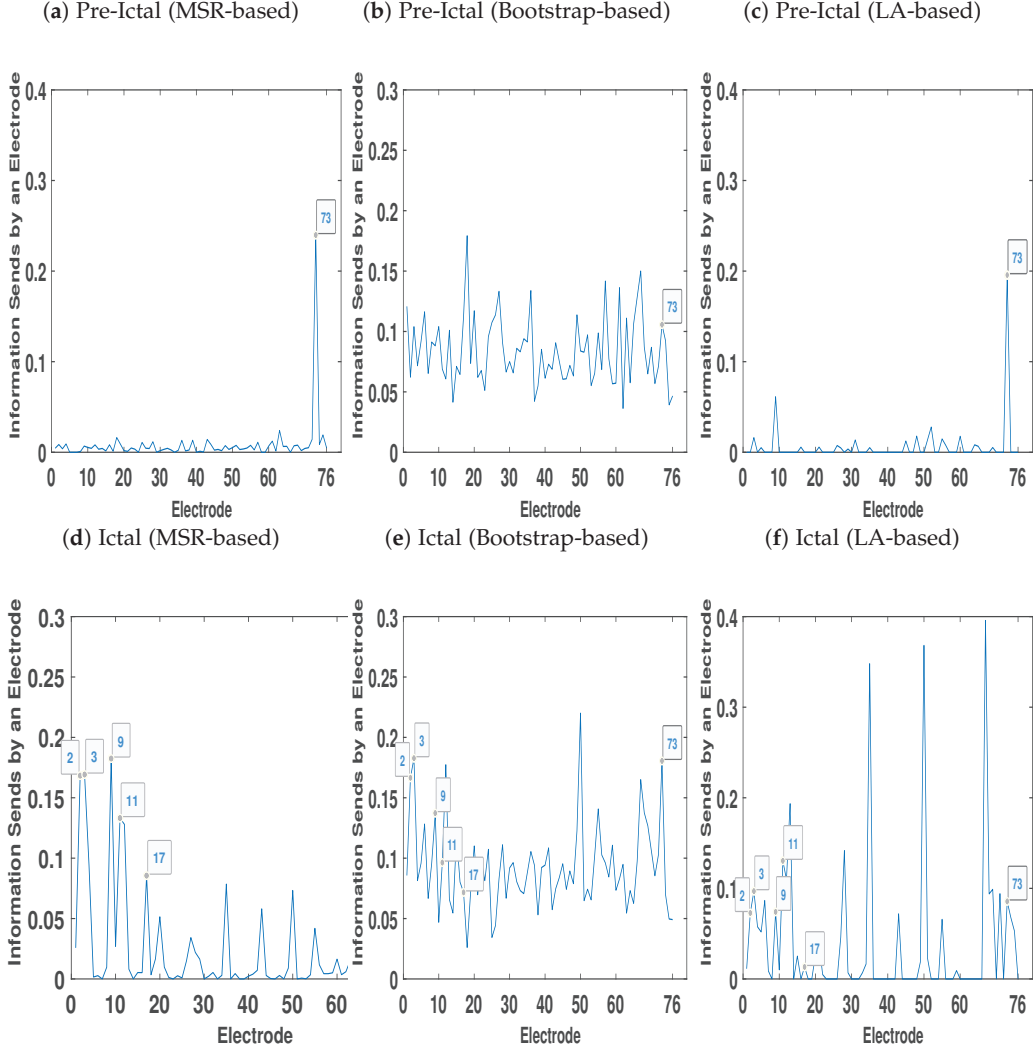
Fig. A.9: Total Information each electrode sends to other contacts at ictal and pre-ictal conditions.

which uses a weighted sum of conditional mutual information (CMI) and nearest neighbor(NN)-based prediction for ranking the candidates and the algorithm is terminated if the highest ranked candidate is not relevant enough to significantly improve the accuracy of the prediction of the target variable. It should be noted that while our simulations on synthetic and real world data indicate that using prediction accuracy can lead to better assessment of directed dependency, we have not been able to prove this from an estimation theoretic point of view. It should also be noted that for the linear Gaussian processes, accuracy of the prediction of the target variable given selected candidates $\text{MSR}(Y_n|\mathcal{U}_n)$, is monotonically equivalent to the conditional entropy $H(Y_n|\mathcal{U}_n)$ [37].

The proposed NUE procedure was compared with the original bootstrap-based NUE algorithm in [13], low-dimensional approximation(LA)-based [21] and Akaike information criterion (AIC)-based [27]. Performance analysis us-

ing simulation data generated by Henon map and autoregressive (AR) models at different lengths and coupling strengths revealed that the proposed mean of the squared (MSR)-based NUE algorithm tends to outperform the existing ones for detecting the directed dependencies. Specifically, the higher true negative rate (TNR) of the proposed MSR-based NUE compared to that of the existing ones may represent better ability of the proposed algorithm to terminate at the correct iteration and, as a result, better functionality of the proposed termination criterion. The poor selectivity (or TNR) of the bootstrap-based is in line with the results observed in [21], where they also found higher false positives for the bootstrap-based procedure compared to that of the LA-based one. The proposed algorithm also attains less false positive in comparison to that of the LA-based approach. The greater true positive rate (TPR) of the MSR-based algorithm with higher λ for small simulated data length and low coupling strength can justify using the weighted sum for ranking candidates. However, the limitation of the proposed NUE algorithm is that, for very low coupling strength, the accuracy of the proposed estimator was not as good as for the the bootstrap-based one.

The applicability of the NUE algorithms in real-word data can be affected by unobserved confounder effects like instantaneous information sharing which can be falsely detected as directed dependencies [31]. The data sequences generated by the AR model were instantly mixed at different mixing strengths in order to simulate an instantaneous coupling (IC) effect. The results showed that, by choosing a proper parameter γ, the proposed MSR-based measure attains significantly better performance than the existing ones. The simulated data results were consistent with the real-data used in this paper where the best results also were obtained for positive γ. The better performance can be of particular importance for such real-world applications like electroencephalography (EEG) and magnetoencephalography in which the volume conduction effect can cause IC [18]. There are also other frameworks like compensated transfer entropy [31], which tries to improve the estimation of the TE in the presence of IC. This measure modified the definition of the transfer entropy to compensate the effect of IC. The NUE algorithms are defined to find the embedding vector for estimating transfer entropy. Therefore, comparison or even modification of the proposed NUE algorithm for restructuring the state-space to estimate compensated transfer entropy deserves an independent and comprehensive study and will be considered in future works.

The proposed MSR-based algorithm with known parameter γ achieved a significant improvement in the computational efficiency. This can be due to the elimination of the computation effort of the bootstrap test which is not included in the proposed MSR-based algorithm. If we consider that the estimation of the CMI dominates the computation of the NUE algorithms (except for the MSR-based with $\lambda = 1$), then the overall computational requirement

of the NUE algorithms which uses bootstrap-based test in the worst case will be $k|\mathscr{C}| + 100k$, where k is the number iterations reported in Tables A.1 and A.2 and $|\mathscr{C}|$ is the cardinality of $\mathscr{C}$. On the other hand, the computational requirement of the proposed NUE algorithm with known parameter γ can be expressed as $k|\mathscr{C}|$. The computational effort of the MSR-based NUE algorithm with $\lambda = 1$ can be considered to be dominated by the estimation of MSR. It is computationally less complex than that of the CMI since it only includes a neighbor search while CMI estimation contains a neighbor search and range searches. Therefore, in very high-dimensional data (like the intracranial EEG data used in the application part where $|\mathscr{C}| = 608$), where execution of the NUE algorithm can be very time-consuming, it is suggested to use $\lambda = 1$, since it will be significantly faster. The proposed NUE algorithm with $\lambda = 1$ also achieved better execution times than that of with $\lambda = 0$ in the simulation data used this paper. As already mentioned in [21, 23], the LA-based approximation of the CMI used in the LA-based NUE algorithm is computationally more expensive, and this is consistent with the execution time reported in this paper where LA-based procedure attains the worst execution time. Better execution time can be especially important for such applications like a scalp EEG-based brain-computer interface where faster time series analyses methods are required. We also consider testing the performance our proposed estimator on high dimensional scalp EEG data in future works.

Another parameter of our proposed NUE algorithm over which one needs to scan is the positive parameter γ. The parameter γ and $\mathrm{MSR}(Y_n|\mathscr{U}_n)$ have the same units, and it defines the required amount of improvement in the accuracy of prediction prior to selecting a variable. Intuitively, the prediction accuracy $MSR(Y_n|\mathscr{U}_n^k)$ can vary between 0 and $\mathrm{var}(y_n)$, where 0 shows that one can perfectly predict Y_n by incorporating $\mathscr{U}_n^k$. The intuition of the worst case of the accuracy of the prediction $MSR(Y_n|\mathscr{U}_n^k)$ can be the case that incorporating $\mathscr{U}_n^k$ does not help the prediction at all and the indices specified by neighbor search in u_n will be uniformly distributed. The obtained $\widehat{y_n}(i|\mathscr{U})$ will be an approximation of mean of y_n and as a result MSR will be approximately $\mathrm{var}(y_n)$. In this paper, we normalize time series related to the realizations of the target processes to have zero mean and unit variance. We therefore scan the parameter γ in the interval between 0 and 1 to tune the algorithm. Therefore, another limitation of our proposed NUE algorithm is that it needs to be tuned by scanning over the parameter γ. The optimal choice of γ will be data dependent. The more accurate investigation of the criterion with which the parameter γ can be selected will be considered in the future works. Moreover, scanning over γ can increase execution time of our proposed algorithm. We suggest tuning the algorithm by using small subset of segments and use the tuned algorithm for the rest of segments. The reason is that the parameter γ can take care of confounder effects found in

the data and will not vary during the segments such as volume conduction effect in neuro-physiological time series [18].

In this paper, TE has been used to assess the directed dependencies. Estimated TE in networks consisting of more than two nodes can be affected by other nodes through, for example, an indirect path or common shared information. One possible approach to reduce such effects is to condition out information coming from other nodes. However, this approach can present bias in the estimated directed dependencies in data in which there is the collider condition [38]. There are other approaches to assess directed dependencies in the network like decomposing TE into unique, synergistic, and redundant information [39]. However, comparison of the estimated conditional TE and decomposing TE deserves an independent and comprehensive study and it is out of the scope of this paper.

A Appendix

A.1 Kraskov–Grassberger–Stögbauer Estimator

Conditional Mutual Information Estimation

The Kraskov–Grassberger–Stögbauer approach [14] is an NN-based estimator which was originally developed in order to estimate mutual information. It was adapted to estimate CMI in the NUE algorithm in [13, 19, 32]. The CMI in (A.3) can be rewritten as the sum/difference of four joint entropies [13, 32]

$$I\left(Y_n; W_n \mid \mathcal{S}_n^{k-1}\right) = h(Y_n, \mathcal{S}_n^{k-1}) - h(\mathcal{S}_n^{k-1}) - h(Y_n, W_n, \mathcal{S}_n^{k-1}) + h(W_n, \mathcal{S}_n^{k-1}).$$
(A.18)

Then, the CMI is estimated by using a NN approach in which the entropy of the higher dimension $h(Y_n, W_n, \mathcal{S}_n^{k-1})$ is estimated through a neighbor search as [13, 32]

$$h(Y_n, W_n, \mathcal{S}_n^{k-1}) \approx -\psi(T) + \psi(N) + (d+1)\langle ln(\epsilon_n(i))\rangle,$$
(A.19)

where ψ is the digamma function, and N is the total number of observations of the vector variable $[Y_n, W_n, \mathcal{S}_n^{k-1}]$. Twice the amount of distance (maximum norm) of ith observation of $[Y_n, W_n, \mathcal{S}_n^{k-1}]$ from its Tth neighbor is denoted by $\epsilon_n(i)$ and $\langle . \rangle$ is the average over all observations. The rest of entropies in (A.18) are estimated by using a range search as

$$h(W_n, \mathcal{S}_n^{k-1}) \approx -\psi(T) + d\left\langle \psi\left(N_{[W_n, \mathcal{S}_n^{k-1}]} + 1\right)\right\rangle$$
$$h(Y_n, \mathcal{S}_n^{k-1}) \approx -\psi(T) + d\left\langle \psi\left(N_{[Y_n, \mathcal{S}_n^{k-1}]} + 1\right)\right\rangle$$
$$h(\mathcal{S}_n^{k-1}) \approx -\psi(T) + (d-1)\left\langle \psi\left(N_{\mathcal{S}_n^{k-1}} + 1\right)\right\rangle.$$
(A.20)

The number of realizations of $[W_n, \mathcal{S}_n^{k-1}]$ whose maximum norm from the ith realization of $[W_n, \mathcal{S}_n^{k-1}]$ is strictly less than $\epsilon_n/2$, which is denoted by $N_{[W_n, \mathcal{S}_n^{k-1}]}$. A similar notation applies to $N_{[Y_n, \mathcal{S}_n^{k-1}]}$ and $N_{\mathcal{S}_n^{k-1}}$. The CMI is finally estimated by replacing (A.19) and (A.20) in (A.18)

$$I\left(Y_n; W_n \mid \mathcal{S}_n^{k-1}\right) = \psi(T) + \left\langle \psi\left(N_{\mathcal{S}_n^{k-1}} + 1\right) - \psi\left(N_{[W_n, \mathcal{S}_n^{k-1}]} + 1\right) - \psi\left(N_{[Y_n, \mathcal{S}_n^{k-1}]} + 1\right) \right\rangle.$$
(A.21)

Conditional Transfer Entropy Estimation

After selecting the most informative candidates and forming the embedding vector $\mathcal{S}_n^k$ using the NUE algorithms, the CTE in (A.2) can be estimated using the same approach explained in Appendix A.1. The CTE can also be expressed as the sum of four joint entropies as

$$\text{CTE}(\mathcal{X} \to \mathcal{Y}|\mathcal{Z}) = h(Y_n, Y_n^-, \mathbf{Z}_n^-) - h(Y_n^-, \mathbf{Z}_n^-) - h(Y_n, Y_n^-, X_n^-, \mathbf{Z}_n^-) + h(Y_n^-, X_n^-, \mathbf{Z}_n^-),$$
(A.22)

where $[X_n^-, Y_n^-, \mathbf{Z}_n^-]$ is replaced by $\mathcal{S}_n^{k-1}$ and $[Y_n^-, \mathbf{Z}_n^-]$ is substituted by $\mathcal{S}_n^{k-1}$ without any past variables of X_n. Then, by using range search in the higher dimension $[Y_n, Y_n^-, \mathbf{Z}_n^-]$ and range search in the rest of dimensions, the CTE can be estimated as

$$\text{CTE}(\mathcal{X} \to \mathcal{Y}|\mathcal{Z}) = \psi(T) + \left\langle \psi\left(N_{[Y_n^-, \mathbf{Z}_n^-]} + 1\right) - \psi\left(N_{[Y_n, Y_n^-, \mathbf{Z}_n^-]} + 1\right) - \psi\left(N_{[X_n^-, Y_n^-, \mathbf{Z}_n^-]} + 1\right) \right\rangle,$$
(A.23)

where $N_{[Y_n^-, \mathbf{Z}_n^-]}$ denotes the number of realizations of whose maximum norm from its ith realization of is strictly less than $\epsilon_n/2$. The same notation applies to $N_{[Y_n, Y_n^-, \mathbf{Z}_n^-]}$ and $N_{[X_n^-, Y_n^-, \mathbf{Z}_n^-]}$.

A.2 Kernel Density Estimation-Based Prediction

In the Akaike information criterion-based termination criterion which is adapted in this paper to stop the NUE algorithm, one needs to predict the target variable Y_n given $\mathcal{U}_n^k = [W_n^k, \mathcal{S}_n^{k-1}]$ by using the kernel density estimation (KDE) approach. The KDE-based prediction is performed as:

$$\widehat{y}_n(i|\mathcal{U}_n^k) = \sum_{i=1}^N \frac{y_n(i)K_h(u_n^k, u_n^k(i))}{\sum_{i=1}^M K_h(u_n^k, u_n^k(i))},$$
(A.24)

where $\widehat{y}_n(i|\mathcal{U}_n^k)$ denotes for estimated i^{th} observation of Y_n and K_h is the Gaussian kernel with Mahalonobis distance (Equation (A.26)) [27]:

$$K_h(u_n^k, u_n^k(i)) = \frac{1}{(\sqrt{2\pi}h)^d} \exp\left(\frac{-\| u_n^k - u_n^k(i)\|}{2h^2}\right),$$
(A.25)

$$\|u_n^k - u_n^k(i)\| = (u_n^k - u_n^k(i))^T \Sigma^{-1}(u_n^k - u_n^k(i)), \qquad \text{(A.26)}$$

where d and Σ are dimension (number of columns) and covariance of u_n^k, respectively. The bandwidth of the kernel function h is chosen for unit variance data as [27, 28]:

$$h = 1.5 \left(\frac{1}{d+2}\right)^{1/(d+4)} N^{-1/(d+4)}. \qquad \text{(A.27)}$$

References

[1] Omidvarnia, A.; Azemi, G.; Boashash, B.; O'Toole, J.M.; Colditz, P.B.; Vanhatalo, S. Measuring time-varying information flow in scalp EEG signals: orthogonalized partial directed coherence. *IEEE Trans. Biomed. Eng.* **2013**, *61*, 680–693.

[2] Cover, T.M.; Thomas, J.A. *Elements of Information Theory*; John Wiley & Sons: Hoboken, NJ, USA, 2012.

[3] Baboukani, P.S.; Azemi, G.; Boashash, B.; Colditz, P.; Omidvarnia, A. A novel multivariate phase synchrony measure: Application to multichannel newborn EEG analysis. *Digit. Signal Process.* **2019**, *84*, 59–68.

[4] Schreiber, T. Measuring information transfer. *Phys. Rev. Lett.* **2000**, *85*, 461.

[5] Baboukani, P.S.; Mohammadi, S.; Azemi, G. Classifying Single-Trial EEG During Motor Imagery Using a Multivariate Mutual Information Based Phase Synchrony Measure. In Proceedings of the 2017 24th National and 2nd International Iranian Conference on Biomedical Engineering (ICBME), Tehran, Iran, 30 November–1 December 2017; pp. 1–4.

[6] Gençağa, D. Transfer Entropy. *Entropy* **2018**, *20*, 288.

[7] Faes, L.; Marinazzo, D.; Stramaglia, S. Multiscale information decomposition: Exact computation for multivariate Gaussian processes. *Entropy* **2017**, *19*, 408.

[8] Derpich, M.S.; Silva, E.I.; Østergaard, J. Fundamental inequalities and identities involving mutual and directed informations in closed-loop systems. *arXiv* **2013**, arXiv:1301.6427.

[9] Massey, J. Causality, feedback and directed information. In Proceedings of the 1990 International Symposium on Information Theory and its Applications (ISITA-90), Waikiki, HI, USA, 27–30 November 1990; pp. 303–305.

[10] Wiener, N. *The Theory of Prediction. Modern Mathematics for Engineers*; McGraw-Hill: New York, NY, USA, 1956; pp. 165–190.

[11] James, R.G.; Barnett, N.; Crutchfield, J.P. Information flows? A critique of transfer entropies. *Phys. Rev. Lett.* **2016**, *116*, 238701.

[12] Lizier, J.T.; Prokopenko, M. Differentiating information transfer and causal effect. *Eur. Phys. J. B* **2010**, *73*, 605–615.

[13] Montalto, A.; Faes, L.; Marinazzo, D. MuTE: A MATLAB toolbox to compare established and novel estimators of the multivariate transfer entropy. *PLoS ONE* **2014**, *9*, e109462.

[14] Kraskov, A.; Stögbauer, H.; Grassberger, P. Estimating mutual information. *Phys. Rev. E* **2004**, *69*, 066138.

[15] Lindner, M.; Vicente, R.; Priesemann, V.; Wibral, M. TRENTOOL: A Matlab open source toolbox to analyse information flow in time series data with transfer entropy. *BMC Neurosci.* **2011**, *12*, 119.

[16] Wibral, M.; Pampu, N.; Priesemann, V.; Siebenhühner, F.; Seiwert, H.; Lindner, M.; Lizier, J.T.; Vicente, R. Measuring information-transfer delays. *PLoS ONE* **2013**, *8*, e55809.

[17] Bossomaier, T.; Barnett, L.; Harré, M.; Lizier, J.T. *An Introduction to Transfer Entropy*; Springer International Publishing: Cham, Switzerland, 2016; pp. 65–95.

[18] Ruiz-Gómez, S.J.; Hornero, R.; Poza, J.; Maturana-Candelas, A.; Pinto, N.; Gómez, C. Computational modeling of the effects of EEG volume conduction on functional connectivity metrics. Application to Alzheimer's disease continuum. *J. Neural Eng.* **2019**, *16*, 066019.

[19] Faes, L.; Marinazzo, D.; Nollo, G.; Porta, A. An information-theoretic framework to map the spatiotemporal dynamics of the scalp electroencephalogram. *IEEE Trans. Biomed. Eng.* **2016**, *63*, 2488–2496.

[20] Mehta, K.; Kliewer, J. Directional and Causal Information Flow in EEG for Assessing Perceived Audio Quality. *IEEE Trans. Mol. Biol. Multi-Scale Commun.* **2017**, *3*, 150–165.

[21] Zhang, J. Low-dimensional approximation searching strategy for transfer entropy from non-uniform embedding. *PLoS ONE* **2018**, *13*, e0194382.

[22] Xiong, W.; Faes, L.; Ivanov, P.C. Entropy measures, entropy estimators, and their performance in quantifying complex dynamics: Effects of artifacts, nonstationarity, and long-range correlations. *Phys. Rev. E* **2017**, *95*, 062114.

[23] Jia, Z.; Lin, Y.; Jiao, Z.; Ma, Y.; Wang, J. Detecting causality in multivariate time series via non-uniform embedding. *Entropy* **2019**, *21*, 1233.

[24] Kugiumtzis, D. Direct-coupling information measure from nonuniform embedding. *Phys. Rev. E* **2013**, *87*, 062918.

[25] Olejarczyk, E.; Marzetti, L.; Pizzella, V.; Zappasodi, F. Comparison of connectivity analyses for resting state EEG data. *J. Neural Eng.* **2017**, *14*, 036017.

[26] Novelli, L.; Wollstadt, P.; Mediano, P.; Wibral, M.; Lizier, J.T. Large-scale directed network inference with multivariate transfer entropy and hierarchical statistical testing. *Netw. Neurosci.* **2019**, *3*, 827–847.

[27] May, R.J.; Maier, H.R.; Dandy, G.C.; Fernando, T.G. Non-linear variable selection for artificial neural networks using partial mutual information. *Environ. Model. Softw.* **2008**, *23*, 1312–1326.

[28] Li, X.; Maier, H.R.; Zecchin, A.C. Improved PMI-based input variable selection approach for artificial neural network and other data driven environmental and water resource models. *Environ. Model. Softw.* **2015**, *65*, 15–29.

[29] Baboukani, P.S.; Graversen, C.; Østergaard, J. Estimation of Directed Dependencies in Time Series Using Conditional Mutual Information and Non-linear Prediction. Accepted for the European Signal Processing Conference (EUSIPCO). European Association for Signal Processing (EURASIP), 2020.

[30] Altman, N.S. An introduction to kernel and nearest-neighbor nonparametric regression. *Am. Stat.* **1992**, *46*, 175–185.

[31] Faes, L.; Nollo, G.; Porta, A. Compensated transfer entropy as a tool for reliably estimating information transfer in physiological time series. *Entropy* **2013**, *15*, 198–219.

[32] Faes, L.; Kugiumtzis, D.; Nollo, G.; Jurysta, F.; Marinazzo, D. Estimating the decomposition of predictive information in multivariate systems. *Phys. Rev. E* **2015**, *91*, 032904.

[33] Danafar, S.; Fukumizu, K.; Gomez, F. Kernel-based Information Criterion. *arXiv* **2014**, arXiv:1408.5810.

[34] Faes, L.; Marinazzo, D.; Montalto, A.; Nollo, G. Lag-specific transfer entropy as a tool to assess cardiovascular and cardiorespiratory information transfer. *IEEE Trans. Biomed. Eng.* **2014**, *61*, 2556–2568.

[35] Kramer, M.A.; Kolaczyk, E.D.; Kirsch, H.E. Emergent network topology at seizure onset in humans. *Epilepsy Res.* **2008**, *79*, 173–186.

References

[36] Wibral, M.; Vicente, R.; Lizier, J.T. *Directed Information Measures in Neuroscience*; Springer: Berlin, Germany, 2014.

[37] Barnett, L.; Barrett, A.B.; Seth, A.K. Granger causality and transfer entropy are equivalent for Gaussian variables. *Phys. Rev. Lett.* **2009**, *103*, 238701.

[38] Cole, S.R.; Platt, R.W.; Schisterman, E.F.; Chu, H.; Westreich, D.; Richardson, D.; Poole, C. Illustrating bias due to conditioning on a collider. *Int. J. Epidemiol.* **2010**, *39*, 417–420.

[39] Williams, P.L.; Beer, R.D. Generalized measures of information transfer. *arXiv* **2011**, arXiv:1102.1507.

Paper B

A Stimuli-Relevant Directed Dependency Index for Time Series

Payam Shahsavari Baboukani, Sergios Theodoridis and Jan Østergaard

Abstract

Transfer entropy can to a certain degree assess the direction in addition to the strength of the couplings within dynamic time series. The greater the transfer entropy, the greater the strength of the dependency between time series. In this work, we are interested in quantifying the effect that a given time series (e.g., an external stimuli) has upon the coupling strength between other time series. Towards that end, we define a directed dependency index based on the difference of two causally conditioned transfer entropies. We then provide a lower bound for the dependency index, and demonstrate on synthetic data that this lower bound can be efficiently computed.

Keywords

Transfer entropy, directed dependecy, mutual information, intrinsic mutual information

1 Introduction

In time-series analysis, it is often desirable to assess the directed dependency between time series [1]. For example, the time series could be observations of physical or biological systems, where any possible directed dependencies in the data would mean that the systems are interacting with each other. One common application is the case of functional connectivity analysis of electroencephalography (EEG) signals [2, 3] where the observations obtained at different scalp electrodes are highly coupled.

Several time series analysis methods such as Granger causality [4, 5] and transfer entropy (TE) [1] have been proposed in order to quantify directed dependencies. While Granger causality is mainly used for analysing linear dependencies, TE is capable of determining both linear and non-linear interactions. In some cases, it is possible to distinguish between direct and indirect (implicit) couplings, where part of the information that two nodes share between them have been conveyed via a third node, see for example Fig. 1. By causally conditioning the estimation of TE between two nodes (say X and Y) on the third node (Z), it is possible to at least partially take the effect of indirect couplings into account [2]. In Fig. B.1, nodes X and Y are directly coupled with the direction from X to Y, and they are also indirectly coupled via Z and S.

In this paper, we are interested in the general problem of quantifying to what degree a given time series is directly influencing the directed dependencies between other time series. Thus, referring to Fig. B.1, we are interested in quantifying and computing a specific part of the information that describes the coupling between nodes X and Y. Specifically, we are only interested in the amount of information that exists within the directed coupling between X and Y and which is due to S but not due to Z. For example, consider

73

the case, where a human subject is exposed to acoustic stimuli and the EEG response is being measured on the scalp. One might then be interested in observing possible changes in the directed dependency from data from one EEG electrode X to another electrode Y, and which is due to changes in the external acoustic stimuli S. However, it is not straight-forward to distinguish whether the changes in the couplings are due to the desired external stimuli, or whether it is due to another stimuli such as other EEG electrodes, visual stimuli or due to artefacts caused by muscle or eye movements or noise.

In [6], the information flow in the human auditory system due to external acoustic stimuli was quantified. In this case, the external stimuli A was first processed by the noisy acoustic environment yielding the output B, which then entered the human auditory system via the human eardrum. The output C of the human auditory system as a response to the stimuli A was then obtained through listening tests. The authors of [6] were then interested in how much information about the stimuli was lost in the human auditory system, and it was shown that this could be quantified via the difference $I(A;B) - I(A;C)$.

We note that [6] considered unidirectional measures and did not need to condition the mutual information. In our case, we consider directed information measures that are causally conditioned. This greatly complicates the problem. Specifically, we introduce a directed coupling index, which is defined as a difference between two causally conditional directed informations and which is on the form $I(X \rightarrow Y \| Z) - \min_{f(\hat{s}|s)} I(X \rightarrow Y \| Z, \hat{S})$, where the latter term includes a minimization over distributions. As was pointed out in [7], it is not known how to compute such a minimization for the case of continuous alphabet sources as is the case here. To circumvent this difficulty, we provide a lower bound to the dependency index, which involves a simpler minimization problem which can be directly computed using recent estimators for causally conditioned transfer entropy [8, 9].

2 Background

2.1 Conditioning can increase the mutual information

It is well known that conditioning cannot increase entropy, i.e., $H(X|Y) \leq H(X)$. This is, however, not always the case for mutual information, where we could have that $I(X;Y|Z) \geq I(X;Y)$, as the following simple example shows. Let $Y = Z \oplus X$, where Z and X are mutually independent binary random variables, and where $\oplus$ denotes XOR. Clearly X and Y are mutually independent and $I(X;Y) = 0$. On the other hand, when conditioning upon
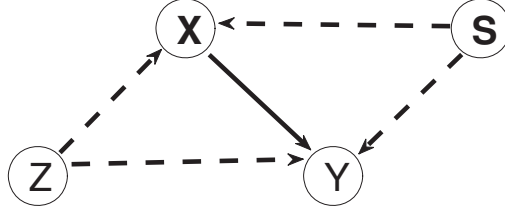
Fig. B.1: The nodes X and Y are directly coupled with each other and indirectly via Z and S.

Z, we obtain:

$$
\begin{aligned}
I(X;Y) &\sum_{x \in \mathcal{X} y \in \mathcal{Y} z \in \mathcal{Z}} p(x,y,z) \log_2 \frac{p(x,y|z)}{p(x|z)p(y|z)} \\
&= sum_{z \in \mathcal{Z}} \sum_{x \in \mathcal{X} y \in \mathcal{Y}} p(x,y|z) \log_2 \frac{p(x,y|z)}{p(x|z)p(y|z)}.
\end{aligned}
\tag{B.1}
$$

Conditioning cannot increase the mutual information if $X - Z - Y$ forms a Markov chain, in that order [10]. To see this, we note that in this case $I(X;Y|Z) = 0$, whereas $I(X;Y) \geq 0$.

2.2 Synergistic, intrinsic, and shared information

As pointed out in e.g. [7], the information measured by the directed information methods and its conditional versions, can be interpreted[1] as consisting of intrinsic information and in addition there could potentially be shared and synergistic information. Thus, the directed information might overestimate the amount of information being conveyed between systems (or signals). Specifically, let Y_0 denote the current sample of the process Y and let X_{-1} denote the past sample of the process X. Then, $I(X_{-1};Y_0)$ quantifies the intrinsic information from the past of X to the current Y in addition to the shared information, which already exist between the variables. Let us now assume that the shared information between X_{-1} and Y_0 is also contained in Y_{-1}. Then, we can simply remove the shared information by conditioning, i.e.: $I(X_{-1};Y_0|Y_{-1})$. Whilst the shared information has been removed, we have now potentially introduced synergistic information, as shown in (**??**).

In [7, 15], the intrinsic mutual information $\tilde{I}(X;Y|Z)$ between between two random variables X and Y given another random variable Z was identified as an upper bound to the secret key agreement rate which is given as:

$$
\tilde{I}(X;Y|Z) \triangleq \min_{f_{\hat{Z}|Z}(\hat{Z}|Z)} I(X;Y|\hat{Z}),
\tag{B.2}
$$

---

[1]There exists a wealth of interpretations and decompositions of the conditional mutual information, cf. [11–14]

which can be interpreted as the minimum conditional mutual information between X and Y given any possible (probabilistic or deterministic) function of Z. In [7], the intrinsic directed dependency between X and Y was defined based on (B.2) as $\tilde{I}(X_{-1}; Y_0 | Y_{-1})$.

For the case where Z has a discrete and finite alphabet, it was shown in [7] that the minimization in (B.2) can easily be computed. For the case where Z has a continuous alphabet, it is not clear how to compute (B.2). If $f_{\hat{Z}|Z}$ is constant, then it can be shown that $\tilde{I}(X; Y | Z) \leq I(X; Y)$ [7]. On the other hand, since one of the possible mappings from Z to $\hat{Z}$ is the identity function, it clearly follows that $\tilde{I}(X; Y | Z) \leq I(X; Y | Z)$.

2.3 Transfer Entropy

We are interested in determining the directed dependency from X to Y in the network of Fig. B.1. We denote by X_i the random variable obtained by sampling the process X at the present time i. Furthermore, let X_i^- be the past of the process X up to but not including X_i. A similar notation applies to Y_i^- and Z_i^-. The transfer entropy from X to Y causally conditioned on Z is then defined as [1, 16]:

$$TE(X \rightarrow Y || Z) \triangleq I(X_i^-; Y_i | Y_i^-, Z_i^-). \tag{B.3}$$

3 Quantifying Stimuli-Relevant directed dependency (SRDD) Index

Let X and Y in Fig. B.1 be the nodes of interest, let S be the external stimuli, and let Z be a (super) node that describes the consensus of the remaining nodes in a potentially complex network. Both S and Z could potentially affect both X and Y.

Let $I(X; Y | Z)$ be the conditional mutual information between X and Y given Z. Due to potential *synergistic* information, we might have that $I(X; Y | Z) > I(X; Y)$. Thus, $I(X; Y | Z)$ does not necessarily mean that we "remove" the information about Z, which is in either X or Y. However, consider now the difference:

$$I(X; Y | Z) - I(X; Y | Z, S). \tag{B.4}$$

In (B.4), any potential synergistic information, which is *only* due to conditioning upon Z, will vanish. In addition, new synergistic information due to conditioning upon S, and jointly upon S, Z could occur. To remove this effect, one can minimize over all possible functions of S as in (B.2). The intuition is now that by using the difference in (B.4), we remove the effect of Z, while at the same time avoiding overestimating the effect of S. Turning this into a

problem that involves dynamic time series, we replace the conditional mutual information expressions in (B.4) with their causally conditioned transfer entropy counterparts [16].

Definition 1 (Stimuli-relevant Directed Dependency (SRDD) Index): We define the stimuli-relevant directed dependency index for $(X^N \to Y^N)$ given Z^N and with stimuli S^N as:

$$
\begin{aligned}
I_{S^N}(X^N \to Y^N | Z^N) &\triangleq \sum_{i=1}^{N} I_S(X^{i-1}; Y_i | Y^{i-1}, Z^{i-1}) \\
I_{S^N}(X^{i-1}; Y_i | Y^{i-1}, Z^{i-1}) &\triangleq I(X^{i-1}; Y_i | Y^{i-1}, Z^{i-1}) \\
&\quad - \min_{f(\hat{s}^N | s^N)} I(X^{i-1}; Y_i | Y^{i-1}, Z^{i-1}, \hat{S}^N).
\end{aligned}
\tag{B.5}
$$

where $X^{i-1} = (X_1, X_2, \dots, X_{i-1})$.

When the processes X, Y, Z, and S are all jointly stationary but otherwise arbitrarily distributed, we ignore the sum in (B.5), and with a slight abuse of notation, we simply define the SRDD index to be given by:

$$
\begin{aligned}
I_S(X \to Y | Z) &\triangleq I(X_i^-; Y_i | Y_i^-, Z_i^-) \\
&\quad - \min_{f(\hat{s}|s)} I(X_i^-; Y_i | Z_i^-, Y_i^- \hat{S}),
\end{aligned}
\tag{B.6}
$$

where the minimization is over all jointly *stationary* distributions $f(\hat{s}, s)$ satisfying $f(\hat{s}, s) = f(\hat{s}|s)f(s)$.

Lemma 1: Let X, Y, Z, S be jointly stationary but otherwise arbitrarily distributed random processes. Then, the SRDD index given in (B.6) can be lower bounded by:

$$
\begin{aligned}
I_S(X \to Y | Z) &\geq I(X_i^-; Y_i | Y_i^-, Z_i^-) \\
&\quad - \min_{\phi \subseteq S_i^-} I(X_i^-; Y_i | Y_i^-, Z_i^-, \phi),
\end{aligned}
\tag{B.7}
$$

where the minimization is over all subsets of the past of S.

Proof: The proof follows immediately since the minimization in (B.7) is over a subset of the set from (B.6). ∎

We note that (B.7) forms a tighter bound than if the minimization is simply replaced by the full amount of information, $\phi = S_i^-$. Moreover, the motivation for restricting the minimization to be over subsets of the sequence S_i^- is to provide the means for efficient estimation of a non-trivial lower bound.

It is possible to move the stimuli away from the conditioning, which can be useful depending upon the choice of estimator. In this case, one needs to minimize over a difference of mutual information terms as is shown below:

Lemma 2: The lower bound in Lemma 1 can be equivalently expressed as:

$$I(X_i^-;Y_i|Y_i^-,Z_i^-) - \min_{\phi \subseteq S_i^-} I(X_i^-;Y_i|Y_i^-,Z_i^-,\phi)$$

$$= \min_{\phi \subseteq S_i^-} \left[I(\phi;y_i|Y_i^-,Z_i^-,X_i^-) - I(\phi;y_i|Z_i^-,y_i^-) \right].$$

Proof: We omit super- and subscripts when it is clear from context to simplify the notation. Assuming that the differential entropies are well defined, we establish the following equivalence by expanding the mutual information in terms of entropies:

$$\begin{aligned}
I(X;Y_i|Y_i^-,Z,S) &= h(Y_i|Y_i^-,Z,S) - h(Y_i|Y_i^-,Z,S,X) \\
&= h(Y_i,Y_i^-,Z,S) - h(Y_i^-,Z,S) \\
&\quad - h(Y_i,Y_i^-,Z,S,X) + h(Y_i^-,Z,S,X) \\
&= h(S|Y_i,Y_i^i,Z) + h(S,Y_i,Y_i^-) - h(S|Y_i^-,Z) - h(Y_i^-,Z) \\
&\quad - h(S|Y_i,Y_i^-,X,Z) - h(Y_i,Y_i^-,X,Z) \\
&\quad + h(S|Y_i^-,Z,X) + h(Y_i^-,X,Z) \\
&= I(S;Y_i|Z,Y_i^-,X) - I(S;Y_i|Y_i^-,Z) \\
&\quad + h(Y_i|Y_i^-,Z) - h(Y_i|Y_i^-,Z,X) \\
&= I(S;Y_i|Z,Y_i^-,X) - I(S;Y_i|Y_i^-,Z) + I(X;Y_i|Y_i^-,Z_i^-).
\end{aligned}$$

The last term does not include S in the conditioning and is identical to the first term on the right hand side of (B.7), which proves the first equality in the lemma. The second equality follows by symmetry in X_i^- and Y_{i-1}. ∎

We will also define a relative SRDD index, which does not depend on the absolute strength of the couplings. We denote this the normalized SRDD index:

$$\hat{I}_S(X \to Y|Z) \triangleq 1 - \frac{\min_{\phi \subseteq S_i^-} I(X_i^-;Y_i|Y_i^-,Z_i^-,\phi)}{I(X_i^-;Y_i|Y_i^-,Z_i^-)}. \tag{B.8}$$

It can easily be seen that $\hat{I}_S(X \to Y|Z) \in [0,1]$, where values close to 1 indicate that the external stimuli S has a great effect upon the coupling strength between X and Y, and a value close to 0 indicates that S has no effect.

3.1 Examples

The following examples show that as long as (partial) information about the stimuli S is shared between the sensors' data, the lower bound is (7) is non-trivially bounded away from zero. In these examples, we let X, Y, Z, and S be mutually independent standard Normal random variables.

Example 1

Assume that a sensor is measuring $\xi_1 = X + Y$ and another sensor is measuring $\xi_2 = X + Z + S$. We are interested in comparing the mutual information between the two sensor measurements conditioned upon knowledge of Z or (Z, S). We therefore obtain:

$$
\begin{aligned}
I(\xi_1; \xi_2 | Z) &= I(X + Y; X + Z + S | Z) \\
&= I(X + Y; X + S) = h(X + Y) - h(X + Y | X + S), \\
I(\xi_1; \xi_2 | Z, S) &= I(X + Y; X + Z + S | Z, S) \\
&= I(X + Y; X) = h(X + Y) - h(Y).
\end{aligned}
$$

Since X, Y, and S are jointly Gaussian, the conditional variance of $X + Y$ given $X + S$ is:

$$
\text{var}(X + Y | X + S) = \text{var}((X + Y) - \alpha(X + S)) \tag{B.9}
$$
$$
= \text{var}(Y) + (1 - \alpha)^2 \text{var}(X) + \alpha^2 \text{var}(S) > \text{var}(Y), \tag{B.10}
$$

where $\alpha \geq 0$ denotes a linear estimator.

Thus, $h(Y) < h(X + Y | X + S)$, which implies that $I(\xi_1; \xi_2 | Z)$ is less than $I(\xi_1; \xi_2 | Z, S)$ and conditioning upon S therefore leads to an increase of mutual information. If the two sensor measurements represents $\xi_1 = X_i^-$ and $\xi_2 = Y_{i-1}$ in (B.7), and Z and S represent Z_i^-, S_i^-, respectively, then the minimum in (B.7) is zero, and it is achieved by letting $\phi = \emptyset$.

Example 2

Let us now assume that $\xi_1 = X + Y + S$ and $\xi_2 = X + Z + S$ so that the external stimuli S is affecting the information captured by both sensors. Then we get

$$
I(\xi_1; \xi_2 | Z) = h(X + Y + S) - h(Y), \tag{B.11}
$$
$$
I(\xi_1; \xi_2 | Z, S) = h(X + Y) - h(Y), \tag{B.12}
$$

where clearly $h(X + Y + S) \geq h(X + Y)$, which implies that $I(\xi_1; \xi_2 | Z, S) \leq I(\xi_1; \xi_2 | Z)$.

4 Computing Stimuli-Relevant directed dependency (SRDD) Index

Let us consider the $M = 4$ nodes network shown in Fig. B.1. Let node S be the stimuli and we are interested in estimating the SRDD between nodes X, Y and Z. It is generally infeasible to take the infinite past of the processes into

account, when estimating the directed dependencies. In this work, we suggest to use Takens' delay embedding approach [17, 18] whereby the infinite past X_i^- is approximated by:

$$X_i^- \approx [X_{i-m}, X_{i-2m}, \ldots, X_{i-dm}],$$

where m and d are the embedding delay and dimension, respectively. Similarly for Y_i^-, S_i^- and Z_i^-.

After replacing the approximated past states of the processes in (B.7) or (B.8), two conditional mutual informations (or transfer entropies) are estimated by using the nearest neighbor-based approach proposed in [9] (which is referred to Kraskov–Stögbauer–Grassberger (KSG) estimator in the literature). The combination of the uniform embedding approach and the KSG estimator has been widely used in the literature to estimate transfer entropy [3, 18, 19].

The conditional mutual informations in (B.7) can be expressed as the sum/difference of four differential joint entropies. The entropy of the set of variables with the highest dimensionality is estimated via a neighbor search and the other three entropies are estimated using range searches [3, 8, 18]. The conditional mutual information is finally estimated as [3, 8, 18]:

$$I(X_i^-; Y_i | Y_i^-, Z_i^-) \approx \psi(K) + \frac{1}{N} \sum_{i=1}^{N} \psi\left(N_{[Y_i^-, Z_i^-]} + 1\right)$$
$$- \psi\left(N_{[Y_i, Y_i^-, Z_i^-]} + 1\right) - \psi\left(N_{[X_i^-, Y_i^-, Z_i^-]} + 1\right),$$

where $N_{[Y_i^-, Z_i^-]}$ denotes the number of realizations (or points) whose maximum norm from $[Y_i^-, Z_i^-]$ is strictly less than twice the maximum norm of $[Y_i, Y_i^-, X_i^-, Z_i^-]$ from its Kth neighbor. Similarly for $N_{[Y_i, Y_i^-, Z_i^-]}$ and $N_{[X_i^-, Y_i^-, Z_i^-]}$.

To solve the minimization in (B.7), we search over all possible subsets (including the empty and the full sets) of $\phi \subseteq [S_{i-m}, S_{i-2m}, \ldots, S_{i-dm}]$.

5   Simulation Study

We use simulated data in order to evaluate our proposed SRDD index in a controlled way. A non-linear autoregressive (AR) model is used to generate multivariate data with controlled directed dependency strengths and stimuli effect. The model reflects the network of Fig. B.1 and is given as:

$$X_i = 0.35X_{i-1} + 0.5Z_{i-2} + 0.6S_{i-1} + \varepsilon_X$$
$$Y_i = 0.35Y_{i-1} + 0.5X_{i-2}^2 + 0.5Z_{i-2} + 0.6S_{i-1} + \varepsilon_Y$$
$$Z_i = 0.35Z_{i-1} + \varepsilon_Z$$
$$S_i = 0.25\sqrt{2}S_{i-1} - 0.2025S_{i-2} + \varepsilon_S,$$

Table B.1: Dependency matrices: a) conditioned transfer entropy on Z, b) on Z, S and c) SRDD index. The direction of dependencies are from columns to the rows. The reported numbers are rounded to two decimal places.

From / To	X	Y	Z
X	0.00	0.00	0.04
Y	0.09	0.00	0.02
Z	0.00	0.00	0.00

a $I(X \rightarrow Y \| Z)$

From / To	X	Y	Z
X	0.00	0.00	0.04
Y	0.05	0.00	0.02
Z	0.00	0.00	0.00

b $I(X \rightarrow Y \| Z, S)$

From / To	X	Y	Z
X	0.00	0.00	0.00
Y	0.04	0.00	0.00
Z	0.00	0.00	0.00

c SRDD index

where ε_X, ε_Y, ε_Z and ε_S are mutually independent zero mean and unit variance white Gaussian processes. We assume that S is the (external) stimuli, which is affecting nodes X and Y. Node X is non-linearly and causally coupled to node Y. There are also directed dependencies from Z to both X and Y.

The SRDD index and the transfer entropy causally conditioned on Z and Z, S (for the sake of comparison) averaged over 50 realizations of the AR model at length $N = 5000$ are reported in Table B.1. The embedding delay m and dimension d were chosen as 1 and 5, respectively. For estimating the transfer entropy and the SRDD index, $K = 10$ neighbors were considered.

As expected, there are non-zero transfer entropies from node X to Y, Z to X and Z to Y in both tables B.1a and B.1b. Adding the external stimuli S to the conditioning process decreases the directed dependency only from node X to Y and it does not affect other couplings. On the other hand, the stimuli can only affect the directed dependency between nodes X and Y, which should lead to a non-zero SRDD index only from node X to Y. This is confirmed in Table B.1c, where only between nodes X and Y there is detected a non-zero directed dependency due to the effect of the stimuli.

6 Conclusions and future works

In this paper, we introduced a new directed dependency index based on the difference of two transfer entropies for quantifying the amount of the directed dependency which is due to a given time series (e.g. stimuli). We provided a lower bound for the proposed index and showed that the lower

bound could be calculated using existing transfer entropy estimators. In a simulation study, we utilized the KSG estimator and demonstrated that the dependency index could be efficiently computed and it was quite accurately able to predict the true dependencies in the data. Other estimators based on binning technique [19] and linear estimators [19] could potentielly also be used to compute the stimuli-relevant directed dependency index.

As an example, we considered a small network containing only a few nodes. However, our proposed index does not depend upon the size of the network, and can therefore be applied to more complex networks. The difficulty is to reliably estimate the transfer entropy for high dimensional problems. A possible solution in the literature to overcome the problem of entropy estimation of high-dimensional data is to select only the most informative subset of candidates among the full set of variables [19]. For the problems considered in this paper, we could potentially use the greedy selection technique of [3, 8, 20, 21] to approximately solve the minimization problem in (B.8), and at the same time reduce the dimensionality of the problem.

References

[1] T. Schreiber, "Measuring information transfer," *Phys. Rev. Lett.*, vol. 85, pp. 461 – 464, 2000.

[2] K. Mehta and J. Kliewer, "Directional and causal information flow in eeg for assessing perceived audio quality," *IEEE Transactions on Molecular, Biological and Multi-Scale Communications*, vol. 3, no. 3, pp. 150–165, 2017.

[3] P.S. Baboukani, C. Graversen, E. Alickovic, and J. Østergaard, "Estimating conditional transfer entropy in time series using mutual information and nonlinear prediction," *Entropy*, vol. 22, no. 10, pp. 1124, 2020.

[4] C.W.J. Granger, "Investigating causal relations by econometric models and cross-spectral methods," *Econometrica*, vol. 37, no. 3, pp. 424 – 438, 1969.

[5] C.W.J. Granger, "Testing for causality: a personal viewpoint," *Journal of Economic Dynamics and control*, vol. 2, pp. 329–352, 1980.

[6] M.Z. Jahromi, A. Zahedi, J. Jensen, and J. Østergaard, "Information loss in the human auditory system," *IEEE/ACM Transactions on Audio, Speech, and Language Processing*, vol. 27, no. 3, pp. 472–481, 2018.

[7] R.G. James, B.D.M. Ayala, B. Zakirov, and J. Crutchfield, "Modes of information flow," 2018.

[8] P.S. Baboukani, G. Graversen, and J. Østergaard, "Estimation of directed dependencies in time series using conditional mutual information and non-linear prediction," pp. 2388–2392, 2021.

[9] A. Kraskov, H. Stögbauer, and P. Grassberger, "Estimating mutual information," *Physical review E*, vol. 69, no. 6, pp. 066138, 2004.

[10] R.W. Yeung, *A First Course in Information Theory*, Springer, 2006.

[11] N. Ay and D. Polani, "Information flows in causal networks," *Advances in complex systems*, vol. 11, no. 1, pp. 17 – 41, 2008.

[12] L. Faes, D. Marinazzo, and S. Stramaglia, "Multiscale information decomposition: Exact computation for multivariate gaussian processes," *Entropy*, vol. 19, no. 8, pp. 408, 2017.

[13] A.B. Barrett, "Exploration of synergistic and redundant information sharing in static and dynamical gaussian systems," *Physical Review E*, vol. 91, no. 5, pp. 052802, 2015.

[14] P.L. Williams and R.D. Beer, "Nonnegative decomposition of multivariate information," *arXiv preprint arXiv:1004.2515*, 2010.

[15] U.M. Maurer and S. Wolf, "Unconditionally secure key agreement and the intrinsic conditional information," *IEEE Transactions on Information Theory*, vol. 45, no. 2, pp. 499–514, 1999.

[16] J. Massey, "Causality, feedback and directed information," pp. 303–305, 1990.

[17] F. Takens, "In dynamical systems of turbulence," *Lecture notes in mathematics*, vol. 898, pp. 366, 1981.

[18] M. Lindner, R. Vicente, V. Priesemann, and M. Wibral, "Trentool: A matlab open source toolbox to analyse information flow in time series data with transfer entropy," *BMC neuroscience*, vol. 12, no. 1, pp. 1–22, 2011.

[19] A. Montalto and L. Faesand D. Marinazzo, "Mute: a matlab toolbox to compare established and novel estimators of the multivariate transfer entropy," *PloS one*, vol. 9, no. 10, pp. e109462, 2014.

[20] Z. Jia, Y. Lin, Z. Jiao, Y. Ma, and J. Wang, "Detecting causality in multivariate time series via non-uniform embedding," *Entropy*, vol. 21, no. 12, pp. 1233, 2019.

[21] J. Zhang, "Low-dimensional approximation searching strategy for transfer entropy from non-uniform embedding," *PloS one*, vol. 13, no. 3, pp. e0194382, 2018.

References

Paper C

EEG Phase Synchrony Reflects SNR Levels During Continuous Speech-in-Noise Tasks

Payam Shahsavari Baboukani, Carina Graversen, Emina Alickovic and Jan Østergaard

Abstract

Comprehension of speech in noise is a challenge for hearing-impaired (HI) individuals. Electroencephalography (EEG) provides a tool to investigate the effect of different levels of signal-to-noise ratio (SNR) of the speech. Most studies with EEG have focused on spectral power in well-defined frequency bands such as alpha band. In this study, we investigate how local functional connectivity, i.e. functional connectivity within a localized region of the brain, is affected by two levels of SNR. Twenty-two HI participants performed a continuous speech in noise task at two different SNRs (+3 dB and +8 dB). The local connectivity within eight regions of interest was computed by using a multivariate phase synchrony measure on EEG data. The results showed that phase synchrony increased in the parietal and frontal area as a response to increasing SNR. We contend that local connectivity measures can be used to discriminate between speech-evoked EEG responses at different SNRs.

Index Terms

Hearing impairment, speech in noise, multivariate phase synchrony, local connectivity, EEG

1 Introduction

Background noise and competing talkers lead to increased listening effort for both normal-hearing (NH) and hearing-impaired (HI) individuals [1]. Previous studies have shown that the presence of background noise can negatively affect a subject's ability to perform a task. Houben et. al. [2] reported that the response time decreased significantly by increasing signal-to-noise ratio (SNR) of an audio signal. In addition, Sarampalis et. al. [3] reported that noise reduction (NR) algorithms in hearing aids (HAs) may reduce listening effort and free up cognitive resources for other tasks. Furthermore, NR algorithms in HAs can improve the performance of listeners during a selective attention task by enhancing the neural representation of speech and reducing the neural representation of background noise [4]. In this paper, we are interested in the change of the listening effort induced by the change SNR value.

A wide variety of methods have been used to assess the performances of subjects during different listening tasks (e.g., see [5]). This include behavioral [2, 3] and physiological measures such as pupillometry [6] and neuroimaging [7]. Neuroimaging measures tend to reflect changes in neural activity during the listening task [7]. Electroencephalography (EEG) has been widely used to measure the neural activity in response to audio stimuli due to its non-invasiveness and high temporal resolution [4, 6, 7].

Various advanced signal processing and information theory techniques have been applied to EEG signals in order to determine the effect of the dif-

ferent SNR values. For example, functional connectivity [8], time-frequency analysis [6], and neural speech tracking [4]. Functional connectivity describes statistical dependencies between neural data and can provide insights about how the brain functions. Transfer entropy [9] and phase synchrony [10, 11] have been proposed in the literature to assess functional connectivity.

Multivariate phase synchrony (MPS) is a standard approach to characterize the interaction within multichannel data and it has been used to assess functional connectivity in multichannel EEG data [10, 11]. Recently, a new MPS measure called circular omega complexity (COC) was proposed, which led to better performance than conventional MPS techniques in some specific cases [11].

Functional connectivity within a small region (for example a cortex) of the brain is called local connectivity. It has been shown that the local connectivity in the frontal cortex changes as the cognitive work load changes [12]. Similarly, The change of the local connectivity was used to classify left and right hand movement motor imagery in [10]. In the present study, we will use COC to assess local connectivity within 8 different regions of interest (ROIs).

Most studies (exceptions include [4, 6, 13]) investigate the effect of SNR when the stimuli is single words or short sentences. However, HI individuals in real-life encounter continuous speech and long sentences.

In this paper, we investigate changes in the local connectivity within EEG signals recorded on HI individuals in response to continuous speech at two different SNRs. Our results show that the phase synchrony reflects significant changes in the parietal and frontal areas as a response to changing SNRs.

2 MATERIALS AND METHODS

In this section we briefly describe the EEG data used in this study. This is followed by the review of the multivariate phase synchrony measure called COC. Finally, steps needed to calculate the local connectivity in the EEG signal to assess the effect of SNR will be explained.

2.1 EEG data

EEG data used in this study is explained in detail in [4], which focused on neural tracking of the speech signals. In the sequel we briefly describe the data and refer to [4] for further details

Participants

Twenty-two native HI Danish speakers (11 males, audiometric threshold = 45 dB HL) aged between 40 and 80 (mean = 67, SD = 11.2) years were recruited

(a) Trial design   (b) Experimental setup
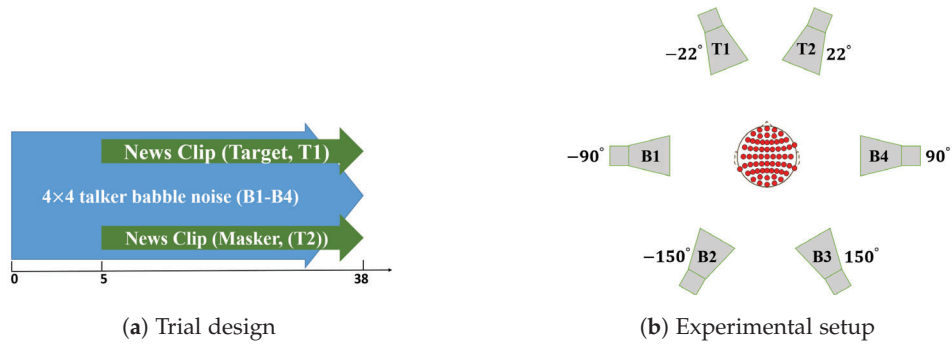
Fig. C.1: Schematic demonstration of the a) trial design and b) experimental setup.

from the Eriksholm Research Centre database. The experimental procedures were approved by the ethics committee for the capital region of Denmark [4].

Experiment Design

All target streams consisted of Danish news clips of neutral content read by the same male and female talker and were presented from two different loudspeakers in the front of the participant ($\pm 22°$ azimuth). The background noise was delivered from the four loudspeakers in the back ($\pm 90°$ and $\pm 150°$ azimuth), each playing a different four-talker babble, leading to an overall effect of 16-talker surrounding babble (see Fig C.1b). Participants were asked to attend to one of the two target talkers (target) while ignoring the contralateral talker (masker) and the background noise.

The SNR was defined as the ratio between signal power of the attended talker and the total signal power of the background noise [4]. The sound pressure level (SPL) of the target talker and background noise was set in a way to generate two different SNR values, +3 dB and +8 dB.

In total 20 trials for each SNR (+3 dB and +8 dB) were used for the analysis per subject. Each trial comprised a short period of silence, 5 s of background noise followed by 33 s of simultaneous target, masker and babble stimuli from all speakers (see Fig C.1a).

EEG data acquisition and preprocessing

The BioSemi ActiveTwo amplifier system (Biosemi, Amsterdam, Netherlands) were utilized to record the EEG data . The international 10–20 system was used to apply the location of 64 scalp electrodes. The EEG signals were sampled at 1,024 Hz.

The preprocessed EEG data used in this study is the same as data used in [4], where all preprocessing procedures are described in detail

Due to technical issues, only data from 19 subjects are included in this study.

2.2 Circular Omega Complexity

In this study, we use the COC phase synchrony measure [11] to assess the local connectivity. The COC measure determines the level of MPS within signals by quantifying the dimensionality of the state-space which is formed based on the instantaneous phase (IP) of the signals [11]. The first step to calculate the COC is to estimate the IP of the signal by using the Hilbert transform [11]. The IP of a mono-component real valued discrete signal $X[n]$ is estimated as:

$$\phi_X = \tan^{-1}\left(\frac{\hat{X}[n]}{X[n]}\right) \tag{C.1}$$

where $\hat{X}[n]$ is the Hilbert transform of $X[n]$. Considering a K-dimensional signal $\mathbf{X}[n]$ and its corresponding K-dimensional IP signal $\text{Œ}_\mathbf{X}$, the circular correlation matrix $C^\mathbf{X}$ is defined as [11]:

$$C^\mathbf{X} = [C^{A,B}]_{K*K}, \tag{C.2}$$

where $C^{A,B}$ is the circular correlation between N time points signal ϕ_A and ϕ_B which is given by [11]:

$$C^{A,B} = \frac{\sum_{n=0}^{N-1} \sin\left(\phi_A[n] - \bar{\phi}_A\right)\sin\left(\phi_B[n] - \bar{\phi}_B\right)}{\sqrt{\sum_{n=0}^{N-1}\sin^2\left(\phi_A[n] - \bar{\phi}_A\right)\left(\phi_B[n] - \bar{\phi}_B\right)}}, \tag{C.3}$$

where $\bar{\phi}_A$ is the circular mean of ϕ_A given by:

$$\bar{\phi}_A = \arg\left(\sum_{n=0}^{N-1}\exp^{i\phi_A[n]}\right). \tag{C.4}$$

The COC is then defined as [11]:

$$COC = 1 + \frac{\sum_{m=0}^{K-1}\bar{\lambda}_m \log\bar{\lambda}_m}{\log K}, \tag{C.5}$$

where $\bar{\lambda}_m = \frac{\lambda_m}{\sum_{i=0}^{K-1}\lambda_i}$ and $\lambda_m; m = 0, \ldots, K-1$ are the eigenvalues of $C^\mathbf{X}$. The COC value varies between 0 and 1 where higher values show that more channels are pair-wise phase correlated, which means that only fewer eigenvalues of the $C^\mathbf{X}$ are significant [11].

2.3 Local Connectivity Assessment in EEG

The effect of SNR in continuous speech on local connectivity will be investigated in this study. Accordingly, the COC of 8 different ROIs will be calculated and compared during two SNR values. The ROIs include left frontal,

frontal, right frontal, left temporal, central, right temporal, parietal and occipital. Table I shows EEG electrodes corresponding to ROIs.

The EEG channels were common average re-referenced to minimize the effect of volume conduction. Additionally, due to the multi-component nature of EEG signals, the analysis was performed on conventional EEG bands; Delta (0.5-4 Hz), Theta (4-8 Hz), Alpha (8-12.5 Hz) and Beta (12.5-25 Hz). Window-based FIR band-pass filters were utilized to filter the EEG channels. Following the analysis done in [11, 14], we also calculate the mean of all band-specific MPS values, which will be referred to average-band MPS value. It can describe the MPS within a ROI over all bands with a single index.

The analysis was performed at the time interval of 32 second duration from 1 to 33 second relative to the onset of the target speaker. The 32 second time interval was divided into 16 non-overlapping 2 second windows and the COC value was extracted for each time window. The local connectivity for each trial and band was then computed by averaging all 16 time windows COC values. In summary, the following steps were performed to assess local connectivity:

- Filter the data to four different bands.

- Estimate the IP of each channel at each band using Eq. (1).

- Extract the COC value at 16 time windows for each band using Eq. (5).

- Compute the local connectivity by averaging all 16 time window COC values for each band.

The aforementioned four steps were repeated for 19 subjects and 40 trials, 20 trials for each SNR value.

Two sample t-test was applied on the obtained values (380 values for each SNR value) to check the significant different local connectivity. The

Table C.1: Mapping EEG electrodes to ROIs

ROI	Electrodes	ROI	Electrodes
Left Frontal	AF7, AF3, F3 F5, F7, Fp1	Frontal	Fp1, Fp2, AF4 AF3, F1, F2
Right Frontal	AF4, AF8, F8 F6, F4, Fp2	Central	FC1, FC2, C1 CP1, C2, CP2
Left Temporal	FT7, T7, TP7 CP5, FC5, C5	Parietal	CP1, CP2, P1 P2, PO4, PO3
Right Temporal	FT8, T8, TP8 CP6, FC6, C6	Occipital	O1, O2, PO3 PO4
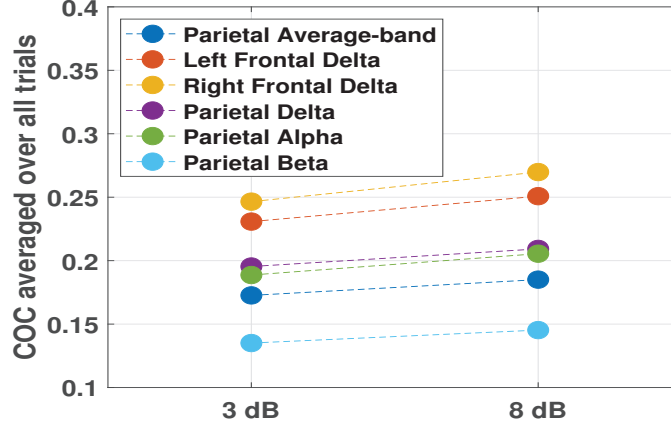
Fig. C.2: The mean values of statistically different local connectivity at two different SNR values, 3dB and 8dB.

null hypothesis is that the mean value of the local connectivity at two SNR values are equal. Since a series (8 ROIs and 5 bands leading to 40 tests) of t-tests were performed, we applied the Bonferroni correction to compensate the multiple comparisons effect. The significance level was therefore chosen as $\alpha = \frac{0.05}{40} = 0.0013$.

3   RESULTS

Table II summarizes the p-values obtained from a two sample t-test applied on the results from all trials. The p-values that are less than the significance level are shown in boldface. As shown in Table II, the parietal ROI shows a significant difference over all the bands, except the theta band. The local connectivity in the left and the right frontal ROIs in the delta band are also statistically different for the two SNR levels.

The mean values over all trials of the statistically different local connectivities are shown in Fig. 2. As illustrated in Fig. 2, all significant local connectivities increase as the SNR level increases. The increase in local connectivity is consistent over subjects; i.e. the mean over all trials for each subject tend to increase when the SNR level increases. As an example, Fig. 3 shows the parietal (averaged over all frequency bands) results averaged over trials for each subject. The blue lines show the increase in local connectivity by increasing the SNR level for each subject while the red line shows otherwise. As shown in Fig. 3, the parietal average-band connectivity attains generally a higher value at 8 dB, except for three subjects (red line).

Table C.2: The p-value of the two sample t-test. The bold face numbers shows the rejection of the null hypothesis. The significance level was $\alpha = \frac{0.05}{40} = 0.0013$.

	Left Frontal	Frontal	Right Frontal	Central	Left Temporal	Parietal	Right Temporal	Occipital
Delta	**3.31e-6**	0.34	**7.66e-7**	0.13	0.002	**2.01e-5**	0.07	0.65
Theta	0.36	0.16	0.12	0.57	0.06	0.007	0.73	0.52
Alpha	0.37	0.68	0.11	0.02	0.04	**7.88e-4**	0.09	0.03
Beta	0.40	0.02	0.65	0.28	0.35	**2.36e-5**	0.55	0.37
Average-Band	0.23	0.20	0.06	0.09	0.02	**4.68e-5**	0.31	0.23

4 DISCUSSION

In this study, we investigated whether a change of SNR level would result in a significant change of the local connectivity in the EEG signal. The target group was hearing impaired subjects and the stimuli was continuous speech in noise. The local connectivity at five frequency bands and 8 ROIs were estimated at two SNR levels of the speech stimuli. The two sample t-test was used to check if the changes were statistically different.

Table II and Fig. 2 show that local connectivity values in parietal, left frontal and right frontal ROIs were significantly higher at +8 dB in comparison to that at +3 dB (harder condition). The increase of connectivity observed in the alpha band in the parietal region when decreasing the difficulty of the task is in line with the results of [6]. In [6], the influence on the EEG power distribution of the SNR level was investigated, and it was concluded that the power in the alpha band in the parietal region was inversely related to the background noise level. It was argued that the reason might be that sustained attention is required over long speech presentation [6] and optimal sustained attention performance is linked to greater alpha oscillation [15]. [16].

The decrease in the local connectivity in the frontal ROIs within the delta band, when the listening situation is more difficult, might be due to the increase in working memory load induced by the SNR level. The decrease in frontal local connectivity within the delta band is consistent with the results reported in [17] in which they also found lower energy near the frontal lobe, when the difficulty of the working memory task increases.

5 FUTURE WORK

The feasibility to discriminate two SNR levels based on local connectivity measures provides future perspectives for hearing care rehabilitation. First, the methodology may be used to gain further understanding of brain processes in realistic listening scenarious for hearing impaired individuals using HAs. Such new understanding may be used to support the development of new signal processing algorithms in HAs. Secondly, further research may be
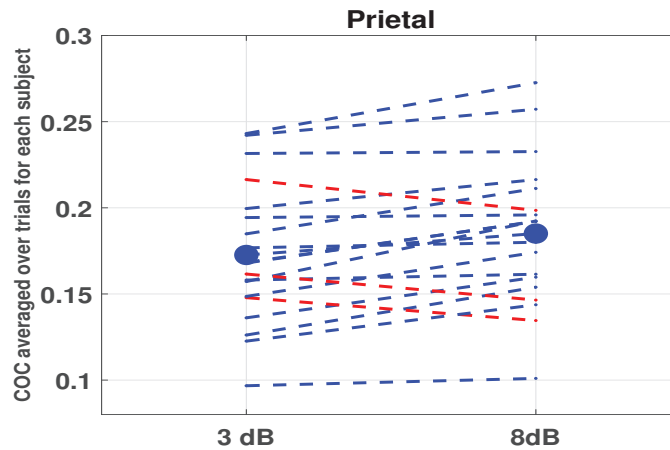
Fig. C.3: The mean over all trials for each subject in the parietal average-band. Blue lines show the increase and red lines a decrease of local connectivity by increasing SNR level.

focused on classification of single-sweep EEG segments to assess the possibility to use local connectivity to control future HAs.

References

[1] S. L. Mattys, M. H. Davis, A. R. Bradlow, and S. K. Scott, "Speech recognition in adverse conditions: A review," *Language and Cognitive Processes*, vol. 27, no. 7-8, pp. 953–978, 2012.

[2] R. Houben, M. van Doorn-Bierman, and W. A. Dreschler, "Using response time to speech as a measure for listening effort," *International journal of audiology*, vol. 52, no. 11, pp. 753–761, 2013.

[3] A. Sarampalis, S. Kalluri, B. Edwards, and E. Hafter, "Objective measures of listening effort: Effects of background noise and noise reduction," *Journal of Speech, Language, and Hearing*, 2009.

[4] E. Alickovic, T. Lunner, D. Wendt, L. Fiedler, R. Hietkamp, E. H. N. Ng, and C. Graversen, "Neural representation enhanced for speech and reduced for background noise with a hearing aid noise reduction scheme during a selective attention task," *Frontiers in neuroscience*, vol. 14, p. 846, 2020.

[5] T. Lunner, E. Alickovic, C. Graversen, E. H. N. Ng, D. Wendt, and G. Keidser, "Three new outcome measures that tap into cognitive processes required for real-life communication," *Ear and hearing*, vol. 41, no. Suppl 1, p. 39S, 2020.

[6] T. Seifi Ala, C. Graversen, D. Wendt, E. Alickovic, W. M. Whitmer, and T. Lunner, "An exploratory study of eeg alpha oscillation and pupil dilation in hearing-aid users during effortful listening to continuous speech," *Plos one*, vol. 15, no. 7, p. e0235782, 2020.

[7] J. E. Peelle, "Listening effort: How the cognitive consequences of acoustic challenge are reflected in brain and behavior," *Ear and hearing*, vol. 39, no. 2, p. 204, 2018.

[8] K. Mehta and J. Kliewer, "Directional and causal information flow in eeg for assessing perceived audio quality," *IEEE Transactions on Molecular, Biological and Multi-Scale Communications*, vol. 3, no. 3, pp. 150–165, 2017.

[9] P. S. Baboukani, C. Graversen, E. Alickovic, and J. Østergaard, "Estimating conditional transfer entropy in time series using mutual information and nonlinear prediction," *Entropy*, vol. 22, no. 10, p. 1124, 2020.

[10] P. S. Baboukani, S. Mohammadi, and G. Azemi, "Classifying single-trial eeg during motor imagery using a multivariate mutual information based phase synchrony measure," in *2017 24th National and 2nd International Iranian Conference on Biomedical Engineering (ICBME)*, pp. 1–4, IEEE, 2017.

[11] P. S. Baboukani, G. Azemi, B. Boashash, P. Colditz, and A. Omidvarnia, "A novel multivariate phase synchrony measure: Application to multichannel newborn eeg analysis," *Digital Signal Processing*, vol. 84, pp. 59–68, 2019.

[12] P. Zarjam, J. Epps, F. Chen, and N. H. Lovell, "Estimating cognitive workload using wavelet entropy-based features during an arithmetic task," *Computers in biology and medicine*, vol. 43, no. 12, pp. 2186–2195, 2013.

[13] E. Alickovic, E. H. N. Ng, L. Fiedler, S. Santurette, H. Innes-Brown, and C. Graversen, "Effects of hearing aid noise reduction on early and late cortical representations of competing talkers in noise," *Frontiers in Neuroscience*, vol. 15, 2021.

[14] L. Frassineti, A. Parente, and C. Manfredi, "Multiparametric eeg analysis of brain network dynamics during neonatal seizures," *Journal of neuroscience methods*, vol. 348, p. 109003, 2021.

[15] J. Hjortkjær, J. Märcher-Rørsted, S. A. Fuglsang, and T. Dau, "Cortical oscillations and entrainment in speech processing during working memory load," *European Journal of Neuroscience*, vol. 51, no. 5, pp. 1279–1289, 2020.

References

[16] J. Fell and N. Axmacher, "The role of phase synchronization in memory processes," *Nature reviews neuroscience*, vol. 12, no. 2, pp. 105–118, 2011.

[17] P. Zarjam, J. Epps, and N. H. Lovell, "Beyond subjective self-rating: Eeg signal classification of cognitive workload," *IEEE Transactions on Autonomous Mental Development*, vol. 7, no. 4, pp. 301–310, 2015.

Paper D

Speech to noise ratio improvement induces nonlinear parietal phase synchrony in hearing aid users

Payam Shahsavari Baboukani, Carina Graversen, Emina Alickovic and Jan Østergaard

Abstract

Objectives: *Comprehension of speech in adverse listening conditions is challenging for hearing-impaired (HI) individuals. Noise reduction (NR) schemes in hearing aids (HAs) have demonstrated the capability to help HI to overcome these challenges. The objective of this study was to investigate the effect of NR processing (inactive, where the NR feature was switched off, vs. active, where the NR feature was switched on) on correlates of listening effort across two different background noise levels [+3 dB signal-to-noise ratio (SNR) and +8 dB SNR] by using a phase synchrony analysis of electroencephalogram (EEG) signals.*

Design: *The EEG was recorded while 22 HI participants fitted with HAs performed a continuous speech in noise (SiN) task in the presence of background noise and competing talker. The phase synchrony within eight regions of interest (ROIs) and four conventional EEG bands was computed by using a multivariate phase synchrony measure.*

Results *The results demonstrated that the activation of NR in HAs affects the EEG phase synchrony in the parietal ROI at low SNR differently than that of at high SNR. The relationship between conditions of the listening task and phase synchrony in the parietal ROI was nonlinear.*

Conclusion: *We showed that the activation of NR schemes in HAs can nonlinearly reduce correlates of listening effort as estimated by EEG-based phase synchrony. We contend that investigation of the phase synchrony within ROIs can reflect the effects of HAs in HI individuals in ecological listening conditions.*

Keywords

istening effort, electroencephalography, noise reduction, phase synchrony, local connectivity, hearing impaired

1 Introduction

Hearing impaired (HI) individuals often report that listening to speech in noisy environments such as competing talkers and background noise demands greater effort, which can lead to negative effects such as increased incidence of fatigue ([Kramer et al.(2006), Wang et al.(2018), Mattys et al.(2012)]), disengagement from conversations ([Jaworski and Stephens(1998)]) and social withdrawal ([Weinstein and Ventry(1982)]). However, current measurements which are used to examine the performance of a listening task (e.g., speech reception threshold) do not typically consider the cognitive factors related to effortful listening ([Houben et al.(2013), Sarampalis et al.(2009)]).

[Pichora-Fuller et al.(2016)] defined the concept of listening effort in a conceptual model as "the deliberate allocation of mental resources to overcome obstacles in goal pursuit when carrying out a task, with listening effort applying more specifically when tasks involve listening." The obstacles

include acoustic challenges experienced by the listener, which is the combination of cognitive factors (e.g., linguistic ability and memory capacity) and acoustic characteristics (e.g., level of background noise and competing talker) ([Peelle(2018)]). Listening effort can also be modulated by the listener's motivation ([Peelle(2018), Pichora-Fuller et al.(2016)]). The goal of studying listening effort is to develop a reliable measurement tool, which can be simultaneously utilized with speech recognition tests and improve the assessment of hearing disability ([Paul et al.(2021)]) and enhance the rehabilitation strategy ([Miles et al.(2017)]).

A wide variety of methods and tools have been used to find correlates of listening effort. This includes subjective rating such as scales ([Krueger et al.(2017)]) and questioners ([Hart and Staveland(1988)]), dual tasks ([Gagne et al.(2017)]), and physiological measures such as pupillometry ([Zekveld et al.(2018)]), skin conductance ([Mackersie and Calderon-Moultrie(2016)]), heart rate ([Mackersie and Calderon-Moultrie(2016)]) and neuroimaging ([Paul et al.(2021)]). Neuroimaging measures tend to reflect changes in the brain activity underlying listening effort. In particular, electroencephalography (EEG) is becoming popular for measuring correlates of listening effort due to its non-invasiveness and high temporal resolution ([Fiedler et al.(2021), Wisniewski et al.(2021), Dimitrijevic et al.(2019), Seifi Ala et al.(2020)]).

A diverse range of signal processing and information theoretic methods have been used to analyze the EEG and extract correlates of listening effort. Some examples include time-frequency analysis, speech tracking and functional connectivity. The change in power in the alpha (8-12 Hz) frequency band at the parietal region ([Dimitrijevic et al.(2017), Petersen et al.(2015)]) and theta (4-8 Hz) frequency band at the frontal region ([Wisniewski et al.(2018), Wisniewski et al.(2015)]) have been reported by using a time-frequency analysis. The coherence between the speech envelope and the corresponding brain signal at the left frontal cortex in the 2-5 Hz frequency range has also been demonstrated that it can be used for predicting correlates of listening effort in speech tracking analysis ([Dimitrijevic et al.(2019)]).

Functional connectivity describes the statistical dependencies between neural data and can give some information about how the brain functions ([Bidelman et al.(2018)]). Functional connectivity analysis in EEG signals has been extensively used to investigate cognitive functions of auditory processing in the brain. Some examples include perceived audio quality assessment ([Mehta and Kliewer(2017)]) and semantic processing ([Zhang et al.(2019)Z]). The effect of acoustic challenges, age-related hearing loss and comprehension of speech on functional connectivity were also investigated in ([Bidelman et al.(2018)], [Bidelman et al.(2019)] and [Zhu et al.(2020)]), respectively.

Functional connectivity can be extracted by using several approaches such as phase synchrony ([Bernarding et al.(2013)]), transfer entropy ([Mehta and

Kliewer(2017), Baboukani et al.(2020), Baboukani et al.(2021b)]) and Pearson correlation ([Bidelman et al.(2019)]). The phase of neural data tends to reflect the timing of neural activity, and phase synchrony describes the interaction between or within brain regions in the neural networks ([Wöstmann et al.(2017a)]). Correlates of listening effort have been estimated using the phase synchrony analysis. Several methods have been used to extract the phase synchrony, such as wavelet phase synchronization stability ([Bernarding et al.(2010), Bernarding et al.(2013)]), the distribution of the mapped phase mean vector on the unit circle ([Bernarding et al.(2014)]) and the entropy of instantaneous phase of EEG signals ([Bernarding et al.(2012), Bernarding et al.(2017)]).

The functional connectivity within a localized region of the brain is called local connectivity. It has been utilized to classify different motor imagery movements [Baboukani et al.(2017)], estimate the cognitive workload ([Zarjam et al.(2013)], investigate schizophrenia [Jalili et al.(2007)] and Alzheimer's disease [Jalili et al.(2013)]). Phase synchrony has also been used to assess the local connectivity. Phase synchrony assessment across multivariate signals (or channels of EEG) in a localized region of the brain by averaging over all possible traditional bi-variate phase synchrony values (e.g. phase coherence, phase locking value) may not provide a full picture of the global synchrony within the signals ([Baboukani et al.(2019), Canolty et al.(2011), Omidvarnia et al.(2013), Oshima et al.(2006), Al-Khassaweneh et al.(2016)]). Alternatively, multivariate measures generalized the traditional bi-variate ones to evaluate phase synchrony within multichannel data ([Baboukani et al.(2019), Omidvarnia et al.(2013), Al-Khassaweneh et al.(2016)]). Local connectivity estimated by multivariate phase synchrony has been used in several works ([Baboukani et al.(2017), Jalili et al.(2013), Al-Khassaweneh et al.(2016)]). A new multivariate phase synchrony measure called circular omega complexity (COC) was recently proposed and shown better performance than conventional multivariate phase synchrony techniques in simulated and real EEG data ([Baboukani et al.(2019)]). Recently, we showed that local connectivity estimated by the COC measure can be used to estimate the correlates of listening effort ([Baboukani et al.(2021)a)]).

Although HI individuals in real-life encounter listening situations which involve continuous speech and long sentences, most of the studies (some exceptions include ([Alickovic et al.(2020), Alickovic et al.(2021), Fiedler et al.(2021)])) investigate the effect of NR processing and SNR when the stimuli is single words or short sentences. ([Dimitrijevic et al.(2017), Miles et al.(2017), Bernarding et al.(2014)]). However, in this study, continuous long stimuli is used in a speech in noise (SiN) task.

Modern hearing aid (HA) devices can help HI individuals through various advanced signal processing approaches ([Winneke et al.(2018), Bernarding et al.(2014), Bernarding et al.(2017)]). In particular, noise reduction (NR)

processing intends to reduce the effect of background noise and enhance the signal-to-noise ratio (SNR). It has shown capability to free up cognitive resources for other tasks during listening and reduce the listening effort ([Sarampalis et al.(2009), Ohlenforst et al.(2018)]). The activation of NR processing can improve speech understanding at low SNRs. Furthermore, it has been also shown that activation of the NR schemes in HAs provides a listening effort enhancement in addition to any effect associated with improved intelligibility ([Ohlenforst et al.(2018)]). In addition to that, NR schemes can improve the performance of the HA users during a selective attention task ([Alickovic et al.(2020), Alickovic et al.(2021)]). [Alickovic et al.(2020)] also showed that the improvement of selective attention task due to NR was different at low SNR than that of at high SNR. Another study on the same data showed that NR changed correlates of listening effort estimated by pupil size differently at the two SNR values, while a time-frequency analysis of EEG signals showed no statistical change due to SNR, NR and the interaction between them ([Fiedler et al.(2021)]). This inspired us to replace conventional power analysis in the time-frequency domain by local connectivity estimates based on multivariate phase synchrony to investigate the effect of NR processing at two SNR values. Inspired by the results in ([Alickovic et al.(2020), Fiedler et al.(2021)]), we hypothesized:

H1: The use of NR in hearing aids affects the EEG phase synchrony within localized regions of the brain (i.e. local connectivity) at low SNR differently than that of at high SNR.

H2: The effect of NR scheme on EEG phase synchrony within localized regions of the brain at different SNR values shows a nonlinear (inverted U-shape) trend.

2 Material and Method

In this section, the EEG data utilized in this study will be briefly explained. It will be followed by the description of the COC measure and steps required to assess local connectivity. Finally, the statistical test used in this study will be described.

2.1 EEG data

The EEG data of this study has been utilized for other analyses in ([Alickovic et al.(2020)] and [Fiedler et al.(2021)]), which focused on neural tracking and pupil dilation, respectively. The EEG analysis of listening effort recruited in ([Fiedler et al.(2021)]) was based on alpha power and did not show significant results.

Participants

We recruited 22 (11 males) native Danish-speaking participants with hearing loss. The stimuli used in this study were based on participants-centered language ([Nicks et al.(2022)]), and consisted of Danish news clips of neutral content. They aged between 40 and 80 years with the mean and standard deviation (SD) age of 69 and 11.2, respectively. The participants were experienced HA users with more than three months of HA usage. Participants had mild-to-moderate sensorineural hearing loss. The audiometric thresholds at 500, 1,000, 2,000, and 4,000 Hz ranged from 33 to 58 dB hearing level, with an average threshold of 45 dB hearing level. The maximum difference between the left and the right ear' averaged audiometric thresholds was less than 8 dB. The experimental procedure was approved by the ethics committee for the capital region of Denmark (journal number H-1-2011-033) and all participants signed a written consent before the experiment.

Hearing Aid Fitting and Signal Processing

All participants were fitted with identical HA models during the experiment. Two pairs of HAs were adapted for each participant: NR inactive and NR active. Rather than NR, all other signal processing settings did not change between the conditions. The Voice Aligned Compression (VAC) rationale ([Le Goff(2015)]) based on each individual's hearing threshold was applied to amplify the sound in both pairs of HAs. In the NR inactive condition, the omnidirectional setting was applied with an added natural slight forward effect of the pinna. In the other pairs, NR active, the combination of minimum variance distortionless response beamformer and a single channel Wiener post filter was applied before the VAC. The articulation-index-weighted SNR improvements ([Ohlenforst et al.(2018)]) were 6.24 dB and 5.17 dB at +3 dB SNR and +8 dB SNR, respectively, for NR active than that for NR inactive ([Alickovic et al.(2020), Fiedler et al.(2021)]).

Experimental Design

The experiment took place in an acoustically shielded listening booth with controlled light conditions. Participants were seated on a chair positioned in the middle of six loudspeakers (Genelec 8040A; Genelec Oy, Iisalmi, Finland) with a distance of 1.2 meter from each loudspeaker (see Figure D.1A), two loudspeakers in the front (at $\pm 22°$ azimuth) and four loudspeakers in the back (at $\pm 90°$ and $\pm 150°$ azimuth). Each of the background loudspeakers (B1-B4 in Figure D.1A) played four-talker babble. The two foreground speakers played the target streams which were spoken by talkers of different gender. Participants were asked to gaze at the screen positioned between the two frontal loudspeakers and were instructed to attend to one of the talkers

in the foreground speakers while ignoring the other talker on the contralateral side and background noise. To-be-attended talkers (either the right or the left side) was indicated by an arrow on the screen (see Figure D.1A).
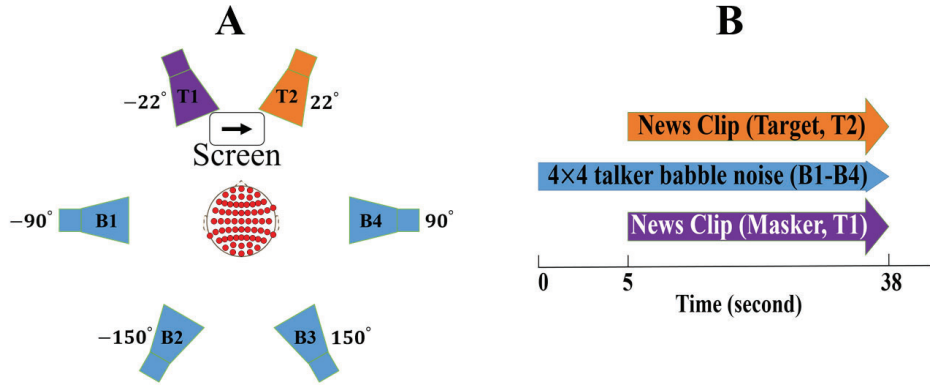
Fig. D.1: Schematic illustration of A) experiment design including six loudspeakers. The target streams (colored as purple and orange) and background noise (colored as blue) were delivered by the two foreground and four background loudspeakers, respectively. The screen located in the middle of the two foreground speakers shows the to-be-attended talker (colored as orange). B) trial design in which five seconds of only background noise and 33 seconds of simultaneous target, masker and background noise stimuli were delivered in each trial.

Stimuli

Continuous 33 seconds long Danish news clips of neutral content were utilized for talker streams. The organization of the location (left or right) and gender (male or female) of the target stream was randomized. Each of the four-talker babble noises delivered by the background loudspeakers consisted of four unique single talkers, two females and two males, speaking different news giving the impression of the 16 talkers active in the background.

The experiment was 2×2 design: the first factor was NR (active vs. inactive) and the second factor was the SNR level (+3 dB vs. + 8 dB). The SNR in our setup was defined as the ratio between the signal power of the attended talker and the total signal power of the background noise, similar to that in ([Das et al.(2018), Alickovic et al.(2020)]). In order to create real-life listening conditions at two levels of difficulty (SNR values of +3 dB and +8 dB), the maskers were set at either 53 or 48 dB, leading to a total of 59 or 54 dB background Sound Pressure Level (SPL). Each of the two foreground loudspeakers was always set at a fixed level of 62 dB SPL, leading to a fixed

level of 65 dB for the foreground talkers.

Procedure

A total of 84 trials were recorded for each participant, organized in a block design. For each of the four blocks (experimental conditions including +3 dB NR inactive, +3 dB NR active, +8 dB NR inactive and +8 dB NR active), 20 trials were conducted. The remaining four trials were used for training. Each trial consisted of a short period of silence, 5 seconds of only background noise (delivered by background loudspeakers) and 33 seconds of simultaneous target, masker and background noise stimuli (see Figure D.1B). After each trial, participants were asked to answer a two-choice question about the content of the attended speech which was displayed on the screen. The HAs were always removed and replaced again between the blocks. The participants were given a rest period after five trials.

EEG Data Acquisition and Pre-processing

The BioSemi ActiveTwo amplifier system (Biosemi, Amsterdam, Netherlands) was used to record EEG data. A total of 64 electrodes on a cap were mounted on the scalp according to the 10-20 international system. The driven right leg and common mode sense electrode were used as a reference for all other recording electrodes. The EEG data were sampled at 1024 Hz. All electrodes were mounted by applying conductive gel to obtain a stable connection and below 50 mv offset voltage.

The pre-processing includes a 0.5 Hz high-pass filter, 95 Hz low-pass filter and downsampling to 512 Hz. Then, The EEG channels with excessive noise were visually identified (on average, 3.1 ± 0.8 channels were rejected) and interpolated from the surrounding clean EEG channels by using the nearest neighbor method in Fieldtrip ([Oostenveld et al.(2011)]). The logistic Infomax independent component analysis algorithm was applied to reduce artifacts caused by eye movements, eye blinks, muscle activity, heartbeats, and single-channel noise, as implemented in Fieldtrip ([Delorme and Makeig(2004), Bell and Sejnowski(1995)]). The components were visually inspected and rejected if clearly reflected as artifacts, on average, 7.9 ± 3.6 of the components were rejected. Finally, the EEG data were epoched from 8 seconds before to 33 seconds after the onset of the target loudspeakers. The EEG data for one subject was removed from further analysis due to being excessively noisy. In addition to that, no data for one block of one participant was recorded due to technical problems.

2.2 Circular Omega Complexity (COC)

The COC measure is used in this study to extract local connectivity. This is a multivariate phase synchrony measure that was recently proposed in ([Baboukani et al.(2019)]) and was shown to perform better than the conventional measures in a particular setup. The COC assesses the level of phase dependency within multivariate signals through quantifying the dimensionality of the state-space formed by their corresponding instantaneous phases ([Baboukani et al.(2019)]).

Estimating the instantaneous phase of a real valued mono-component discrete signal $X \in \mathbb{R}^{1 \times N}$ is the first step to calculate the COC. A Hilbert transform-based approach is commonly used whereby the instantaneous phase is estimated as ([Baboukani et al.(2019)]):

$$\phi_X[n] = \tan^{-1}\left(\frac{\hat{X}[n]}{X[n]}\right), \tag{D.1}$$

where $\hat{X}[n]$ and $\phi_X[n]$ are the Hilbert transform and instantaneous phase of $X[n]$, respectively. The next step is calculating the circular correlation matrix. Considering a K-channels signal $\mathbf{X} \in \mathbb{R}^{K \times N}$ and its corresponding instantaneous phase signal $\mathbf{Œ_X} \in \mathbb{R}^{K \times N}$, the circular correlation matrix $C^{\mathbf{X}} \in \mathbb{R}^{K \times K}$ is defined as ([Baboukani et al.(2019)]):

$$C^{\mathbf{X}} = [C^{(m,l)}], \tag{D.2}$$

where $m, l \in \{1, 2, \ldots K\}$. The circular correlation between the instantaneous phase ϕ_m and ϕ_l is noted by $C^{(m,l)}$ where ϕ_m and ϕ_l are the mth and l^{th} rows of $\mathbf{Œ_X}$, respectively. The circular correlation $C^{(m,l)}$ is given as ([Baboukani et al.(2019)]):

$$C^{(m,l)} = \frac{\sum_{n=1}^{N} \sin\left(\phi_m[n] - \bar{\phi}_m\right) \sin\left(\phi_l[n] - \bar{\phi}_l\right)}{\sqrt{\sum_{n=1}^{N} \sin^2\left(\phi_n[n] - \bar{\phi}_m\right) \sin^2\left(\phi_l[n] - \bar{\phi}_l\right)}}, \tag{D.3}$$

where the circular mean $\bar{\phi}_m$ is given by ([Baboukani et al.(2019)]):

$$\bar{\phi}_m = \arg\left(\sum_{n=1}^{N} \exp^{i\phi_m[n]}\right). \tag{D.4}$$

It was shown in ([Baboukani et al.(2019)]) that the eigenvalues of $C^{\mathbf{X}}$ can be used as an index for the dimensionality of the state-space formed by $\mathbf{Œ_X}$ whereby the level of phase synchronization can be determined. The COC was then defined as ([Baboukani et al.(2019)]):

$$COC = 1 + \frac{\sum_{i=1}^{K} \bar{\lambda}_i \log \bar{\lambda}_i}{\log K}, \tag{D.5}$$

where $\bar{\lambda}_i = \frac{\lambda_m}{\sum_{j=1}^{K} \lambda_j}$ and $\lambda_i; i = 1, \ldots, K$ are the eigenvalues of C^X. The COC varies between 0 and 1 where higher values show that the channels within C^X are more phase synchronized, which means that only fewer eigenvalues of the C^X are significant ([Baboukani et al.(2019)]).

2.3 Local Connectivity Assessment

The effect of NR at two SNR values on local connectivity will be explored in this paper. Listening in adverse conditions can possibly engage multiple cognitive processes such as working memory and distractor inhibition ([Wisniewski et al.(2021)]), which can possibly change the local connectivity within different brain regions and frequency bands. We, therefore, did not restrict our analysis to one specific band or ROI and local connectivity within eight ROIs and four conventional EEG bands will be examined. The ROIs include left frontal, frontal, right frontal, left temporal, central, right temporal, parietal and occipital, similar to that in ([Mehta and Kliewer(2017)]). Table D.1 and Figure D.2 show the electrodes and their corresponding positions of different ROIs, respectively [1]. The EEG bands consist of Delta (0.5-4 Hz), Theta (4-8 Hz), Alpha (8-12.5 Hz) and Beta (12.5-25 Hz). The EEG channels were filtered by using Window-based FIR band-pass filters. Filtering to narrow frequency bands can also reduce the multi-component nature of EEG signals and can improve the estimation of the instantaneous phase signals by using the Hilbert transform technique ([Boashash and Aïssa-El-Bey(2018)]). The EEG channels were common average re-referenced to reduce the effect of volume conduction.

The local connectivity of each trial of the experiment was estimated during the time interval that frontal loudspeakers were presenting the target streams (33 seconds). We also omitted the first second of the delivering target streams to minimize the effects of event-related potential which led to a 32 seconds time period (1 to 33 second relative to the onset of the target streams). The 32 seconds time span was then divided into 16 non-overlapping 2 seconds windows [2]. The COC was then quantified for each of the windows and the average over all windows was considered as an indicator of the strength of local connectivity. The higher the average of COC values over time windows is, the more channels within the ROI are phase synchronized. The higher phase synchrony is considered as higher local connectivity in this study. The steps required to assess local connectivity in a specific band and ROI can be

---

[1]An alternative groups of electrodes for frontal, central, parietal and occipital ROIs, which include the midline electrodes located in the regions, such as Fz, Pz, Cz and Oz, produced the same trend of results.

[2]An alternative longer length (such as 10 seconds) of time windows leads to better estimation of COC. However, the results produced by longer or equal to 2 seconds time windows were following the same trend.

summarized as follows:

S1) Band-pass filter the EEG channels in the ROI to a conventional EEG band.

S2) Estimate the instantaneous phase of the filtered channels.

S3) Extract the COC value for each of the 2 seconds time windows.

S4) Average the COC values corresponding to time windows.

The aforementioned steps were repeated for eight ROIs and four EEG bands leading to 32 local connectivity values for each trial.
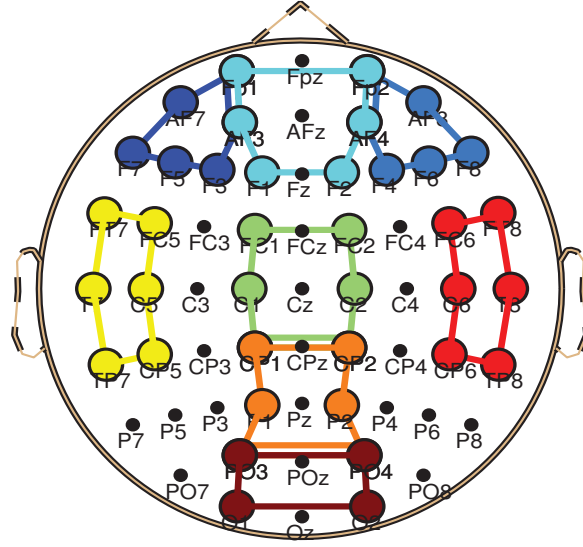
Fig. D.2: The electrode position of ROIs, different colors show different ROIs. The lines in the figure show schematic presentations of the ROIs. The ROIs include left frontal (dark blue), frontal (aqua), right frontal (light blue), left temporal (yellow), central (green), right temporal (red), parietal (orange) and occipital (brown)

2.4 Statistical Test

All the statistical analysis was performed in RStudio ([RStudio Team(2021)]). In order to investigate the effect of NR at two SNR values on local connectivity (our first hypothesis H1), two-way Linear mixed effect (LMM) ANOVA was applied by using lme4 ([Bates et al.(2014)]) and lmerTest ([Kuznetsova et al.(2017)]) packages. We fitted separate LMM ANOVA models for local connectivity values estimated at each ROI and band. Local connectivity values were treated as a continuous variable and normalized by using

2. Material and Method

ROI	Electrodes	ROI	Electrodes
Left Frontal	**AF7, AF3, F3 F5, F7, Fp1**	**Frontal**	**Fp1, Fp2, AF4 AF3, F1, F2**
Right Frontal	**AF4, AF8, F8 F6, F4, Fp2**	**Central**	**FC1, FC2, C1 CP1, C2, CP2**
Left Temporal	**FT7, T7, TP7 CP5, FC5, C5**	**Parietal**	**CP1, CP2, P1 P2, PO4, PO3**
Right Temporal	**FT8, T8, TP8 CP6, FC6, C6**	**Occipital**	**O1, O2, PO3 PO4**

$COC_{normalized} = \frac{COC - M}{S}$, where the M and S are the mean and standard deviation of the local connectivity values at specific band and ROI calculated over all experimental conditions and all subjects. The experiment factor NR was treated as a factor variable with two levels, inactive and active. The experiment factor SNR was also treated as a factor variable with two levels, high (+8 dB) and low (+3 dB). The local connectivity was modeled as a function of fixed factors NR, SNR and their interaction, and the participants were treated as a random effect. The analysis was conducted based on subject-averaged local connectivity values. We will also report the results based on single trial models for the statistically significant local connectivity, in which the interaction between participants and trials was treated as a random effect.

In order to investigate our second hypothesis which is about the relationship between local connectivity and the four experimental conditions- +3 dB active, +3 dB inactive, +8 dB active and +8 dB inactive, we applied the measured SNR improvement of the NR processing, see Section 2.1 for more details. The SNR improvements of the active NR scheme were 6.24 dB and 5.17 dB at 3 dB SNR and 8 dB SNR, respectively. This process reduces the two factors SNR and NR of the experiment to only one factor SNR, with values of 3 dB, 8 dB, 9.24 dB and 13.17 dB. Then, one-way LMM ANOVA was applied to model local connectivity as a function of fixed factor SNR which was treated as a continuous variable. Two models were used for each local connectivity: the first model included the quadratic (nonlinear) term alongside with the linear term for the fixed factor SNR and the second model only consisted of the linear term. The participants were treated as a random effect. Similar to the two-way LMM ANOVA, the results based on single trial models for the statistically significant trends will be reported.

Since a series (eight ROIs and four bands leading to 32 models) of LMM ANOVA models were applied, we used the Bonferroni correction to compensate for the multiple comparisons effect. The significance levels for all

the two-way and one-way LMM ANOVA models were therefore chosen as $\alpha = \frac{0.05}{32} = 0.0016$.

3 Results

Participants were prompted with a two-choice question related to the content of the attended speech after each trial. They correctly answered 86% of the questions. This indicates that the participants followed the task as instructed. However, after applying a two-way LMM ANOVA on the behavioral performances, there was no statistical effect of NR, SNR, and their interaction, with the p-values of 0.25, 0.06, and 0.37, respectively.

To test the hypothesis H1, two-way LMM ANOVA was applied to local connectivity at each ROI and band, which modeled the normalized local connectivity as a function of fixed factors NR and SNR. Table D.2a, D.2b and D.2c summarized the p-values obtained from applying two-way LMM ANOVA on the average over trials for each subject local connectivity. As shown in able D.2a, we found a significant interaction of SNR and NR on local connectivity at the parietal region alpha frequency band (will be referred to as parietal alpha hereinafter), $F_{59.02} = 12.28, p = 0.0009$. Note that, as mentioned in section 2.1, the EEG data of one block for one subject was not recorded. Therefore, our data is unbalanced and the denominator degree of freedom (DF) is estimated by using Satterthwaite's method. As there is no p-value less than 0.0016 in Table D.2b and Table D.2c, no significant main effect was found for SNR and NR. The results of applying LMM ANOVA on single trial data were in line with the average trial analysis. The interaction between SNR and NR was statistically significant at parietal alpha, $F_{1228.5} = 83.59, p < 0.0001$.

The one-way LMM ANOVA was applied to average trial data after applying the SNR improvement of the NR processing to investigate the hypothesis H2. The normalized local connectivity was modeled as a function of continuous fixed factor SNR by using two separate one-way LMM ANOVA to study the relationship between the normalized local connectivity and experiment conditions. The first model was based on including the quadratic term for the fixed factor SNR and the second model only consisted of the linear term. Table D.3a shows the results of the first model in which quadratic term alongside with linear term were included. As shown in Table D.3a, the nonlinear trend between local connectivity and SNR at parietal alpha was statistically significant, $F_{60.22} = 11.92, p = 0.0010$. We found no linear relationship between the experimental conditions and local connectivity, as there is no p-value less than the significant level in Table D.3b. The nonlinear trend between local connectivity and SNR at parietal alpha was also significant by single trial analysis, $F_{1229.5} = 76.36, p < 0.0001$.

For the purposes of visualization, Figure D.3 and Figure D.4 plot regres-

sion line and 95% confidence interval for the nonlinear trend between normalized local connectivity and experimental conditions at both individual and average trial analysis, respectively. The inverted U-shaped relationship shows that local connectivity at parietal alpha is higher for +3 dB active and +8 dB inactive and lower for +3 dB inactive and +8 dB active. The figures also show that NR processing at lower SNR (+3 dB) leads to an increase in the local connectivity at parietal alpha while NR processing at higher SNR (+8 dB) leads to a decrease.
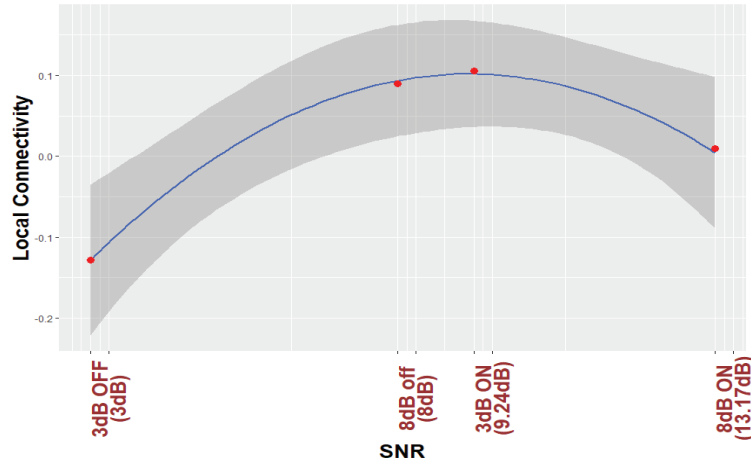
Fig. D.3: Parietal alpha local connectivity is regressed based on different listening conditions. The analysis is performed by single trial data and the red points show the average over all trials and all subjects for different listening conditions.
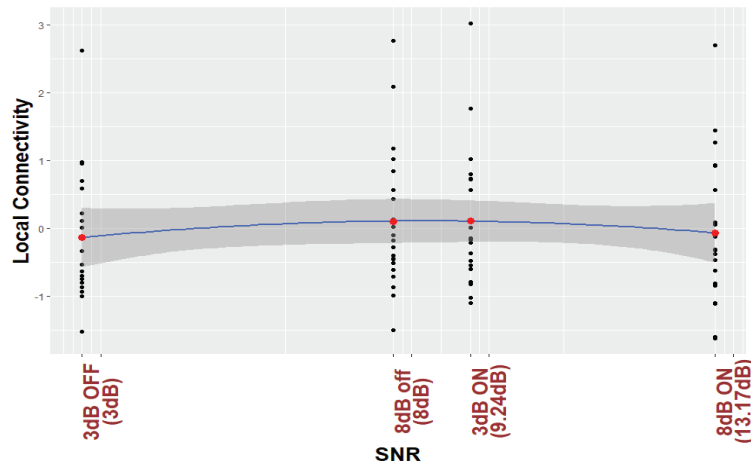
Fig. D.4: Parietal alpha local connectivity is regressed based on different listening conditions. The analysis is performed by average over trials data. The black points in the figure show the average over trials for subjects and the red points show the average over black points for different listening conditions.

Table D.2: P-values of the two-way LMM ANOVA. (A) P-values for interaction between two factors SNR and NR. (B) P-values of the main factor SNR. (C) P-values of the main factor NR. The two factors are SNR values, +3 dB and +8 dB, and NR schemes, on and off. The boldface numbers show the rejection of the null hypothesis. The significance level was Bonferroni corrected, $\alpha = \frac{0.05}{32} = 0.0016$.

a A

	Left Frontal	Frontal	Right Frontal	Central	Left Temporal	Parietal	Right Temporal	Occipital
Delta	0.3083	0.9577	0.9004	0.2891	0.7109	0.0086	0.5054	0.6982
Theta	0.5986	0.9038	0.8941	0.2419	0.8460	0.0098	0.1991	0.8890
Alpha	0.5811	0.7302	0.6898	0.1370	0.5116	**0.0009**	0.04	0.6041
Beta	0.6868	0.3757	0.5041	0.2295	0.8981	0.0033	0.1544	0.7814

b B

	Left Frontal	Frontal	Right Frontal	Central	Left Temporal	Parietal	Right Temporal	Occipital
Delta	0.6430	0.1143	0.0535	0.6862	0.4565	0.7421	0.9075	0.7022
Theta	0.4882	0.0497	0.5245	0.3467	0.8811	0.4504	0.1736	0.9586
Alpha	0.6072	0.1096	0.6841	0.8241	0.8235	0.6635	0.0981	0.1719
Beta	0.2794	0.0757	0.9245	0.4805	0.6725	0.9951	0.0260	0.3742

c C

	Left Frontal	Frontal	Right Frontal	Central	Left Temporal	Parietal	Right Temporal	Occipital
Delta	0.5015	0.8633	0.7418	0.4164	0.8241	0.6195	0.6881	0.5722
Theta	0.7668	0.9642	0.5383	0.4872	0.6733	0.3703	0.8001	0.8816
Alpha	0.6963	0.7806	0.2371	0.7766	0.6075	0.4634	0.5812	0.2326
Beta	0.7135	0.5241	0.2805	0.8134	0.7648	0.7150	0.8649	0.4089

4 Discussion

4.1 Summary

In a sample of 22 HIs, we studied the effect of NR processing in HAs on the EEG local connectivity during a continuous SiN task. Inspired by the results reported in ([Alickovic et al.(2020), Fiedler et al.(2021)]), we hypothesized that the effect of NR schemes on local connectivity differs at the two SNR values, +3 dB and +8 dB, of the experiment. Consistent with our hypothesis (H1), we found a significant interaction between the factors of the experiment, SNR and NR, at parietal alpha by using both average-trial and single-trial analysis, which would suggest that NR processing affects the local connectivity at low SNR differently than that of at high SNR. It should be noted that the p-values corresponded to the interaction at the parietal and all frequency bands are small. However, the dominant significant change due to the interaction between SNR and NR appears to be at the alpha band as only the parietal alpha band survives a correction for multiple comparisons.

The articulation-index-weighted SNR improvements ([Ohlenforst et al.(2018)]) of the NR processing was applied, which reduces the two factors of the experiment to only one factor SNR with values +3 dB, +8 dB, +9.24 and +13.17

dB. We then investigated the relationship between the experimental conditions and local connectivity. We found a significant inverted U-shaped function at parietal alpha by both single and average trial analysis, which was in line with our second hypothesis H2. Since this study is the first work, to our knowledge, that investigates the effect of different levels of listening effort and NR schemes in HA on local connectivity, the results will be discussed in terms of hypothesized functions in the following sections.

4.2 NR Schemes in HAs Reduce the Listening Effort

Recent studies have shown that the activation of advanced signal processing algorithms in HAs provides hearing benefits for HIs, particularly in adverse listening conditions ([Ohlenforst et al.(2018), Sarampalis et al.(2009), Winneke et al.(2018)]). Studies focusing on changes or benefits in speech intelligibility may not provide a complete picture of the processes involved in speech recognition ([Sarampalis et al.(2009), Dillon and Lovegrove(1993), Ohlenforst et al.(2018)]). In particular, NR processing, which is the main focus of this study, can reduce listening effort and free up cognitive resources for other tasks while it may not have positive effects on speech reception threshold ([Sarampalis et al.(2009)]). The effects of NR schemes have been investigated when the stimuli is a single word or sentence ([Dimitrijevic et al.(2017), Miles et al.(2017), Ohlenforst et al.(2018)]). However, HI individuals encounter long speech in real ecological situations. For this reason, long continuous news clips were presented at different SNR levels. Our first finding based on speech tracking analysis of the EEG data published in ([Alickovic et al.(2020)]) showed that NR processing can improve the performance of HAs during a selective auditory attention task. Then, [Fiedler et al.(2021)] showed that the NR schemes can also reduce the listening effort estimated by pupillometry. However, the neural index of listening effort estimated by spectral power analysis of the EEG data did not show any statistical change. It inspired us to recruit a new correlate of listening effort estimated by local connectivity in EEG data to investigate the effect of NR schemes during a long continuous SiN task.

As shown in Table D.2a, the interaction between SNR and NR on local connectivity is statistically significant. This suggests that NR processing affects the local connectivity differently at the two SNR values of the experiment, which is in line with pupillometry results reported in ([Fiedler et al.(2021), Ohlenforst et al.(2018)]) where they also found a different effect of NR schemes at different SNR values. This result is also consistent with results published in ([Alickovic et al.(2020)]) in which they found that NR processing improved the performance of the selective attention task differently at the two SNR values. We also investigated the relationship between correlates of listening effort and the experimental conditions by applying the

SNR-improvement of NR processing. As demonstrated in Table D.3a and Figure D.3 and Figure D.4, we found inverted U-shaped trend. We believe that this study is the first work that showed the nonlinear trend of neural estimation of correlates of listening effort as a result of NR processing at different SNR values during a continuous long SiN task. This result is consistent with pupil dilation analysis in ([Ohlenforst et al.(2018)]) and EEG analysis in ([Paul et al.(2021), Decruy et al.(2020), Wisniewski et al.(2017), Marsella et al.(2017)]) where nonlinear relationship due to NR processing at different SNR values and different levels of listening difficulty were found, respectively.

4.3 Local Connectivity is Modulated by Top-down Cognitive Functions or Changes of Brain Networks

Most of the existing studies in the literature which investigated the listening effort by using EEG signals tend to focus on spectral power features and particularly event-related spectral perturbation (ERSP) (c.f Section 4.5). Finding a relationship between local connectivity estimated at scalp level, which is the case in this study, and power change can be controversial and even two features can be significantly uncorrelated, as it is the case in ([Jalili et al.(2007)]) study where no significant correlation was found between power change and local connectivity in Schizophrenia EEG data analysis. There might be possibilities to discuss the relationship based on Firefly model presented in ([Burgess(2012)]) or the model presented in ([Jirsa(2009)]). However, we believe that the local connectivity estimated in this study can violate the required assumptions of these models. Nonetheless, the studies which investigate spectral power changes during effortful listening described the possible top-down cognitive functions or brain networks that can lead to the change in the power features. There are two theories which can connect top-down cognitive function or brain networks and local connectivity.

The first theory is based on the phase reset model in which phase locking of ongoing EEG activity can be a modulatory effect of top-down functions of the brain ([Bernarding et al.(2017)]). [Peelle et al.(2013)] found that neural data and the envelope of the external acoustic stimuli become more phase-locked when linguistic information is available. They concluded that the phase-locking of the neural oscillations does not rely only on the sensory cues and top-down cognitive function can also modulate phase locking. [Dimitrijevic et al.(2019)] also found that the phase-locked cortical representation can be modulated by top-down cognitive function related to different levels of listening effort. [Bernarding et al.(2017)] demonstrated that the distribution of the phase of the ongoing EEG signal can be modulated by the top-down cognitive functions related to different listening effort. Considering these aspects, one interpretation can be that local connectivity estimated by multivari-

Table D.3: P-values of the one-way LMM ANOVA. (A) P-values for the quadratic term. (B) P-values for the linear term. The local connectivity at different ROIs and bands is independently modeled by different listening conditions. The conditions are +3 dB inactive (+3 dB), +8 dB inactive (+8 dB), +3 dB active (9.24 dB), and +8 dB active (13.17 dB). The boldface numbers show the rejection of the null hypothesis. The significance level was Bonferroni corrected, $\alpha = \frac{0.05}{32} = 0.0016$.

a A

	Left Frontal	Frontal	Right Frontal	Central	Left Temporal	Parietal	Right Temporal	Occipital
Delta	0.3358	0.9458	0.9256	0.3253	0.6948	0.0094	0.4790	0.6577
Theta	0.6181	0.9998	0.9405	0.2151	0.8761	0.0129	0.2118	0.8773
Alpha	0.6061	0.7128	0.6102	0.1282	0.5417	**0.0010**	0.0593	0.5358
Beta	0.7114	0.4093	0.5719	0.2195	0.9201	0.0035	0.1618	0.8435

b B

	Left Frontal	Frontal	Right Frontal	Central	Left Temporal	Parietal	Right Temporal	Occipital
Delta	0.3699	0.2595	0.3415	0.6413	0.7490	0.4511	0.7277	0.5054
Theta	0.8699	0.2342	0.9215	0.2923	0.65551	0.6869	0.5770	0.8868
Alpha	0.9773	0.2288	0.5105	0.7980	0.7522	0.3106	0.6534	0.9599
Beta	0.3135	0.0942	0.3961	0.5875	0.9849	0.6326	0.2555	0.9071

ate phase synchrony is also modulated by the top-down cognitive functions related to the listening effort.

The second theory explains that change of local connectivity estimated by phase synchronization can be one of the mechanisms for coordinating the information transfer in brain networks ([Olejarczyk et al.(2017), Helfrich et al.(2016)]). For example, [Helfrich et al.(2016)] showed that local parieto-occipital phase coupling at the alpha band controls the inter-hemispheric information transfer. Additionally, [Olejarczyk et al.(2017)] reported the increase in local phase coupling in closed eyes compared to open eyes in a resting-state EEG analysis and they concluded that fronto-parietal information transfer can be regulated by local phase synchrony. Regarding these aspects, it can be interpreted that local connectivity estimated by phase synchrony also coordinates the information transfer related to effortful listening and NR schemes in HAs.

4.4 Significant Change at Parietal Alpha Local Connectivity

Most prior studies that investigated EEG correlates of listening effort have tended to restrict their analysis to a single EEG band and region ([Wisniewski et al.(2015), Dimitrijevic et al.(2019), Seifi Ala et al.(2020)]). However, [Wisniewski et al.(2021)] conducted a comprehensive study in which they investigated a fuller range of the EEG power spectrum and independent source activities. They found several significant changes in different regions and bands. They concluded that listening in adverse conditions can possibly engage multiple cognitive processes. Consistent with [Wisniewski et al.(2021)],

NR processing can also engage multiple cognitive processes which can possibly change the local connectivity. As the effect of NR processing in HAs on local connectivity in ecologically adverse conditions was investigated for the first time in this paper, we did not restrict our analysis to one specific EEG band and region. Local connectivity at a total of eight ROIs and four conventional EEG bands were therefore examined.

Frontal theta and parietal alpha activity at the sensor level have been mainly reported in the literature as the regions and bands that can be used to estimate correlates of listening effort ([Wisniewski et al.(2018), Wisniewski et al.(2017), Fiedler et al.(2021), Dimitrijevic et al.(2019)]). The change in the frontal theta activity is mostly observed in experiments in which non-speech stimuli were used ([Wisniewski et al.(2018), Wisniewski et al.(2017)]). This tends to reflect the internal attention and it does not show general endogenously exerted effort related to externally generated object representations (e.g., competing speech streams and background noise) ([Wisniewski et al.(2018)]). As the change of listening effort in this study is mostly due to changes in externally represented speech stimuli, we did not observe any significant change in frontal theta local connectivity, which is in line with the results reported in ([Seifi Ala et al.(2020)]) that significant change of frontal theta change was not observed as a results changes in the speech stimuli characteristics. On the other hand, the change of parietal alpha activity has been widely observed when listening effort was examined in experiments with speech stimuli ([Fiedler et al.(2021), Dimitrijevic et al.(2017), Dimitrijevic et al.(2019), Paul et al.(2021), Seifi Ala et al.(2020), Petersen et al.(2015), McMahon et al.(2016), Wöstmann et al.(2017b)Wöstmann, Lim, and Obleser, Wöstmann et al.(2015), Miles et al.(2017), Marsella et al.(2017)]), which is line with our results where we only found significant change at the parietal alpha activity.

4.5 Top-down Cognitive Functions in Listening Effort

The direction (i.e. increase, decrease or inverted U-shape) of the parietal alpha activity modulation found in the literature has been controversial. Some studies reported that higher listening effort leads to increase in parietal alpha power (relative to the baseline) arguing that it reflects the inhibition of neural activity in task-irrelevant brain area ([Dimitrijevic et al.(2017), Dimitrijevic et al.(2019), Paul et al.(2021), Petersen et al.(2015), McMahon et al.(2016), Wöstmann et al.(2017b)Wöstmann, Lim, and Obleser, Wöstmann et al.(2015), Miles et al.(2017), Marsella et al.(2017)]). In contrast, other studies showed that more demanding conditions lead to decrease in parietal alpha power ([Seifi Ala et al.(2020), Fiedler et al.(2021)]). The first explanation for the contradictory results is that multiple sources of alpha power contribute to parietal alpha power and the balance between suppression and enhancement

can be determined by the stimuli and task design ([Fiedler et al.(2021), Wisniewski et al.(2021), Seifi Ala et al.(2020), Dimitrijevic et al.(2017)]). [Seifi Ala et al.(2020)] observed lower parietal alpha power related to more difficult conditions during long speech listening. It was discussed in ([Seifi Ala et al.(2020)]) that sustained attention and constant update of information in working memory is required when the stimuli is long, which would lead to contradictory results. Another explanation for the opposite direction can be related to the inverted U-shape relationship. Depending on the level of difficulties of the experiment, estimated correlates of listening effort can be on one or the other side of the inverted U's maximum, which would result in an increase or decrease in parietal alpha power, respectively ([Fiedler et al.(2021)]).

The last relationship between listening conditions and parietal alpha power reported in the literature is an inverted U-shape ([Paul et al.(2021), Decruy et al.(2020), Wisniewski et al.(2017), Marsella et al.(2017)]). There are two explanations for the observed nonlinear trend. One theory is that during difficult conditions subjects disengaged and gave up to perform the task, which can influence the parietal alpha changes ([Marsella et al.(2017)]). The second explanation is that at very high levels of difficulty, other sensory networks might be activated to help speech understanding which leads to an inverse direction of parietal alpha modulation compared to that of at lower difficulty levels ([Paul et al.(2021)]). The supportive sensory networks under very hard conditions can be related to sustained attention and constant update of information in working memory as reported in ([Seifi Ala et al.(2020)]).

4.6 Parietal Alpha Local Connectivity is Modulated by Listening Effort

Referring to Figure D.3 and Table D.3a, we also found a significant nonlinear trend in local connectivity at parietal alpha. As shown in Figure D.3, an increase in levels of difficulty in listening (decrease in SNR values) from the condition +8 dB ON (NR: active) to +8 dB off (NR: inactive) leads to an increase in local connectivity. Consistent with results reported in ([Dimitrijevic et al.(2017), Dimitrijevic et al.(2019), Paul et al.(2021), Petersen et al.(2015), McMahon et al.(2016), Wöstmann et al.(2017b)Wöstmann, Lim, and Obleser, Wöstmann et al.(2015), Miles et al.(2017), Marsella et al.(2017)]), the increase of the parietal alpha power can be due to inhibition cognitive function. Considering the first theory mentioned in Section 4.3, the inhibition top-down cognitive function can lead to the modulation of local connectivity. This interpretation is in line with the results of ([Mathewson et al.(2009), Paul et al.(2021)]) where the authors also found that phase synchronization in parietal alpha increases due to inhibition cognitive function. The change of local connectivity due to inhibition function can also be supported by the second

theory mentioned in Section 4.3. The inhibition function mostly engages the fronto-parietal network. We interpreted that the local connectivity at parietal alpha can also coordinate the fronto-parietal information transfer. This interpretation is in line with the results reported in ([Olejarczyk et al.(2017)]) where the authors also found that phase synchrony in parietal alpha coordinates the fronto-parietal information transfer in rest-state EEG analysis.

As shown in Figure D.3, in the more difficult condition (i.e., at +3 dB) the local connectivity decreases, whereas in the easier condition (i.e., at + 8dB) the local connectivity increases. In line with EEG band power analysis results, this change can be due to either giving up during more difficult conditions ([Marsella et al.(2017)]) or other sensory networks that might be activated to help speech understanding during such listening conditions ([Paul et al.(2021)]). Our findings provide evidence that the change from increase to decrease in local connectivity under more difficult conditions could be due to the activation of other networks at the lowest SNR value. Considering the second theory mentioned in Section 4.3 which describes that local connectivity estimated by phase synchrony can coordinate the information transfer in brain networks, the change of direction in local connectivity modulation at +3 dB OFF condition can also be due to activation of other sensory networks which can be coordinated by local connectivity at parietal alpha. One possible sensory network can be due to sustained attention and constant update of information in working memory which is in line with the results reported in ([Seifi Ala et al.(2020)]). It was discussed in ([Seifi Ala et al.(2020)]) that sustained attention and constant update of information in working memory is required when the stimuli is long. This was also observed during a Stenberg task in which encoding and retention phases were entangled and a contradictory increase in parietal alpha power was reported as a result of higher working memory loads ([Jensen et al.(2002), Hjortkjær et al.(2020), Seifi Ala et al.(2020)]). Kim et al. found that the brain network involved in updating function engaged in an n-back level experimental paradigm mostly includes the parietal cortex which is served as a main hub for the cognitive network ([Kim et al.(2017)]). They also found a substantially different pattern during the most demanding condition compared to easier conditions. Considering the second theory in Section 4.3, the change of direction of the local connectivity modulation at the hardest condition in our experiment can also be due to substantially different networks involved in updating function.

4.7 Limitations

The local connectivity at eight ROIs and four EEG frequency bands were investigated in this study. The selection of the ROIs was similar to that in ([Mehta and Kliewer(2017)]) where they used 128 electrodes and we adapted their ROI selections with 64 electrodes setup. However, there might be a

better selection of ROIs, which can lead to different results. Additionally, considering that we had two states of NR processing and two SNR values, our experiment had four listening conditions. We checked the relationship between local connectivity and listening conditions and we found a nonlinear trend. Examination with more SNR values is required and it can provide more insights and we expect to observe a complete inverted U-shape relationship with more SNR values.

[Obleser and Kayser(2019)] showed that the phase locking between neural data and the envelope of the speech can be modulated by the behavioral performance of the task. There is a possibility that local connectivity is also modulated by the performance of the task or subjective rating of listening effort (often refereed to as self-report or experienced listening effort) ([Paul et al.(2021)]), similar to the first theory in Section 4.3. The behavioral performance evaluation was accomplished by asking a two-choice question about the to-be-attended speech stream at the end of each trial in our experiment. Our investigation of the effect of the experimental factors on the behavioral performance published in ([Fiedler et al.(2021)]) did not show any significant effect of NR, SNR or their interactions on the behavioral performance. The behavioral performance was though well above the chance level (50%) and the participants followed the task as instructed. However, the lack of valuable behavioral performance or subjective ratings of listening effort prevented us from checking the possibility that local connectivity is modulated by them.

The second theory in Section 4.3 explained that local connectivity can coordinate the information transfer in brain networks. We interpreted that local connectivity at parietal alpha can also coordinate the large-scale connectivity engaged in inhibition function and constant update of the working memory and referred to the studies in which these information transfers were studied. There is a possibility that other brain networks are also engaged during a continuous long SiN task, which could be provided by a large-scale connectivity investigation.

5 Conclusion

We investigated the effect of activation of NR processing on EEG-based phase synchrony measure within localized regions of the brain at eight regions of interest and four conventional EEG frequency bands during a longer continuous speech in noise (SiN) task with two SNR levels. We demonstrated that the effect of noise reduction (NR) processing algorithms on EEG-based phase synchrony has a non-linear trend in the parietal region of interest, specifically in the alpha band. The interpretation of the phase synchrony modulation is in line with the literature. These results confirmed that the EEG-based phase

synchrony within localized regions of the brain contains informative features which can reflect the effects of HA signal processing algorithms in HA users. Taken together, our study provided further evidence that the NR processing algorithms in HAs positively affect HA users in their everyday natural listening environments.

References

[Al-Khassaweneh et al.(2016)] Al-Khassaweneh, M., Villafane-Delgado, M., Mutlu, A. Y., and Aviyente, S. (2016). A measure of multivariate phase synchrony using hyperdimensional geometry. *IEEE Transactions on Signal Processing* 64, 2774–2787

[Alickovic et al.(2020)] Alickovic, E., Lunner, T., Wendt, D., Fiedler, L., Hietkamp, R., Ng, E. H. N., et al. (2020). Neural representation enhanced for speech and reduced for background noise with a hearing aid noise reduction scheme during a selective attention task. *Frontiers in neuroscience* 14, 846

[Alickovic et al.(2021)] Alickovic, E., Ng, E. H. N., Fiedler, L., Santurette, S., Innes-Brown, H., and Graversen, C. (2021). Effects of hearing aid noise reduction on early and late cortical representations of competing talkers in noise. *Frontiers in Neuroscience* 15:636060

[Baboukani et al.(2019)] Baboukani, P. S., Azemi, G., Boashash, B., Colditz, P., and Omidvarnia, A. (2019). A novel multivariate phase synchrony measure: Application to multichannel newborn eeg analysis. *Digital Signal Processing* 84, 59–68

[Baboukani et al.(2020)] Baboukani, P. S., Graversen, C., Alickovic, E., and Østergaard, J. (2020). Estimating conditional transfer entropy in time series using mutual information and nonlinear prediction. *Entropy* 22, 1124

[Baboukani et al.(2021)a)] Baboukani, P. S., Graversen, C., Alickovic, E., and Østergaard, J. (2021a). Eeg phase synchrony reflects snr levels during continuous speech-in-noise tasks. In *2021 43rd Annual International Conference of the IEEE Engineering in Medicine & Biology Society (EMBC)* (IEEE), 531–534

[Baboukani et al.(2021b)] Baboukani, P. S., Graversen, C., and Østergaard, J. (2021b). Estimation of directed dependencies in time series using conditional mutual information and non-linear prediction. In *2020 28th European Signal Processing Conference (EUSIPCO)* (IEEE), 2388–2392

References

[Baboukani et al.(2017)] Baboukani, P. S., Mohammadi, S., and Azemi, G. (2017). Classifying single-trial eeg during motor imagery using a multivariate mutual information based phase synchrony measure. In *2017 24th National and 2nd International Iranian Conference on Biomedical Engineering (ICBME)* (IEEE), 1–4

[Bates et al.(2014)] Bates, D., Mächler, M., Bolker, B., and Walker, S. (2014). Fitting linear mixed-effects models using lme4. *Journal of Statistical Software* 67, 1–48

[Bell and Sejnowski(1995)] Bell, A. J. and Sejnowski, T. J. (1995). An information-maximization approach to blind separation and blind deconvolution. *Neural computation* 7, 1129–1159

[Bernarding et al.(2010)] Bernarding, C., Corona-Strauss, F. I., Latzel, M., and Strauss, D. J. (2010). Auditory streaming and listening effort: an event related potential study. In *2010 Annual International Conference of the IEEE Engineering in Medicine and Biology* (IEEE), 6817–6820

[Bernarding et al.(2012)] Bernarding, C., Strauss, D. J., Hannemann, R., and Corona-Strauss, F. I. (2012). Quantification of listening effort correlates in the oscillatory eeg activity: a feasibility study. In *2012 Annual International Conference of the IEEE Engineering in Medicine and Biology Society* (IEEE), 4615–4618

[Bernarding et al.(2013)] Bernarding, C., Strauss, D. J., Hannemann, R., Seidler, H., and Corona-Strauss, F. I. (2013). Neural correlates of listening effort related factors: Influence of age and hearing impairment. *Brain research bulletin* 91, 21–30

[Bernarding et al.(2014)] Bernarding, C., Strauss, D. J., Hannemann, R., Seidler, H., and Corona-Strauss, F. I. (2014). Objective assessment of listening effort in the oscillatory eeg: Comparison of different hearing aid configurations. In *2014 36th Annual International Conference of the IEEE Engineering in Medicine and Biology Society* (IEEE), 2653–2656

[Bernarding et al.(2017)] Bernarding, C., Strauss, D. J., Hannemann, R., Seidler, H., and Corona-Strauss, F. I. (2017). Neurodynamic evaluation of hearing aid features using eeg correlates of listening effort. *Cognitive neurodynamics* 11, 203–215

[Bidelman et al.(2018)] Bidelman, G. M., Davis, M. K., and Pridgen, M. H. (2018). Brainstem-cortical functional connectivity for speech is differentially challenged by noise and reverberation. *Hearing research* 367, 149–160

[Bidelman et al.(2019)] Bidelman, G. M., Mahmud, M. S., Yeasin, M., Shen, D., Arnott, S. R., and Alain, C. (2019). Age-related hearing loss increases full-brain connectivity while reversing directed signaling within the dorsal–ventral pathway for speech. *Brain Structure and Function* 224, 2661–2676

[Boashash and Aïssa-El-Bey(2018)] Boashash, B. and Aïssa-El-Bey, A. (2018). Robust multisensor time–frequency signal processing: A tutorial review with illustrations of performance enhancement in selected application areas. *Digital Signal Processing* 77, 153–186

[Burgess(2012)] Burgess, A. P. (2012). Towards a unified understanding of event-related changes in the eeg: The firefly model of synchronization through cross-frequency phase modulation. *PLOS ONE* 7, 1–21

[Canolty et al.(2011)] Canolty, R. T., Cadieu, C. F., Koepsell, K., Knight, R. T., and Carmena, J. M. (2011). Multivariate phase–amplitude cross-frequency coupling in neurophysiological signals. *IEEE Transactions on Biomedical Engineering* 59, 8–11

[Das et al.(2018)] Das, N., Bertrand, A., and Francart, T. (2018). Eeg-based auditory attention detection: boundary conditions for background noise and speaker positions. *Journal of neural engineering* 15, 066017

[Decruy et al.(2020)] Decruy, L., Lesenfants, D., Vanthornhout, J., and Francart, T. (2020). Top-down modulation of neural envelope tracking: the interplay with behavioral, self-report and neural measures of listening effort. *European Journal of Neuroscience* 52, 3375–3393

[Delorme and Makeig(2004)] Delorme, A. and Makeig, S. (2004). Eeglab: an open source toolbox for analysis of single-trial eeg dynamics including independent component analysis. *Journal of neuroscience methods* 134, 9–21

[Dillon and Lovegrove(1993)] Dillon, H. and Lovegrove, R. (1993). Single microphone noise reduction systems for hearing aids: A review and an evaluation. *Acoustical factors affecting hearing aid performance* 20, 353–70

[Dimitrijevic et al.(2017)] Dimitrijevic, A., Smith, M. L., Kadis, D. S., and Moore, D. R. (2017). Cortical alpha oscillations predict speech intelligibility. *Frontiers in human neuroscience* 11, 88

[Dimitrijevic et al.(2019)] Dimitrijevic, A., Smith, M. L., Kadis, D. S., and Moore, D. R. (2019). Neural indices of listening effort in noisy environments. *Scientific Reports* 9, 1–10

References

[Fiedler et al.(2021)] Fiedler, L., Ala, T. S., Graversen, C., Alickovic, E., Lunner, T., and Wendt, D. (2021). Hearing aid noise reduction lowers the sustained listening effort during continuous speech in noise—a combined pupillometry and eeg study. *Ear and hearing* 42, 1590–1601

[Gagne et al.(2017)] Gagne, J.-P., Besser, J., and Lemke, U. (2017). Behavioral assessment of listening effort using a dual-task paradigm: A review. *Trends in hearing* 21, 2331216516687287

[Hart and Staveland(1988)] Hart, S. G. and Staveland, L. E. (1988). Development of nasa-tlx (task load index): Results of empirical and theoretical research. In *Advances in psychology* (Elsevier), vol. 52. 139–183

[Helfrich et al.(2016)] Helfrich, R. F., Knepper, H., Nolte, G., Sengelmann, M., König, P., Schneider, T. R., et al. (2016). Spectral fingerprints of large-scale cortical dynamics during ambiguous motion perception. *Human brain mapping* 37, 4099–4111

[Hjortkjær et al.(2020)] Hjortkjær, J., Märcher-Rørsted, J., Fuglsang, S. A., and Dau, T. (2020). Cortical oscillations and entrainment in speech processing during working memory load. *European Journal of Neuroscience* 51, 1279–1289

[Houben et al.(2013)] Houben, R., van Doorn-Bierman, M., and Dreschler, W. A. (2013). Using response time to speech as a measure for listening effort. *International journal of audiology* 52, 753–761

[Jalili et al.(2013)] Jalili, M., Barzegaran, E., and Knyazeva, M. G. (2013). Synchronization of eeg: bivariate and multivariate measures. *IEEE Transactions on Neural Systems and Rehabilitation Engineering* 22, 212–221

[Jalili et al.(2007)] Jalili, M., Lavoie, S., Deppen, P., Meuli, R., Do, K. Q., Cuénod, M., et al. (2007). Dysconnection topography in schizophrenia revealed with state-space analysis of eeg. *PloS one* 2, e1059

[Jaworski and Stephens(1998)] Jaworski, A. and Stephens, D. (1998). Self-reports on silence as a face-saving strategy by people with hearing impairment. *International Journal of Applied Linguistics* 8, 61–80

[Jensen et al.(2002)] Jensen, O., Gelfand, J., Kounios, J., and Lisman, J. E. (2002). Oscillations in the alpha band (9–12 hz) increase with memory load during retention in a short-term memory task. *Cerebral cortex* 12, 877–882

[Jirsa(2009)] Jirsa, V. K. (2009). Neural field dynamics with local and global connectivity and time delay. *Philosophical Transactions of the Royal Society A: Mathematical, Physical and Engineering Sciences* 367, 1131–1143

[Kim et al.(2017)] Kim, N. Y., Wittenberg, E., and Nam, C. S. (2017). Behavioral and neural correlates of executive function: interplay between inhibition and updating processes. *Frontiers in neuroscience* 11, 378

[Kramer et al.(2006)] Kramer, S. E., Kapteyn, T. S., and Houtgast, T. (2006). Occupational performance: Comparing normally-hearing and hearing-impaired employees using the amsterdam checklist for hearing and work: Desempeño laboral: Comparación de empleados con audición normal o alterada usando el listado amsterdam para audición y trabajo. *International journal of audiology* 45, 503–512

[Krueger et al.(2017)] Krueger, M., Schulte, M., Brand, T., and Holube, I. (2017). Development of an adaptive scaling method for subjective listening effort. *The Journal of the Acoustical Society of America* 141, 4680–4693

[Kuznetsova et al.(2017)] Kuznetsova, A., Brockhoff, P. B., and Christensen, R. H. (2017). lmertest package: tests in linear mixed effects models. *Journal of statistical software* 82, 1–26

[Le Goff(2015)] Le Goff, N. (2015). Amplifying soft sounds—a personal matter. *Oticon Whitepaper*

[Mackersie and Calderon-Moultrie(2016)] Mackersie, C. L. and Calderon-Moultrie, N. (2016). Autonomic nervous system reactivity during speech repetition tasks: Heart rate variability and skin conductance. *Ear and Hearing* 37, 118S–125S

[Marsella et al.(2017)] Marsella, P., Scorpecci, A., Cartocci, G., Giannantonio, S., Maglione, A. G., Venuti, I., et al. (2017). Eeg activity as an objective measure of cognitive load during effortful listening: A study on pediatric subjects with bilateral, asymmetric sensorineural hearing loss. *International journal of pediatric otorhinolaryngology* 99, 1–7

[Mathewson et al.(2009)] Mathewson, K. E., Gratton, G., Fabiani, M., Beck, D. M., and Ro, T. (2009). To see or not to see: prestimulus α phase predicts visual awareness. *Journal of Neuroscience* 29, 2725–2732

[Mattys et al.(2012)] Mattys, S. L., Davis, M. H., Bradlow, A. R., and Scott, S. K. (2012). Speech recognition in adverse conditions: A review. *Language and Cognitive Processes* 27, 953–978

[McMahon et al.(2016)] McMahon, C. M., Boisvert, I., de Lissa, P., Granger, L., Ibrahim, R., Lo, C. Y., et al. (2016). Monitoring alpha oscillations and pupil dilation across a performance-intensity function. *Frontiers in Psychology* 7, 745

References

[Mehta and Kliewer(2017)] Mehta, K. and Kliewer, J. (2017). Directional and causal information flow in eeg for assessing perceived audio quality. *IEEE Transactions on Molecular, Biological and Multi-Scale Communications* 3, 150–165

[Miles et al.(2017)] Miles, K., McMahon, C., Boisvert, I., Ibrahim, R., De Lissa, P., Graham, P., et al. (2017). Objective assessment of listening effort: Coregistration of pupillometry and eeg. *Trends in hearing* 21, 2331216517706396

[Nicks et al.(2022)] Nicks, S., Johnson, A. L., Traxler, B., Bush, M. L., Brame, L., Hamilton, T., et al. (2022). The use of person-centered language in medical research articles focusing on hearing loss or deafness. *Ear and Hearing* 43, 703–711

[Obleser and Kayser(2019)] Obleser, J. and Kayser, C. (2019). Neural entrainment and attentional selection in the listening brain. *Trends in cognitive sciences* 23, 913–926

[Ohlenforst et al.(2018)] Ohlenforst, B., Wendt, D., Kramer, S. E., Naylor, G., Zekveld, A. A., and Lunner, T. (2018). Impact of snr, masker type and noise reduction processing on sentence recognition performance and listening effort as indicated by the pupil dilation response. *Hearing research* 365, 90–99

[Olejarczyk et al.(2017)] Olejarczyk, E., Marzetti, L., Pizzella, V., and Zappasodi, F. (2017). Comparison of connectivity analyses for resting state eeg data. *Journal of neural engineering* 14, 036017

[Omidvarnia et al.(2013)] Omidvarnia, A., Azemi, G., Colditz, P. B., and Boashash, B. (2013). A time–frequency based approach for generalized phase synchrony assessment in nonstationary multivariate signals. *Digital Signal Processing* 23, 780–790

[Oostenveld et al.(2011)] Oostenveld, R., Fries, P., Maris, E., and Schoffelen, J.-M. (2011). Fieldtrip: open source software for advanced analysis of meg, eeg, and invasive electrophysiological data. *Computational intelligence and neuroscience* 2011

[Oshima et al.(2006)] Oshima, K., Carmeli, C., and Hasler, M. (2006). State change detection using multivariate synchronization measure from physiological signals. *Journal of Signal Processing* 10, 223–226

[Paul et al.(2021)] Paul, B. T., Chen, J., Le, T., Lin, V., and Dimitrijevic, A. (2021). Cortical alpha oscillations in cochlear implant users reflect subjective listening effort during speech-in-noise perception. *Plos one* 16, e0254162

References

[Peelle(2018)] Peelle, J. E. (2018). Listening effort: How the cognitive consequences of acoustic challenge are reflected in brain and behavior. *Ear and hearing* 39, 204

[Peelle et al.(2013)] Peelle, J. E., Gross, J., and Davis, M. H. (2013). Phase-locked responses to speech in human auditory cortex are enhanced during comprehension. *Cerebral cortex* 23, 1378–1387

[Petersen et al.(2015)] Petersen, E. B., Wöstmann, M., Obleser, J., Stenfelt, S., and Lunner, T. (2015). Hearing loss impacts neural alpha oscillations under adverse listening conditions. *Frontiers in psychology* 6, 177

[Pichora-Fuller et al.(2016)] Pichora-Fuller, M. K., Kramer, S. E., Eckert, M. A., Edwards, B., Hornsby, B. W., Humes, L. E., et al. (2016). Hearing impairment and cognitive energy: The framework for understanding effortful listening (fuel). *Ear and hearing* 37, 5S–27S

[RStudio Team(2021)] RStudio Team (2021). *RStudio: Integrated Development Environment for R*. RStudio, PBC, Boston, MA

[Sarampalis et al.(2009)] Sarampalis, A., Kalluri, S., Edwards, B., and Hafter, E. (2009). Objective measures of listening effort: Effects of background noise and noise reduction 52, 1230–1240

[Seifi Ala et al.(2020)] Seifi Ala, T., Graversen, C., Wendt, D., Alickovic, E., Whitmer, W. M., and Lunner, T. (2020). An exploratory study of eeg alpha oscillation and pupil dilation in hearing-aid users during effortful listening to continuous speech. *Plos one* 15, e0235782

[Wang et al.(2018)] Wang, Y., Naylor, G., Kramer, S. E., Zekveld, A. A., Wendt, D., Ohlenforst, B., et al. (2018). Relations between self-reported daily-life fatigue, hearing status, and pupil dilation during a speech perception in noise task. *Ear and Hearing* 39, 573

[Weinstein and Ventry(1982)] Weinstein, B. E. and Ventry, I. M. (1982). Hearing impairment and social isolation in the elderly. *Journal of Speech, Language, and Hearing Research* 25, 593–599

[Winneke et al.(2018)] Winneke, A., De Vos, M., Wagener, K. C., Derleth, P., Latzel, M., Appell, J., et al. (2018). Listening effort and eeg as measures of performance of modern hearing aid algorithms. *Audiology Online* 24198, 1–13

[Wisniewski et al.(2018)] Wisniewski, M. G., Iyer, N., Thompson, E. R., and Simpson, B. D. (2018). Sustained frontal midline theta enhancements during effortful listening track working memory demands. *Hearing research* 358, 37–41

References

[Wisniewski et al.(2017)] Wisniewski, M. G., Thompson, E. R., and Iyer, N. (2017). Theta-and alpha-power enhancements in the electroencephalogram as an auditory delayed match-to-sample task becomes impossibly difficult. *Psychophysiology* 54, 1916–1928

[Wisniewski et al.(2015)] Wisniewski, M. G., Thompson, E. R., Iyer, N., Estepp, J. R., Goder-Reiser, M. N., and Sullivan, S. C. (2015). Frontal midline θ power as an index of listening effort. *Neuroreport* 26, 94–99

[Wisniewski et al.(2021)] Wisniewski, M. G., Zakrzewski, A. C., Bell, D. R., and Wheeler, M. (2021). Eeg power spectral dynamics associated with listening in adverse conditions. *Psychophysiology* 58, e13877

[Wöstmann et al.(2017a)] Wöstmann, M., Fiedler, L., and Obleser, J. (2017a). Tracking the signal, cracking the code: Speech and speech comprehension in non-invasive human electrophysiology. *Language, Cognition and Neuroscience* 32, 855–869

[Wöstmann et al.(2015)] Wöstmann, M., Herrmann, B., Wilsch, A., and Obleser, J. (2015). Neural alpha dynamics in younger and older listeners reflect acoustic challenges and predictive benefits. *Journal of Neuroscience* 35, 1458–1467

[Wöstmann et al.(2017b)Wöstmann, Lim, and Obleser] Wöstmann, M., Lim, S.-J., and Obleser, J. (2017b). The human neural alpha response to speech is a proxy of attentional control. *Cerebral cortex* 27, 3307–3317

[Zarjam et al.(2013)] Zarjam, P., Epps, J., Chen, F., and Lovell, N. H. (2013). Estimating cognitive workload using wavelet entropy-based features during an arithmetic task. *Computers in biology and medicine* 43, 2186–2195

[Zekveld et al.(2018)] Zekveld, A. A., Koelewijn, T., and Kramer, S. E. (2018). The pupil dilation response to auditory stimuli: current state of knowledge. *Trends in hearing* 22, 2331216518777174

[Zhang et al.(2019)Z] Zhang, G., Si, Y., and Dang, J. (2019). Revealing the dynamic brain connectivity from perception of speech sound to semantic processing by eeg. *Neuroscience* 415, 70–76

[Zhu et al.(2020)] Zhu, Y., Liu, J., Ristaniemi, T., and Cong, F. (2020). Distinct patterns of functional connectivity during the comprehension of natural, narrative speech. *International journal of neural systems* 30, 2050007